ADVANCED OPTIMIZATION TECHNIQUES AND HYBRID MICROGRID DESIGN FOR SOLAR ENERGY INTEGRATION AND MPPT ENHANCEMENT USING MODIFIED FIREFLY ALGORITHM

by

MANA ABUSAQ

A dissertation proposal submitted in partial fulfillment of the
requirements for the degree of

DOCTOR OF PHILOSOPHY IN ELECTRICAL AND COMPUTER ENGINEERING

2025

Oakland University
Rochester, Michigan

Doctoral Advisory Committee:

Mohamed Zohdy, Ph.D., Chair
Hoda S. Abdel-Aty-Zohdy, Ph.D.
Steven Louis, Ph.D.
Mohammad-Reza Siadat, Ph.D.
Erica Ruegg, Ph.D.

For Every Great Dream, There Is A Long Journey

To My Father.
To My Mother.
To My Sisters and Brothers.
To My Family, Asma, Jaber and Nader.
To Myself, Mana…

ACKNOWLEDGMENTS

First and foremost, I would like to express my sincere gratitude to my advisor, Dr. Mohamed A. Zohdy, for his unwavering guidance, encouragement, and invaluable insights throughout this research journey. His expertise, patience, and constructive feedback have played a crucial role in shaping this dissertation.

I am also deeply grateful to Dr. Hoda S. Zohdy, Dr. Steven Louis, Dr. Mohammad-Reza Siadat, and Dr. Erica Ruegg, for their time, effort, and invaluable suggestions, which have greatly enhanced the quality of this work. Their expertise and insightful discussions have been instrumental in refining my research approach.

A special appreciation goes to Oakland University for providing the necessary resources and a research environment that enabled the successful completion of this work. I would also like to acknowledge the Technical and Vocational Training Corporation (TVTC) for their financial support, which made this research possible.

My heartfelt thanks extend to my colleagues and fellow researchers for their continuous support, inspiring discussions, and collaborative spirit. Their encouragement and shared knowledge have made this journey both enriching and enjoyable.

I am incredibly grateful to my beloved parents for their unwavering love, guidance, and support, which have been the foundation of my journey. My heartfelt appreciation also goes to my dear sisters and brothers for their constant encouragement and belief in me. A special and profound gratitude is reserved for my wonderful wife, Asma, whose patience, understanding, and unwavering support have been my greatest source of strength. Lastly, to my two precious sons, Jaber and Nader, your presence has been my greatest motivation and inspiration, reminding me every day of the importance of perseverance and hard work.

Lastly, I extend my appreciation to all individuals, known and unknown, who contributed to this work in one way or another. Without their support, this dissertation would not have been possible.

Mana Abusaq

ABSTRACT

ADVANCED OPTIMIZATION TECHNIQUES AND HYBRID MICROGRID DESIGN FOR SOLAR ENERGY INTEGRATION AND MPPT ENHANCEMENT USING MODIFIED FIREFLY ALGORITHM

by

MANA ABUSAQ

Adviser: Mohamed A. Zohdy, Ph.D.

Present-day, microgrid systems, particularly systems engaging photovoltaic (PV) technologies, are gaining increasing attention as they offer promising solutions for a resilient and sustainable power demand worldwide. Saudi Arabia, with its enormous solar resources, is great positioned to embrace renewable energy alternatives. However, the southern region, particularly Najran Provenience, remains unutilized despite its significant solar potential. This thesis comprehensively investigates the design and sizing of microgrids of this area following enhancing system reliability and optimizing performance using the professional capabilities for the scientific research.

The first study examines a grid-connected hybrid microgrid for the Najran Secondary Industrial Institute (NSII) utilizing the Hybrid Optimization of Multiple Energy Resources (HOMER) software. The system integrates PV, battery storage system (BSS), diesel generator (DG) and grid. In this study, the system's reliability was assessed using the Loss of Power Supply Probability (LPSP). The LPSP was maintained at zero, indicating no unmet load for all scenarios. The design of the grid-connected balances the technological, economic and environmental considerations, insuring the system's resilience and cost-effectiveness.

The second study shifts the focus to an off-grid system. The off-grid solar-powered microgrid interduces a novel approach for sizing the microgrid using a Modified Firefly Algorithm (MFA). This modified algorithm enhances the convergence speed and solution quality which is a significant improvement over the traditional firefly algorithm (FA). The system's reliability was evaluated under two scenarios, with LPSP values of 0.01 and 0.1. This innovative MFA demonstrated superior performance in optimizing the sizing of the system's components, particularly in scenarios where reliability is critical.

The third study focuses on the impact of partial shading conditions (PSC) on photovoltaic systems and the effectiveness of maximum power point tracking (MPPT) algorithms. A comparative analysis was conducted to evaluate the performance of four MPPT techniques: Perturb and Observe (P&O), Particle Swarm Optimization (PSO), FA, and MFA. The results demonstrate that MFA consistently outperforms the other algorithms in tracking the maximum power point (MPP) under PSCs. Additionally, the study investigates the influence of varying load resistance on the efficiency of MPPT tracking, revealing that MFA exhibits higher adaptability and stability across different conditions. The research findings highlight the importance of employing advanced MPPT techniques to enhance PV system efficiency under challenging environmental conditions.

Together, these studies enrich the deployment of renewable energy systems in Saudi Arabia's southern regions by highlighting the potential of the advance and novel techniques in designing the methodologies of these microgrid. This research, by addressing both grid-connected and off- grid, contributes to the Saudi Arabia's immense efforts to diversify its energy sources under Vision 2030.

TABLE OF CONTENTS

TABLE OF CONTENTS - Continued

LIST OF TABLES

LIST OF TABLES - Continued

LIST OF FIGURES

LIST OF FIGURES - Continued

LIST OF FIGURES - Continued

CHAPTER ONE

INTRODUCTION

1.1 Saudi Arabia's Path to Renewable Energy

The growing demand for energy has brought microgrids to the forefront as an energy solution in today’s world. These systems, utilizing renewable energy sources (RES), are transforming energy distribution by providing reliable, clean, and cost-effective power. By reducing dependency on power grids microgrids empower communities with resilient, localized energy. This integration is not only cost savings but also minimizing the environmental impacts by reducing carbon emission and promotion of cleaner energy sources making them an essential part of modern energy infrastructure. Saudi Arabia, due to its vast landmass and favorable weather conditions, is Ideally located to capitalized on renewable energy, particularly the solar power. Situated within the Sun Belt, the country receives abundant solar irradiance throughout the year, making it a primal choice for solar system mega projects. The combination of the vast desert landscape and high solar irradiance provides a perfect medium for capturing solar energy, creating valuable opportunity to produce sustainable energy for both rural and urban areas.

While Saudi Arabia is rich, in oil reserves. Heavily depends on them for its economy in the run this can have negative consequences. The country’s economy is affected by fluctuating oil prices which makes it susceptible to changes in the market. Furthermore, burning fossil fuels leads to air pollution and greenhouse gas emissions which have effects on both the environment and public health [1]. Therefore, the country faces the dual challenge of maintaining its economic stability with reducing its environmental impact as the world transitions toward using more sustainable energy sources.

In response, the country has launched the Saudi National Renewable Energy Program (NREP) intends to increase the share of the RES in the electricity generation from 1% in 2018 to reach 50% by 2030 through several mega project around the country. Table 1.1. Shows the RE mega projects in Saudi Arabia [2].

Table 1.1 Mega projects in Saudi Arabia

Year	**Status**	**Project**		**Project type**	**Capacity (MW)**
2017	Operating	1	Sakaka	PV	300
		2	Duwmat Al Jandal	Wind	400
2019	Partially operating	3	Al-Shuaiba	PV	600
		4	Jeddah	PV	300
		5	Rabigh	PV	300
		6	Qurrayat	PV	200
		7	Madina	PV	50
		8	Rafha	PV	20
2020	Under Construction	9	Layla	PV	80
		10	Wadi Aldwaser	PV	120
		11	Ar Rass	PV	700
		13	Saad	PV	300
		14	Red Sea	PV	340
		15	Alkahfa	PV	1425
		16	Almaala	PV	410

Table 1.2 Mega projects in Saudi Arabia (continued)

Year	Status		Project	Project type	Capacity (MW)
		17	NEOM	PV	2200
		18	NEOM	Wind	1650
		19	Al-Faisaliah	PV	600
		20	Duba	PV	550
		21	Dhahran	PV	10.5
		22	Medyan Umluj	Wind	400
2022	Power purchased agreement signed	23	Yanbu	Wind	700
		24	Al Ghat	Wind	600
		25	Waad Al Shamal	Wind	500
		26	Al henakiyah	PV	1100
		27	Tabarjal	PV	400
2023	Announced	28	As Sadawi	PV	2000
		29	Almas'a	PV	1000
		30	Al henakiyah	PV	400
		31	Rabigh 2	PV	300
		32	Al-Shuaiba 2	PV	2000
		33	Sudair	PV	1500
		34	Ar Rass 2	PV	2000
		35	Saad 2	PV	1125

However, despite its potential, Najran Province remains largely untapped for renewable energy projects. As a region enjoys high sola irradiance throughout the year which gives it the ideality for one of the solar energy projects in the country.

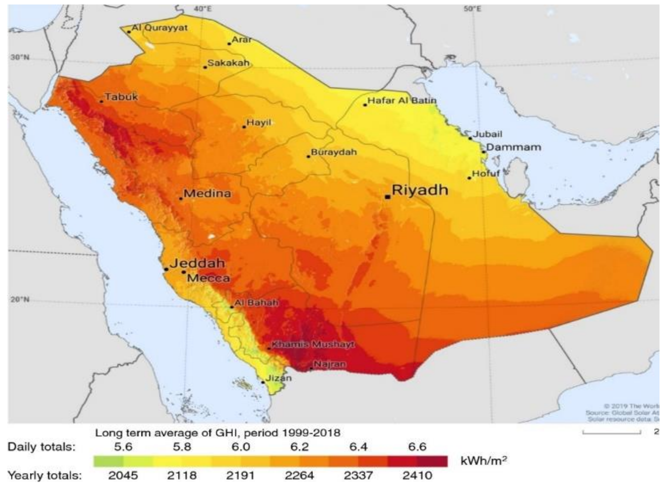

Figure 1.1 Map of the global horizontal solar irradiation of Saudi Arabia

Recently, many studies have highlighted the feasibility of integrating the renewable energy projects in Saudi Arabia, emphasizing their potential in both economic and environmental aspects by reducing the dependency on the fossil fuel [3][4][5][6][7][8]. Wherefore, research studying the expanding photovoltaic system in regions like Najran could significantly expand the dependency on the renewable energy resources in the country. As Saudi Arabia continues to achieve a sustainable energy future, the importance of focusing on underutilized regions becomes clear. By exploiting these regions' solar potential, Saudi Arabia can accelerate its growth, progress and development toward a greener and more sustainable energy scene.

1.2 Motivation

Despite Saudi Arabia's vast solar potential, Najran Province in the south region remains untapped in terms of the renewable energy development. This lack of development contrasts with the Kingdom's Vision 2030 goals of reducing the dependency on fossil fuel by increasing renewable energy production. All the governmental, private and residential sectors in the region rely on costly and environmentally harmful fossil fuel- based generators. conducting research that focuses on designing live grid-connected and off-grid models with realistic data, especially for one of the biggest government facilities in the region, using the modern and innovative techniques to ensure the system high reliability, will undoubtedly have a positive impact in guiding the authorities toward harnessing the potential energy in the region. This work not only contributes to closing the energy gap in untapped areas but also aligns with the United Nations' Sustainable Development 7th goal, which is to provide affordable and clean energy for all [9].

Figure 1.2 UN Sustainable Development Goals

1.3 Thesis Objectives

The objective of this research is to design and develop an optimized solar photovoltaic (PV) microgrid system for the southern regions of Saudi Arabia, focusing on both grid-connected and off-grid applications. This study aims to improve the efficiency and reliability of microgrid system sizing through advanced algorithmic optimization and system design strategies. The research presented in this dissertation is based on prior work conducted by the author, which has resulted in three published papers: [10], [11], and [12]. Each of these papers focuses on different aspects of microgrid optimization, and their findings have been expanded and integrated into this dissertation to create a comprehensive framework for microgrid system development.

Research Methods:

This thesis follows a structured research approach to collect data and derive insights using the following methodologies:

- Theoretical Framework:
    - Review foundational concepts of photovoltaic systems, battery storage (BS), and power converters.
    - Examine financial metrics such as Net Present Cost (NPC) and Levelized Cost of Energy (LCOE) to assess the economic feasibility of different microgrid configurations.
    - Analyze Maximum Power Point (MPP) and Maximum Power Point Tracking (MPPT) strategies for efficient solar energy utilization.
- Grid-Connected Systems Analysis:

    This section builds upon previous work presented in [10], where an optimized hybrid microgrid system was designed for the Najran Secondary Industrial Institute. The study explored:

    - The optimal tilt angle for solar panels to maximize energy capture.
    - The best system configuration that balances economic and technical constraints for grid-connected microgrids.
    - The resilience of the system under different environmental and operational conditions.
- Off-Grid Systems Development:

This research builds upon the methodology outlined in [11], where the Modified Firefly Algorithm (MFA) was implemented for optimizing the configuration of off-grid microgrids. The key research objectives in this area include:

- Implementing the MFA to optimize the design and sizing of off-grid microgrid components, ensuring cost-effective and reliable operation.
- Evaluating system reliability using the Loss of Power Supply Probability (LPSP) as a key performance metric.
- Conducting comparative analyses between the MFA-optimized system and configurations optimized using the standard Firefly Algorithm (FA) to validate the effectiveness of the MFA.

- MPPT:

The implementation of MPPT algorithms in this dissertation is based on the research presented in [12], where the Modified Firefly Algorithm (MFA) was applied to track the Maximum Power Point (MPP) of a PV system under Partial Shading Conditions (PSCs). The research objectives in this section include:

- Develop and apply the MFA for real-time MPPT in a photovoltaic system operating under Partial Shading Conditions (PSCs).
- Validate the effectiveness of the MFA by comparing its tracking efficiency against conventional MPPT algorithms, including Perturb and Observe (P&O), Particle Swarm Optimization (PSO), and the standard FA under PSCs.

- Investigate the effect of varying load resistance in a DC-DC boost converter on the MPPT performance of the MFA, particularly under PSCs.
- Conducting MATLAB/Simulink-based simulations to evaluate system performance under different environmental conditions and load variations, ensuring the robustness of the MFA in dynamic operating conditions.

Key Design Considerations:

The design process will focus on the optimal integration of system components to ensure that load profiles are effectively met, and system reliability is prioritized. This research will also introduce innovative approaches for the optimal sizing of off-grid microgrid systems, integrating cutting-edge algorithmic strategies to enhance operational efficiency and sustainability under varying environmental conditions.

1.4 Thesis Outline

This dissertation is structured into six chapters, covering the fundamental principles, system design, optimization techniques, and performance evaluation of microgrid systems.

Chapter 2 provides an overview of the fundamentals of microgrid systems, detailing key components of hybrid microgrid architectures and their electrical modeling. A special focus is given to solar photovoltaic (PV) systems, emphasizing their role in harvesting solar energy and their integration into microgrid configurations.

Chapter 3 explores the design and implementation of a grid-connected hybrid microgrid system, evaluating both its economic and technical performance under various operational conditions. The analysis in this chapter is based on prior research conducted by the author, as presented in [10], where HOMER Pro was used to determine the optimal microgrid configuration.

Chapter 4 focuses on the optimization of off-grid microgrid sizing using the Modified Firefly Algorithm (MFA). This chapter also evaluates the reliability of the optimized microgrid system by comparing it with configurations optimized using the standard Firefly Algorithm (FA). The research findings presented in this chapter build upon the methodology developed in [11], where MATLAB scripting was utilized for algorithmic implementation and performance validation.

Chapter 5 presents an advanced study on Maximum Power Point Tracking (MPPT) under Partial Shading Conditions (PSCs) using the MFA. The effectiveness of the algorithm is validated by comparing its tracking performance with conventional MPPT algorithms, including Perturb and Observe (P&O), Particle Swarm Optimization (PSO), and FA. The work in this chapter is an extension of [12], with further refinements in algorithmic design and real-world applicability.

Chapter 6 concludes the dissertation by summarizing the key findings, discussing the broader implications of this research, and outlining potential future research directions in microgrid system optimization and renewable energy integration.

CHAPTER TWO

FUNDAMENTALS OF MICROGRID POWER SYSTEMS

2.1 Microgrid Types

A microgrid is small-scale power systems incorporating distributed energy resources, viewed as essential components of future smart grids [13]. A typical microgrid system can be configured as either AC or DC-coupled, commonly referred to as an AC microgrid or DC microgrid, respectively. Each type has its own advantages and disadvantages, depending on the application [14]. Additionally, microgrids can be either grid-tied (connected to the main utility grid) or operate independently as off-grid systems. Conducting a system-level analysis is crucial to determine the most suitable topology for a specific use case. This involves evaluating the type of power generation, the microgrid's size, and the nature of the loads [15].

2.1.1 Grid-tied Microgrids

In a grid-tied AC microgrid, as illustrated in Figure 2.1, the DC power generated from DC sources is converted into AC to supply power to AC loads. This configuration is optimal for "grid-direct" systems, where DC power from solar panels is transmitted to a home via AC wiring connected to the grid. In such microgrids, grid-tied inverters enable DC sources to power the loads, charge the energy storage system (ESS), and direct any surplus energy back to the grid. Figure 2.1 shows that the DC power is converted to AC by the inverter, which can then be used by the load or reconverted to DC by the inverter/charger to charge the ESS. The stored ESS energy can also be converted back to AC to supply power to the AC loads.

In a grid-tied DC microgrid, as shown in Figure 2.2, DC sources and the energy storage system (ESS) are connected through a DC/DC charge controller. This configuration is more efficient at storing solar energy because it transfers the DC power from the PV panels directly to the ESS, bypassing the need to convert it to AC for the grid or load and then back to DC for storage. By eliminating this extra conversion step, the system achieves a modest efficiency improvement compared to an AC microgrid.

2.1.2 Off-grid Microgrids

Off-grid microgrids, also referred to as stand-alone or islanded systems, function similarly to grid-tied microgrids but without connection to the main grid. In an off-grid AC microgrid, depicted in Figure 2.3, the system operates independently from the national grid. The energy generated from DC sources, such as solar panels, is first converted into AC power using an inverter to power AC loads. This configuration is useful for remote locations where grid access is unavailable. The ESS plays a crucial role in ensuring power availability when generation is insufficient, such as during periods of low solar output.

Similarly, in an off-grid DC microgrid, shown in Figure 2.4, the DC power from renewable sources is used directly to power DC loads or to charge the ESS through a DC/DC charge controller. This setup avoids unnecessary power conversion, enhancing the system's overall efficiency compared to an off-grid AC microgrid. Both configurations offer flexibility depending on the types of loads and power generation sources available. Further details regarding the components and operation modes of off-grid microgrids will be discussed in the following sections.

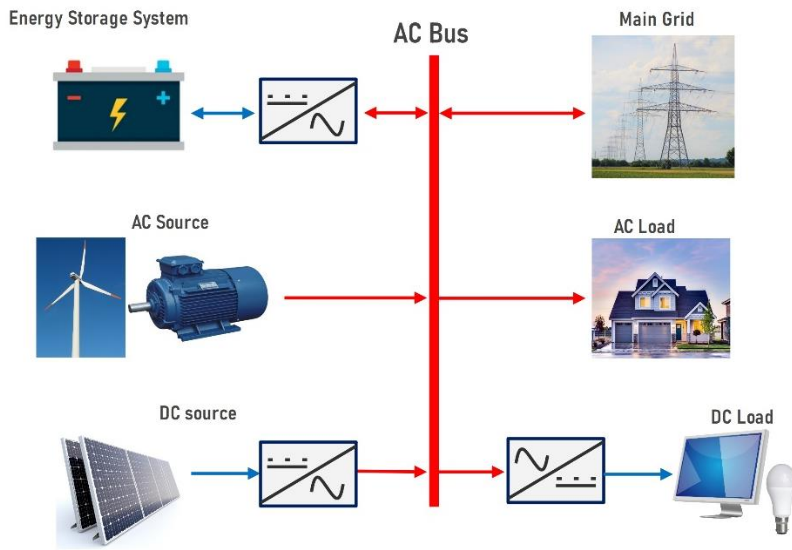

Figure 2.1 Grid-tied AC microgrid topology

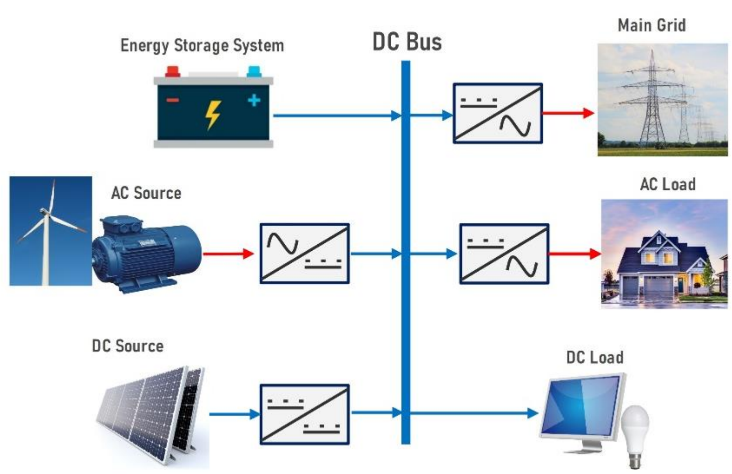

Figure 2.2 Grid-tied DC microgrid topology

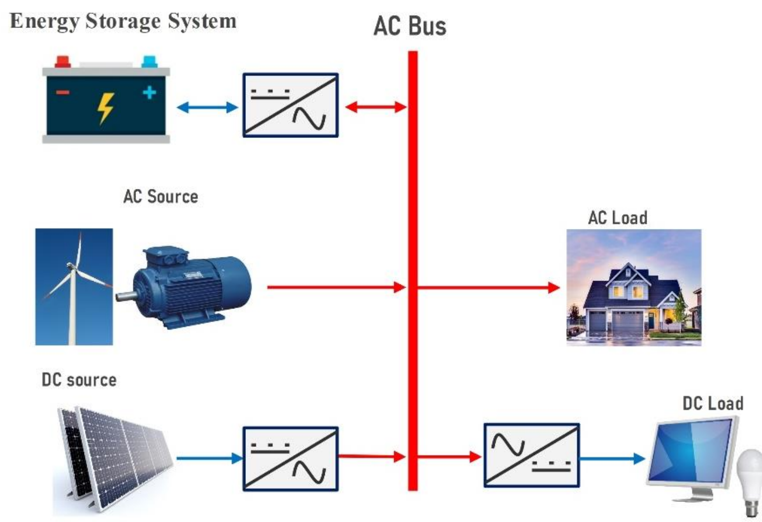

Figure 2.3 Off-grid AC microgrid topology

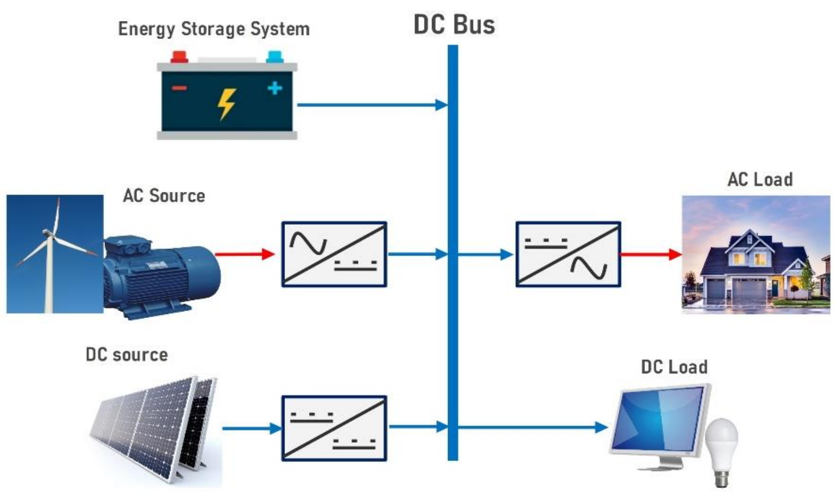

Figure 2.4 Off-grid DC microgrid topology

2.2 Solar Photovoltaics

2.2.1 PV Generator

Solar energy is highly intermittent and unpredictable, varying regionally, seasonally, and throughout the day due to the sun's movement across the sky. Photovoltaic (PV) cells function as the primary component in capturing solar energy, converting sunlight (irradiation) into electrical energy using semiconductor devices. A PV cell functions as a diode, allowing current flow when exposed to sunlight (photons). The basic construction of a monocrystalline silicon PV cell is shown in Figure 2.5, incorporating performance-enhancing features like a current mesh, anti-reflective coating, and cover glass . PV cells are combined to create PV modules, also known as solar panels. These modules serve as the fundamental units of PV arrays, which are utilized in solar power systems. Figure 2.6 demonstrates the relationship between a PV cell, a PV module (comprised of multiple PV cells), and a PV array (formed from several PV modules).

The equivalent electrical circuit of a PV cell is shown in Figure 2.7. When there is no current flowing through the load (I = 0), the open-circuit voltage and diode current can be described using equations (2.1) and (2.2), respectively [16].

$$V_{oc} = V_{PV} + R_{sh} * I_{sh} \tag{2.1}$$

$$I_D = I_d * \left(e^{\frac{Q*(V_{OC})}{A*K*T}} - 1\right) \tag{2.2}$$

Where I_{sh} is the shunt leakage current, R_{sh} is the shunt resistance, I_D is the diode current, I_d is the saturation current of the diode, Q is the electron charge (1.6 x 10^-19 C), A is the curve fitting constant, K is Boltzmann's constant (1.38 x 10^-23 J/K), and T is the temperature in Kelvin (K).

Therefore, the total load current can be expressed as:

$$I_{PV} = I_{ph} - I_D - I_{sh} \tag{2.3}$$

In equation (2.3),in this model the shunt resistance is assumed as infinite. Therefore, I_{sh}, the shunt leakage current, is usually negligible and can be ignored in most calculations. The open-circuit voltage (when $I_{PV} = 0$) is derived from equation (2.4):

$$I_{PV} = I_{ph} - I_d \left[exp\left(\frac{Q*V_{oc}}{A*K*T}\right) - 1\right] - \frac{V_{oc}}{R_{sh}} \tag{2.4}$$

$$V_{oc} = \frac{A*K*T}{Q} * \log_n\left(\frac{I_{ph}}{I_d} - 1\right) \tag{2.5}$$

2.2.2 PV Operation

The output power of a PV module is characterized by its current-voltage (I-V) curve, which is dependent on the operating point at any given time. Figure 2.8 shows typical I-V and P-V curves, respectively, for a PV cell. The point where the I-V curve bends is known as the maximum power point (MPP). The MPP is crucial for ensuring that the PV cell operates at its peak efficiency, maximizing the power output under varying conditions.

To achieve maximum efficiency, Maximum Power Point Tracking (MPPT) controllers are used in PV systems to ensure that the PV modules operate near their maximum power point. As shown in Figure 2.8, the characteristics of the PV cell change significantly with operating voltage and current. This variability must be managed by sophisticated control algorithms, which adjust the load to keep the PV module operating near the MPP.

In summary, solar photovoltaic cells play a critical role in converting solar energy into usable electricity, and their operation is governed by the intrinsic properties of semiconductor materials and the conditions under which they operate. PV systems are becoming increasingly popular due to their ability to generate clean, renewable energy with relatively low operating costs and high reliability over time. However, their intermittent nature necessitates advanced control techniques like MPPT and hybrid energy storage to ensure a stable power supply.

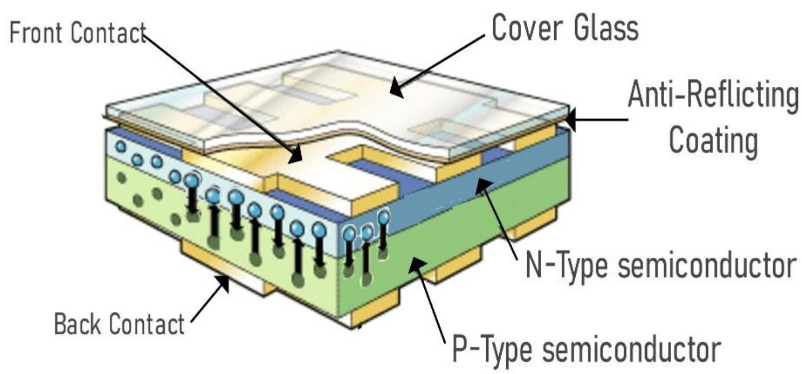

Figure 2.5 PV cell basic construction

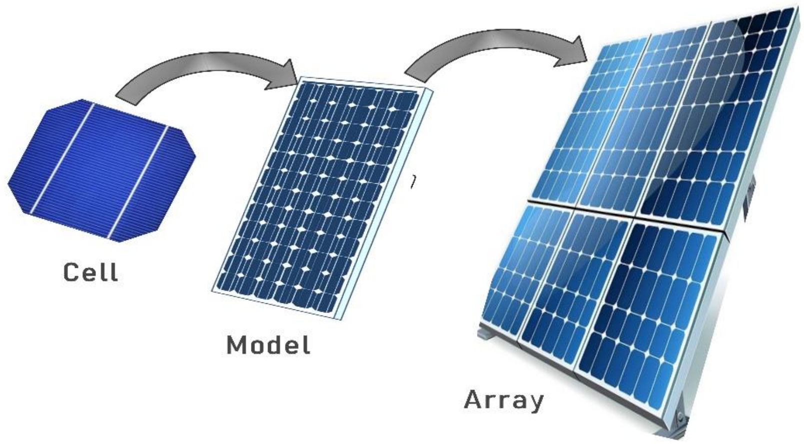

Figure 2.6 PV cell to array structure

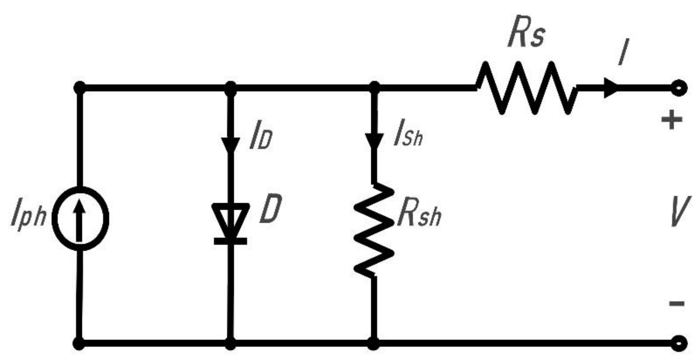

Figure 2.7 PV cell equivalent circuit

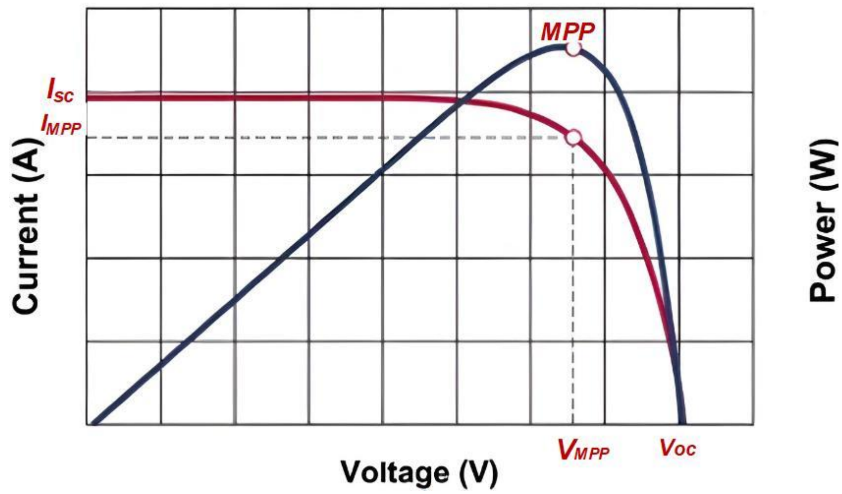

Figure 2.8 The maximum power point curve

2.3 Storage System

2.3.1 Storage Systems Types

Storage systems are integral to energy storage solutions, particularly in the microgrid environment. The most used storage system technologies include lead-acid batteries and lithium-ion batteries, both of which have distinct advantages and disadvantages in terms of cost, energy density, and cycle life [17].

Additionally, flywheel energy storage systems (FESS) are an emerging and highly efficient storage technology, especially in short-term high-power applications. Flywheels store kinetic energy in a rotating mass, which is converted into electrical energy when needed. The main advantages of flywheel storage systems are their high-power output, fast response time, and long lifecycle compared to conventional batteries. Flywheels can withstand many more charge and discharge cycles, which makes them particularly useful for applications where frequent cycling is necessary [18].

Supercapacitors also play a significant role in hybrid energy storage systems due to their high-power density and ability to deliver rapid bursts of energy. Although their energy density is low compared to batteries, their fast charge/discharge capability makes them ideal for complementing batteries in a hybrid storage system [19]. Table 2.1 shows a comparison of the three ESS technologies.

Table 2.1 Comparison of different types of energy storage

Type	**Efficiency (%)**	**Specific Energy (Wh/kg)**	**Specific Power (W/kg)**	**Charging Time**	**Service Life (Years)**
Flywheel	85–95%	5–150	180–1800	minutes	>20
Chemical Battery	70–80%	3–15	100–700	hours	3–15
Supercapacitor	80–95%	0.2–10	7000–18000	minutes	>20

2.3.2 BSS Equivalent Circuit

The equivalent circuit of a lead-acid battery consists of several elements that replicate the internal electrical dynamics of the battery, including an overvoltage capacitance and charge/discharge resistances as shown in Figure 2.1.

Flywheel systems, on the other hand, do not have an equivalent electrical circuit but function mechanically. Energy is stored kinetically and is later converted into electrical energy using a motor-generator system. Flywheels are ideal for short-term storage applications requiring frequent cycling and rapid energy release, making them a key component of modern microgrids [18].

2.3.3 Role in The Microgrids

Battery storage systems play a crucial role in ensuring the stability of a microgrid by balancing supply and demand. In a grid-tied microgrid, BSSs are used for peak shaving, demand-side management, and energy arbitrage. They store excess energy produced during off-peak hours and release it during high demand, reducing the need for grid-supplied energy and cutting costs.

In off-grid microgrid, BSS acts as the main storage component, storing energy from renewable sources (e.g., solar or wind) when generation is high and supplying it when generation is low. The combination of BSS with flywheels can significantly enhance the grid’s reliability, as flywheels handle high-power surges while batteries provide long-term storage. This hybrid approach improves the efficiency and longevity of the microgrid's energy storage system.

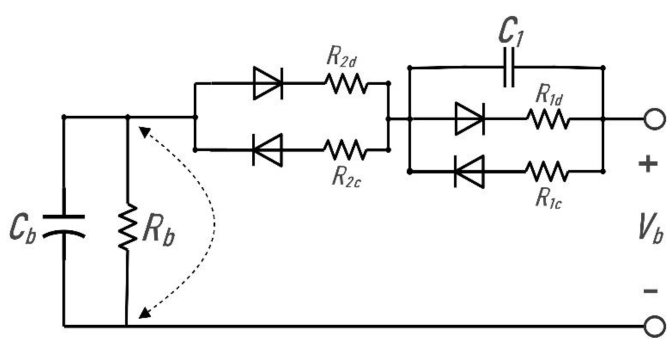

Figure 2.9 The equivalent circuit of lead-acid battery

Where : *C1* : overvoltage capacitance

Cb : battery capacity

R1c : charge overvoltage resistance

R1d : discharge overvoltage resistance

Rp : self-discharge resistance

R2c : internal resistance for charge

R2d : internal resistance for discharge

Vb : battery voltage

Voc : open circuit voltage

2.4 Electrical Load in Microgrids

The concept of electrical load refers to the amount of power or energy consumed by devices and systems connected to a particular circuit or network. It essentially indicates the demand imposed on the power supply system. Electrical load is typically measured in terms of current (amperes) or power (watts) and plays a pivotal role in the design, management, and optimization of microgrids. A proper understanding of electrical loads and their handling is crucial for ensuring the stability and reliability of the microgrid system. The behavior of electrical loads directly impacts the operation of generation sources, energy storage systems, and other components of a microgrid.

In a microgrid, electrical loads can be categorized based on their importance. Critical loads, such as medical equipment and essential communication systems, require an uninterrupted power supply, while non-critical loads, like household appliances, can be reduced or disconnected during peak demand periods. Effective load management strategies are vital in microgrids to ensure system balance. Techniques such as demand response and load shedding help in managing power during periods of high demand or limited supply[20]. These methods optimize energy distribution, reduce operational costs, and enhance the overall efficiency and resilience of the microgrid.

2.5 Converter

Converters are fundamental components in microgrids, enabling the integration of renewable energy sources and storage systems into the power network. The primary role of converters in microgrids is to manage the conversion of power between AC and DC systems. Since most renewable energy sources, such as solar photovoltaic (PV) systems and batteries generate or store power in DC, and most household and industrial appliances run on AC, converters ensure compatibility between these different types of power systems. Inverters (DC to AC converters) are used to convert the DC power generated by solar panels into AC power for use in homes or the grid. Conversely, rectifiers (AC to DC converters) are essential in charging batteries or operating DC appliances. The integration of bidirectional converters also allows energy to flow in both directions, which is crucial for energy storage systems (ESS), enabling them to charge during periods of excess energy generation and discharge when energy demand exceeds supply[21].

One of the key functions of converters in microgrids is to control voltage and frequency. In off-grid or islanded microgrid operation, converters regulate the voltage and frequency to ensure that all components of the microgrid are synchronized[22]. This is achieved through voltage-source inverters (VSIs), which generate a stable AC output with a controlled magnitude and frequency.

Converters also play a significant role in enhancing power quality and managing harmonics in microgrids. Renewable energy sources, such as solar PV and wind, often generate power with fluctuations, leading to issues like voltage sags, swells, and harmonics[23]. Converters with pulse-width modulation (PWM) control strategies help in reducing these harmonics by regulating the switching frequency of the converter, which in turn smoothens the power waveform. The total harmonic distortion (THD) in a microgrid is minimized using high-frequency switching techniques, with the THD percentage calculated as [24]:

$$THD = \sqrt{\sum_{n=2}^{\infty} \left(\frac{V_n}{V_1}\right)^2} * 100\% \qquad (2.6)$$

whereV_n is the voltage of the V_{th} harmonic and V_1 is the fundamental frequency voltage. By minimizing the THD, converters improve the efficiency and longevity of electrical devices connected to the microgrid, ensuring that both the energy generated from renewable sources and the energy stored in batteries are utilized in the most efficient manner.

CHAPTER THREE

OPTIMIZING RENEWABLE ENERGY INTEGRATION THROUGH INNOVATIVE HYBRID MICROGRID DESIGN: A CASE STUDY OF NAJRAN SECONDARY INDUSTRIAL INSTITUTE IN SAUDI ARABIA

3.1 Introduction

The increasing global demand for electricity, driven by globalization, has resulted in greater reliance on diverse energy sources. This shift necessitates addressing environmental concerns, particularly the reduction of carbon dioxide (CO_2) emissions and their associated economic impacts. As a response, microgrids (MGs) have emerged as a sustainable energy solution. Saudi Arabia presents a unique case, as it remains one of the few nations that directly utilize crude oil for electricity generation, with approximately 60% of its power derived from oil, while the remainder is sourced from natural gas, as illustrated in Figure 3.1. The power generation sector, alongside other energy-intensive industries, contributed to a 300% increase in CO_2 emissions between 1990 and 2019 [25]. Despite its reliance on fossil fuels, Saudi Arabia holds substantial untapped renewable energy potential, including solar, wind, geothermal, and waste-to-energy resources. Leveraging these resources presents an opportunity for the country to diversify its energy portfolio and reduce its carbon footprint, aligning with global sustainability objectives [26]. As part of Vision 2030, Saudi Arabia aims to expand its energy sector while increasing the share of non-associated natural gas and decreasing dependence on oil-based electricity generation. The Saudi National Renewable Energy Program (NREP) targets 50% of the nation’s electricity generation from renewable sources by 2030 [27],

[28]. The NREP includes 13 projects with a total installed capacity of 4,870 MW, of which 91.8% is derived from solar energy, while 8.2% comes from wind power. By 2024, these projects are expected to generate approximately 15,108,701 MWh annually, sufficient to meet the electricity demands of 692,557 households. Furthermore, this transition is projected to reduce fossil fuel consumption, leading to an estimated 9,828,156-ton reduction in CO_2 emissions per year by 2024 [29]. With these efforts, Saudi Arabia is actively working toward becoming a global leader in energy sustainability, aiming to achieve net-zero greenhouse gas emissions by 2060.

This chapter examines the underutilization of renewable energy resources in Saudi Arabia, with a case study focused on the Najran Secondary Industrial Institute (NSII). An in-depth analysis of a hybrid microgrid (MG) system at NSII is conducted, evaluating six different cases with varying tilt and azimuth angles. A benchmark analysis is performed to compare the optimal angles against the default settings provided by Hybrid Optimization of Multiple Energy Resources (HOMER) software. Given the roof area limitations at NSII, this study proposes an approach that ensures a reliable power supply while balancing technological feasibility, economic viability, and environmental sustainability within the selected model.

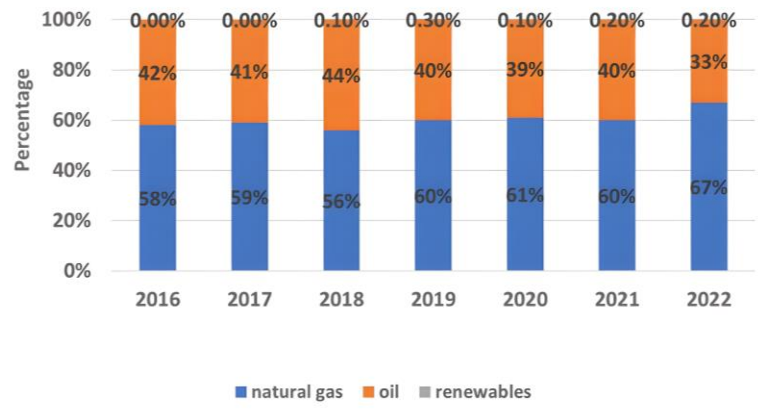

Figure 3.1 Power generation by sources in Saudi Arabia (2016 to 2022) [30]

3.2 Literature Review

The case study in [31] focused on the design of a solar photovoltaic (PV) microgrid for a hospital in Dhaka. The study involved an assessment of the electrical load and solar profiles, followed by an optimization problem aimed at minimizing cost and emissions while maximizing reliability. The optimization was performed using HOMER software. In [4], the authors analyzed a grid-connected PV–wind system for a 15,000 kWh/day community electrical load amid Saudi Arabia's rising energy demands. The study utilized HOMER software and King Abdullah City for Atomic and Renewable Energy (KACARE) data to evaluate four cities, identifying Yanbu as the most viable location due to lower costs and emissions, highlighting its potential for replication in similar climates globally. Alhawsawi, in [32], applied HOMER software to design an optimal hybrid renewable energy system for a microgrid at Oakland University, focusing on meeting unmet electrical loads and reducing greenhouse gas emissions. The system incorporated solar PV, an energy storage system (ESS), combined heat and power (CHP), and wind turbines (WT), ensuring flexibility and scalability. The results demonstrated a sustainable energy solution, achieving a peak electrical load of 9.958 MW, a net present cost (NPC) of USD 30M, and a levelized cost of energy (LCOE) of 0.00274 USD/kWh. The authors of [33] investigated the integration of renewable energy sources (RESs), particularly solar PV and wind energy, as a means of achieving Saudi Arabia's strategic energy objectives. An optimal microgrid system for the Islamic University of Madinah was analyzed by comparing three alternatives: PV-only, wind-only, and hybrid systems. Utilizing real weather data, the study found that a PV system could supply up to 3.03% of the university's annual electricity demand with an LCOE of 0.051 USD/kWh. The wind and hybrid systems provided different cost-benefit trade-offs but contributed to emission reductions, aligning with Saudi Arabia's sustainability goals. To address the growing energy demand of electric vehicles (EVs) and their impact on the grid, researchers applied HOMER software to design and optimize a PV–wind hybrid charging station with global applicability. The optimal configuration consisted of 44.4% wind energy and 55.6% solar energy, generating 843,150 kWh annually at a cost of 0.064 USD/kWh [34]. A study conducted by the authors of [35] focused on New Sohag University in Egypt, comparing two microgrid configurations based on renewable energy sources. The first system consisted of PV, a diesel generator (DG), and a converter, while the second configuration incorporated an energy storage system (ESS), including batteries for long-term storage and flywheels for short-term power stability. Using HOMER software, the study assessed the economic and environmental performance of both systems, analyzing costs, CO_2 emissions, and diesel consumption. Dahiru et al. [36] conducted a techno-economic evaluation using HOMER software to analyze the performance of renewable energy-based distributed grids across various tropical regions. A specific case study in the Sudan Savannah region of Nigeria proposed six scenarios for grid-connected nanogrids to supply a daily residential energy demand of 355 kWh and a per capita energy consumption of 150 kWh. The results indicated an LCOE ranging between 0.0110 USD/kWh and 0.0095 USD/kWh, along with an NPC between USD 366,210 and USD 288,680, where negative values suggested potential for significant grid export. Notably, a renewable energy fraction of up to 98% was achieved, with greenhouse gas emissions as low as 2,328 tons per year.

Islam et al. [37] investigated a hybrid PV/wind/hydro system incorporating pumped hydro storage (PHS) to meet the electricity demands of a community in Newfoundland, Canada. This PHS-based hybrid system was compared with battery-based setups, evaluating techno-economic and environmental advantages over traditional battery and diesel-only systems. The results highlighted that the hybrid system significantly reduced electricity costs to 0.136 USD/kWh, whereas a diesel-only configuration had a much higher cost of 0.355 USD/kWh, leading to substantial savings in diesel consumption and CO_2 emissions annually. Additionally, the PHS-based system demonstrated superior cost and energy efficiency over battery storage systems (BSSs), with hydro integration reducing energy costs by 58% compared to a PV/wind/PHS configuration alone. The authors of [38] focused on the optimal sizing of hybrid energy storage by integrating a fuel cell (FC) system and a supercapacitor (SC) for off-grid renewable applications, emphasizing both reliability and cost efficiency. The optimized system was designed for a 20-year operational lifespan, comprising 1351 kW of PV panels and an 80 kW fuel cell stack, along with other essential components. The PV system contributed 98.2% of the total electricity production, achieving an NPC of USD 26.5M and an LCOE of 4.78 USD/kWh. Furthermore, a sensitivity analysis revealed that hydrogen storage costs had a significant impact on overall system feasibility. The six cases analyzed in [39] assessed the feasibility of hybridized energy systems incorporating PV, wind turbines (WT), diesel generators (DGs), and battery storage systems (BSSs) for a remote village in northern Bangladesh. Utilizing HOMER software, the optimal configuration was identified as a system consisting of 73 kW of PV arrays, a 57 kW diesel generator, and a 387 kWh BSS. This setup achieved an LCOE of 0.37 USD/kWh and an NPC of USD 357,284, resulting in CO_2 emission reductions of approximately 62% compared to the kerosene-based system and 67% compared to the grid system. Leveraging HOMER software's advanced capabilities, the authors of [40] proposed an innovative integration of distributed and centralized generation, incorporating a solar thermal system alongside five other technologies. Their study, which focused on a combined heat and power (CHP) microgrid design for a remote community in Newfoundland, demonstrated that renewable energy sources could supply the entire electricity demand and the majority of thermal loads, proving to be more cost-effective than a diesel-only setup. A study conducted on the island of Favignana, Italy[41] employed HOMER software to explore sustainable energy solutions, particularly in the integration of hydrogen and battery storage for electricity production and public transportation. The research assessed the feasibility of using electric fuel cell (FC) vehicles and hydrogen-compressed natural gas (CNG) vehicles. The findings revealed that a hybrid storage system combining batteries and an electrolyzer emerged as a viable solution to enhance energy independence and support the decarbonization of the transport sector in small islands, aligning with economic and environmental sustainability objectives.

Islam [42] conducted a study on the integration of a hybrid renewable energy system (HRES) in a large office building, focusing on reducing reliance on grid electricity and evaluating the economic impact of incorporating green vehicles. Using HOMER software, the study found that implementing solar PV reduced grid electricity consumption by 43%, lowered the unit electricity cost by 10%, and led to a more than 90% reduction in emissions. A separate study [43] introduced a grid-connected renewable energy system as an economically and technologically advanced solution for electrifying a rural village in India. The research focused on determining the optimal sizing of an integrated renewable energy system (IRES) coupled with the grid to ensure a stable power supply. By incorporating solar PV, a battery storage system (BSS), and grid connectivity, the study conducted sensitivity analyses and techno-economic evaluations using HOMER software. Various electrical load profiles were assessed through a demand response strategy. The study identified the optimal system configuration, which achieved the lowest Levelized Cost of Energy (LCOE) and Total Net Present Cost (TNPC) while maintaining the highest renewable fraction, effectively minimizing CO_2 emissions. This demonstrated the system's capability to provide reliable 24/7 power, even in areas with limited grid availability. A techno-economic performance assessment of grid-connected PV power systems across five distinct climate zones in China was conducted in [44], utilizing HOMER software for evaluation. The study analyzed key factors, including monthly average electricity production, economic feasibility, and environmental impact, concluding that grid/PV hybrid systems are technically, economically, and environmentally viable across all studied climate zones.

A study examining the resilience of a proposed microgrid (MG) [45], which incorporated solar PV, wind turbines (WT), an energy storage system (ESS), a diesel generator (DG), and converters, utilized HOMER software to assess its operational robustness. Various randomized power outages were simulated across multiple days within the annual cycle to analyze the MG's ability to withstand real-world disruptions. Additionally, the study introduced a novel resilience index, providing a quantitative metric to evaluate the extent of unmet electrical load demands during such disturbances. In [46], the authors used HOMER software to investigate the feasibility of significant renewable energy integration into a remote, sub-tropical island's power system. The study compared the benefits of a hybrid MG against a diesel-only power system, analyzing technical, financial, and environmental factors. The results indicated that the existing diesel-based system imposed a high economic burden on the island's residents. In contrast, a PV/wind/diesel/battery hybrid MG was found to be the most cost-effective alternative, offering lower Net Present Cost (NPC) and per-unit electricity costs while achieving a 56% renewable energy share and reducing CO_2 emissions by 23%. Sawle et al. [47] conducted a study on an electrical load of approximately 900 kWh/day with a peak demand of nearly 100 kW in Ukai City, India. Using HOMER software, the study evaluated four different hybrid MG configurations to determine the most feasible energy system. The optimal system consisted of PV, WT, micro-hydro (MH), converters, batteries, DG, and a biodiesel generator (BG). This configuration achieved the lowest Cost of Energy (COE) at USD 0.196/kWh and NPC at USD 831,217, while maintaining a high renewable energy fraction of 81.2% and significantly reducing emissions, making it an environmentally sustainable solution. Table 3.1 provides a summary of the most relevant studies discussed in this literature review.

Table 3.1 Survey of previous work

Reference/ Location	**Grid Dependency**	**HRES Components**	**Objectives**	**Main Constraints**	**Resilience / Reliability**	**Sensitivity**
[33] Saudi Arabia	On-grid	PV WT	Economic Environmental	$P_{PV,Cap}$, $P_{WT,Cap}$	-	-
[34] Turky	OFF-Grid	PV WT BSS	Economic	Roof Area,	-	Data Uncertainty analyzed
[36] Nigeria	On-grid	PV DG BSS	Economic Environmental Reliability	DoD	Unmet Load	RE fraction
[37] Canada	OFF-Grid	PV WT Hydro BSS PHS DG	Economic Environmental	Annual capacity shortage, Hourly load operating reserve, Penalties over CO2 emissions	Unmet Load	The variation of solar radiation, wind speed, PV capital cost, water flow rates, load demand, and losses in pipe flow.
[38] South Africa	OFF-Grid	PV SC FC	Economic Reliability	Annual capacity shortage = 2%, Economics constraints, SoC	Unmet Load	Sensitively analyzed the variation of the cost of hydrogen storage

Table 3.1 Survey of previous work (continued)

Reference/ Location	Grid Dependency	HRES Components	Objectives	Main Constraints	Resilience / Reliability	Sensitivity
[41] Italy	OFF-Grid	PV BSS FC DG	Economic Environmental Reliability	f_{RE}, $P_{PV,Cap}$,	-	Sensitively analyzed the variation of economic and technical parameters
[42] France	ON-Grid	PV Hydro	Economic Environmental Reliability	Min(f_{RE}) = 35% Max Annual capacity shortage = 0%, Operating Reserve = 0%	-	Sensitively analyzed the variation of Electric load, H_2 load, economic and technical parameters in
[43] India	ON-Grid	PV BSS	Economic Environmental Reliability	Grid Time Constrained, Initial Cost, Load Demand Balance, P_{BSS}, SoC, f_{RE}	-	Sensitively analyzed the variation of grid price against the economic parameters.

Table 3.1 Survey of previous work (continued)

Reference/ Location	**Grid Dependency**	**HRES Components**	**Objectives**	**Main Constraints**	**Resilience / Reliability**	**Sensitivity**
[45] Iran	ON-Grid	PV WT BSS DG	Economic Environmental Reliability	SOC	The ratio of the cumulative supplied electric load reduced by the unmet load to the total supplied electric load	Sensitively analyzed applied by emerging electric outages
[39] Bangladesh	OFF-Grid	PV WT DG BSS	Economic Environmental Reliability	minimum starting threshold of DG = 25% of the maximum capacity of the DG, SoC	-	Sensitively analyzed the variation of economical parameters
[40] Canada	OFF-Grid	PV WT FC Hydro	Economic	$P_{inv, Cap}$, $P_{PV,Cap}$, $P_{WT,Cap}$, $P_{FC,Cap}$	-	-

3.3 System Description

3.3.1 PV

A photovoltaic (PV) cell is a device that directly converts light energy into electricity through a physical and chemical process known as the photovoltaic effect. These cells belong to a category of photoelectric devices, meaning that their electrical properties, such as current, voltage, and resistance, change when exposed to natural sunlight or artificial light sources. PV cells serve as fundamental components in PV modules, commonly referred to as solar panels. Additionally, they can function as photo detectors, detecting light or electromagnetic radiation within a specific spectrum and measuring its intensity [48].

3.3.2 ESS

Energy storage refers to the process of capturing and retaining energy for later use, ensuring its availability when required by a system. It plays a crucial role in managing supply–demand fluctuations and facilitating the integration of renewable energy sources (RES) into the grid. Energy storage systems (ESS) cater to both short- and long-term energy needs, providing frequency regulation, grid stability, and efficient energy management. By acting as a reserve power source, energy storage enhances the reliability and efficiency of the electrical supply network [49]. Several types of energy storage technologies have been developed, including pumped hydro power, compressed air energy storage (CAES), batteries, flywheels, supercapacitors, and hydrogen-based storage systems.

3.3.3 Electrical Load

The term electrical load refers to the amount of power or energy consumed by devices and systems within a specific circuit or network, representing the demand placed on the power supply. Electrical load is typically measured in amperes (current) or watts (power). A thorough understanding of electrical loads and their management is essential for maintaining system stability and operational efficiency.

3.3.4 DG

In a hybrid microgrid (MG), a diesel generator (DG) plays a crucial role in ensuring a stable and reliable power supply. It serves multiple functions, including backup power, supply stability, peak shaving, energy cost optimization, and emergency power provision, particularly in critical infrastructure such as hospitals. Ultimately, the DG complements renewable energy sources (RESs) by maintaining a continuous and dependable energy supply, especially during periods of low renewable generation or unexpected demand surges.

3.4 System Mathematics Modeling

3.4.1 PV Modeling

The photovoltaic (PV) system is essential for converting solar energy into electricity. Its power output is significantly affected by various environmental factors, such as ambient temperature and solar radiation intensity. To accurately model and predict the PV system's performance, the following equation was utilized [50], [51]:

$$P_{PV} = Y_{PV} \cdot f_{PV} \left(\frac{G_T}{G_{T,STC}}\right) \left[1 + \alpha_P \left(T_C - T_{C,STC}\right)\right] \tag{3.1}$$

where f_{PV} represents the PV derating factor (%), while Y_{PV} denotes the rated capacity of the PV array (kW). G_T refers to the global solar radiation incident on the PV array surface at the current time step (kW/m²), whereas $G_{T,STC}$ = 1 kW/m² represents the standard incident radiation under standard test conditions (STC) at 25°C. Additionally, α_P is the temperature coefficient of power (%/°C). The parameters T_C and $T_{C,STC}$ indicate the PV cell temperature under actual operating conditions and the temperature under STC, respectively. The PV cell temperature is determined using the following equation [52].

$$T_C = T_a + \left[\frac{NOCT - 20}{800}\right] * G_T \tag{3.2}$$

where T_a represents the ambient temperature (°C), and $NOCT$ refers to the nominal operating cell temperature, which generally ranges between 45°C and 47°C.

3.4.2 BSS Modeling

In microgrid systems, renewable energy sources (RESs) experience continuous fluctuations and intermittency in power generation due to their reliance on environmental conditions. Energy storage systems (ESSs), particularly battery banks, play a crucial role in mitigating these fluctuations and ensuring a stable power supply. Acting as a buffer, the battery bank stores surplus energy generated during peak production periods and delivers it when renewable generation is insufficient. This mechanism ensures a steady and uninterrupted power supply, reducing the risks associated with variable energy output. In extreme scenarios where RES generation falls short of meeting the energy demand, the system can utilize alternative power sources, such as diesel generators, to compensate for the deficit. However, the incorporation of battery storage systems significantly decreases reliance on non-renewable backup sources, thereby fostering a more sustainable and resilient energy framework within the MG.

The State of Charge (SoC) of a Battery Storage System (BSS), contingent upon its charging or discharging state, is determined using the following equation[53], [54]:

$$SoC(t+\Delta t) = SoC(t) + (1-\sigma_b) + \left(P_{RES}(t) \times \eta_{inv} - \frac{P_L(t)}{\eta_{inv}}\right) \times \eta_C \times \Delta t \qquad (3.3)$$

$$SoC(t+\Delta t) = SoC(t) - (1-\sigma_b) + \left(\frac{P_L(t)}{\eta_D} - P_{RES}(t) \times \eta_{inv}\right) \times \eta_D \times \Delta t \qquad (3.4)$$

where $P_L(t)$ represents the electrical load demand, while $P_{PV}(t)$ denotes the PV output power (kW). The parameter η_{inv} refers to the inverter efficiency (%), and σ_b indicates the self-discharge rate of the BSS (%). Additionally, η_C and η_D correspond to the charging and discharging efficiencies of the BSS (%), respectively.

To ensure the long-term operational lifespan of ESSs, it is essential to keep the SoC within the defined maximum (SoC_{max}) and minimum (SoC_{min}) limits, as expressed in the following equation:

$$SoC_{min} \leq SoC \leq SoC_{max} \tag{3.5}$$

3.4.3 Converter Modeling

Converters are essential components in MG systems, enabling the seamless transfer of energy between various system elements. They operate as inverters, converting direct current (DC) into alternating current (AC), and as rectifiers, transforming AC into DC. This functionality is particularly critical in hybrid MG systems, where maintaining a consistent energy exchange between DC and AC subsystems is necessary for stable operation. The capacity and operational constraints of the inverter (P_{inv}) are defined by the following equations [45], [55]:

$$P_{inv} = \frac{E_L(\max)}{\eta_{dc/ac}} \tag{3.6}$$

$$\eta_{dc/ac}\left[P_{BSS,ch/dis}(t) + P_{PV}(t)\right] \leq P_{inv} \tag{3.7}$$

$$\eta_{ac/dc}[P_G(t)] \leq P_{inv} \tag{3.8}$$

where P_{inv} represents the converter capacity (kW), and E_L(max) denotes the maximum electrical load demand (Wh). The parameters $\eta_{dc/ac}$ and $\eta_{ac/dc}$ correspond to the conversion efficiencies for DC to AC and AC to DC processes, respectively. Additionally, $P_{BSS,ch/dis}$ refers to the charging and discharging power of the BSS, while P_{PV} and P_G indicate the power generated by the PV system and the power imported/exported to the grid, respectively.

3.4.4 DG Modeling

An automatically sized genset generator was integrated using the HOMER library. This generator dynamically adjusts its capacity to match the electrical load demand, effectively preventing capacity shortages across all sensitivity scenarios.

3.5 Simulation Methodology

HOMER is a critical tool for designing and analyzing various hybrid energy configurations, including renewable microgrids, grid-connected energy systems, and islanded hybrid energy systems, among others [56]. The primary function of HOMER is to determine the minimum economic objectives, such as the NPC [57] and the LCOE, while also assessing the reliability and performance objectives of the system. Users provide input parameters, including energy source types, energy storage components, electrical load demand, and associated costs. In response, HOMER generates key output metrics, such as NPC, LCOE, surplus energy, fuel consumption, and renewable energy utilization. Additionally, the software assists in selecting the optimal control strategy for the system by offering control methodologies like Load Following (LF) and Cycle Charging (CC) [58]. Figure 3.2 presents the flowchart of the HOMER optimization process.

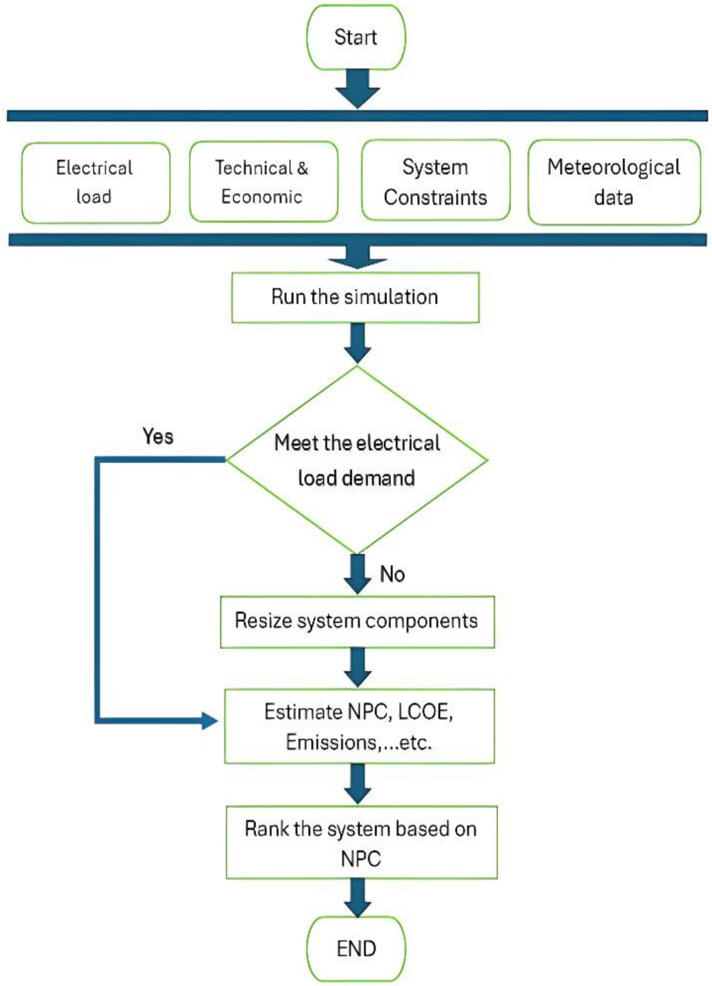

Figure 3.2 Homer flowchart

3.5.1 HOMER Software Dispatch Strategy (Controller)

In HOMER software, a dispatch strategy establishes the operational rules governing the function of generators and battery banks within a power system. The software supports the simulation of two primary dispatch strategies, with the optimal selection depending on multiple factors, including generator and battery bank sizes, fuel prices, operation and maintenance (O&M) costs, the proportion of renewable energy in the system, and the characteristics of renewable resources.

- Load Following (LF) Strategy: The LF strategy ensures that generators produce only the required amount of power to meet the instantaneous electrical demand, leaving battery charging primarily to renewable energy sources. This approach is particularly effective in systems with a high penetration of renewable energy, especially when generation occasionally exceeds demand.
- Cycle Charging (CC) Strategy: The CC strategy operates generators at full capacity, directing any excess power to charge the battery storage system. This approach is most effective in systems with limited or no renewable energy sources, ensuring maximum utilization of generator capacity to store energy for later use.

3.5.2 HOMER Software Optimization Criteria

- Economic:
  - Total NPC: This metric reflects the overall financial performance of the system by accounting for all costs and revenues incurred throughout its operational lifespan. It encompasses initial capital investment, replacement costs, operation and maintenance (O&M) expenses, fuel expenditures, potential emissions penalties, and costs related to purchasing power from the main grid. On the revenue side, it considers the salvage value, and the income generated from selling excess power back to the grid [56].

$$C_{NPC,tot} = \frac{C_{ann,tot}}{CRF(i,N)} \tag{3.9}$$

$$CRF(i,N) = \frac{i(1+i)^N}{(1+i)^N - 1} \tag{3.10}$$

where $C_{NPC,tot}$ represents the total NPC, while $C_{ann,tot}$ denotes the total annualized costs (USD/year). The term *CRF()* refers to the Capital Recovery Factor, *N* indicates the project lifetime, and *i* represents the discount rate.

- LCOE: This metric is widely recognized in the energy sector as a standard economic indicator. HOMER defines the Levelized Cost of Energy (LCOE) as the average cost per kWh of useful electrical energy produced by the system [56], [59].

- $$LCOE = \frac{C_{ann,tot} - C_{boiler} H_{served}}{E_{served}} \tag{3.11}$$

where C_{boiler} represents the marginal cost of the boiler (USD/kWh), while H_{served} denotes the total served thermal load (kWh/year). This term is zero in systems without thermal loads. Additionally, E_{served} indicates the total electrical load (kWh/year).

- Environmental

HOMER is capable of estimating the emissions of six key pollutants, including carbon dioxide (CO_2), sulfur dioxide (SO_2), nitrogen oxides (NO_x), particulate matter (PM), unburned hydrocarbons (UHC), and carbon monoxide (CO). This feature is crucial in the design of microgrids (MGs), as it aids in minimizing toxic gas emissions and promoting environmentally sustainable energy solutions [60].

- Reliability
  - Unmet Load: In MGs, a shortfall in power generation results in unserved electrical load. The fraction of unmet electrical load (f_{unmet}) is determined by the ratio of unserved electrical load (E_{unmet}) to the total annual electrical demand (E_{demand}), as expressed in the following equation [56].

$$f_{unmet} = \frac{E_{unmet}}{E_{demand}} \tag{3.12}$$

  - Capacity Shortage: This refers to the deficit that arises when the system's actual operating capacity falls below the required capacity needed to meet both the electrical load and reserve load within a given timeframe. The capacity shortage fraction (f_{cs}) is determined by the total capacity shortage (E_{cs}) occurring throughout the year, divided by the total annual electrical load, as described in the following equation [56].

$$f_{cs} = \frac{E_{cs}}{E_{demand}} \tag{3.13}$$

3.5.3 Constraints

- Maximum Annual Capacity Shortage: This represents the permissible limit for the f_{cs}, ensuring that the system operates within an acceptable threshold.
- Minimum Renewable Fraction: This constraint defines the minimum proportion of the electrical load that must be met exclusively by renewable energy sources, restricting reliance on non-renewable components.

$$f_{ren} = 1 - \frac{E_{nonren} + H_{nonren}}{E_{served} + H_{served}} \tag{3.14}$$

where f_{ren} represents the renewable fraction (%), while E_{nonren} denotes the annual energy production (kWh/year) from non-renewable sources. Additionally, E_{served} refers to the total electrical load served by the system (kWh/year). The parameters H_{nonren} and H_{served} correspond to the thermal energy generated from non-renewable sources and the total thermal load served, respectively [56]. In systems without thermal production, both the thermal served load and thermal energy production are considered zero.

3.6 Case Study

In this study, a hybrid MG system was designed and implemented for a Saudi government facility, specifically the Technical and Vocational Training Corporation (TVTC)'s Najran Secondary Industrial Institute (NSII) and subsequently evaluated. The existing grid-only system has a Net Present Cost (NPC) of USD 7.02 million and a Levelized Cost of Energy (LCOE) of 0.098 USD/kWh. The primary objective of this research was to determine the most cost-effective, reliable, and environmentally sustainable configuration, while ensuring compliance with economic and technical constraints. To assess system resilience, multiple grid outage scenarios were analyzed. Figure 3.3 presents the schematic diagram of the proposed system, whereas Figure 3.4 provides an aerial view of the site, highlighting the rooftops designated for the installation. The total available rooftop area for the system was calculated to be 12,000m².

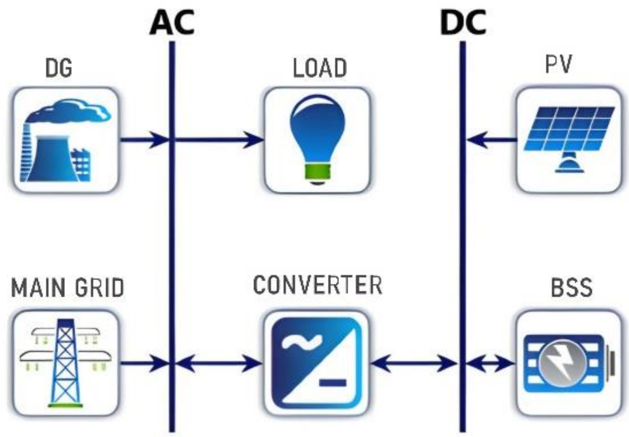

Figure 3.3 A schematic of the proposed system

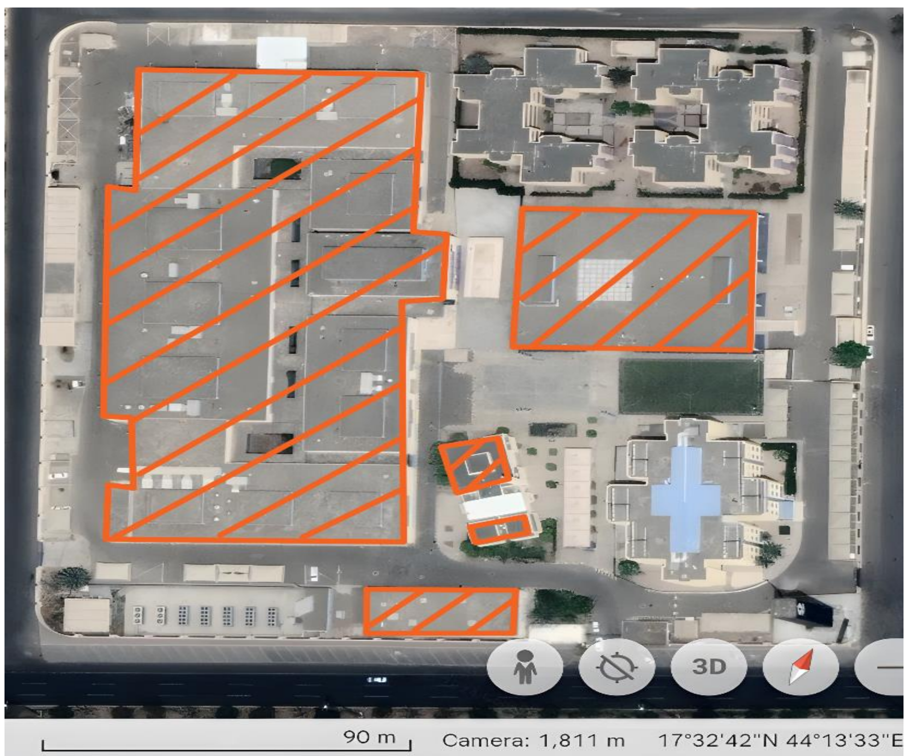

Figure 3.4 An aerial view of NSII's roofs (source: Google Earth)

3.6.1 Input Data

- Meteorological Data

The Najran Secondary Industrial Institute (NSII), located at 17°32.4′ N, 44°13.6′ E, is situated in the central region of Najran City, in the southern part of Saudi Arabia. This region experiences a humid subtropical climate with a dry-winter zone, classified as “CWa” under the Köppen–Geiger climate classification system [61]. With consistent solar exposure throughout the year [62], the area is highly favorable for solar energy applications, as depicted in Figure 3.5. To enhance accuracy in system modeling, global horizontal irradiance (GHI) data were sourced from King Abdullah City for Atomic and Renewable Energy (KACARE). Figures 3.6 and 3.7 illustrate the GHI, clearness index data, and annual average ambient temperature. The average annual GHI recorded at NSII was 7.07 kWh/m²/day.

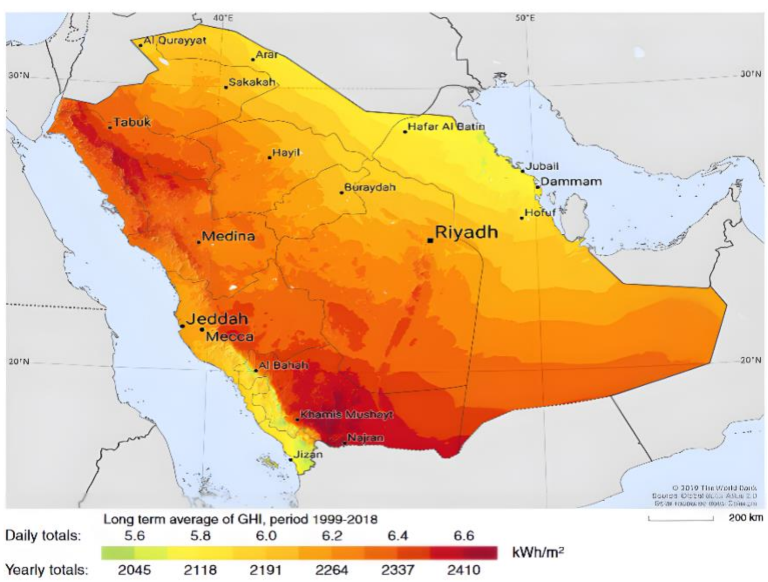

Figure 3.5 Map of the solar irradiation of Saudi Arabia [62]

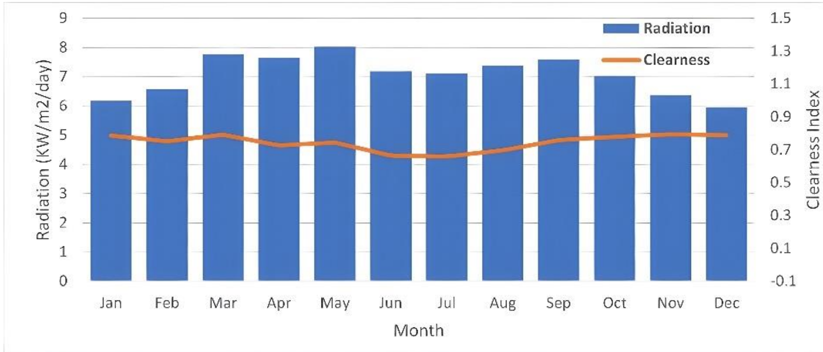

Figure 3.6 Annual GHI and clearness index

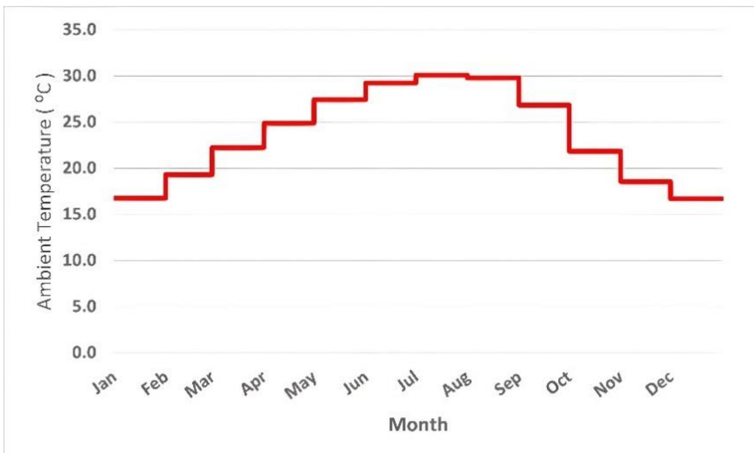

Figure 3.7 Annual average ambient temperature

- Electrical Load Data

The electrical load data for the study site was obtained from electricity bills covering an entire year**.** Figure 3.8 presents the average monthly electrical load profile for NSII, highlighting an increase in demand during the warmer months due to the higher usage of air conditioning systems**.** The highest demand occurs in September, making it crucial to ensure the system design can accommodate peak electricity consumption during this period. Table 3.2 provides additional details on the electrical load characteristics. According to the table, the peak electrical load was 2160 kW, while the hourly average electrical load was 327.32 kWh. The total annual electrical demand was recorded at 2,865,749 kWh. Additionally, the electrical load factor, a dimensionless value computed by dividing the average load by the peak load, was 0.15.

Table 3.2 Annual electrical load data

Metric	**Value**
Peak load	2160 KW
Load average	327.32 KWh
Load factor	0.15
Total annual load demand	2,865,749 KW

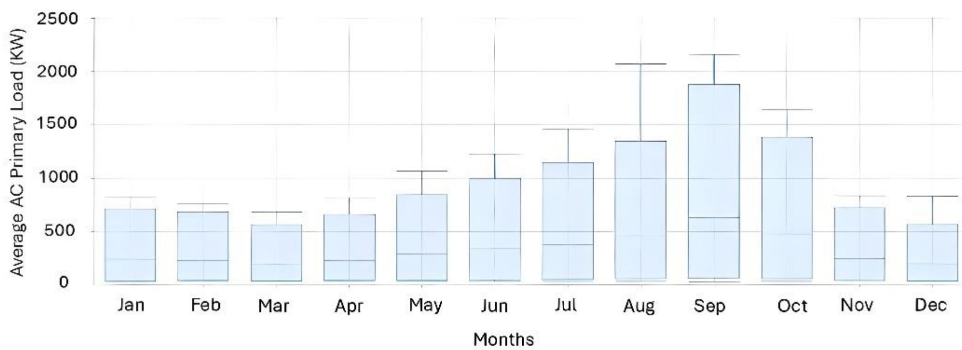

Figure 3.8 The average monthly electrical load

- Technical and Economic Data for System Components

In Saudi Arabia, the electricity generation cost for government facilities is set at 0.098 USD/kWh, inclusive of Value Added Tax (VAT). According to the Arab Petroleum Investments Corporation (APICORP), which operates under the Organization of Arab Petroleum Exporting Countries (OAPEC), there have been no changes in the governmental electricity tariff [63]. While the proposed MG is expected to produce surplus energy, this study does not account for selling excess energy back to the main grid. As a result, the analysis presents a conservative estimate of the system’s economic viability. Table 3.3 provides a summary of the key financial and technical specifications of the system components.

Table 3.3 Technical and economic data

Component	Parameter	details	Value	Unit
PV	Manufacturer	Trina Solar		
	Dimensions	Length	2.384	m
		Width	1.3	m
	Rated Capacity		0.66	kW
	Temperature Coefficient		-0.34	%/ºC
	Operating Temperature		43	ºC
	Efficiency		21.25	%
	Panel lifetime		25	Year
	Capital Cost		147	$/kWh
	Replacement cost		110	$/kWh
	O&M cost		10	$/Year
BSS	Manufacturer	Generic		
	Nominal voltage		600	V
	Nominal capacity		100	kWh
	Nominal Capacity		167	Ah
	Roundtrip efficiency		90	%
	Maximum charge current		167	A
	Initial SOC		100	%
	Minimum SOC		20	%
	Maximum discharge current		500	A
	Lifetime		5	Year
	Capital Cost		100	$/kWh
	Replacement cost		100	$/kWh
	O$M cost		10	$/Year

Table 3.3 Technical and economic data (continued)

Component	Parameter	details	Value	Unit
Converter	Manufacturer	Schneider		
	Capacity		1	kW
	Capital Cost		280	$
	Replacement cost		280	$
	O&M		10	$/Year
	Efficiency		97	%
	Lifetime		25	Year
DG	Capital Cost		500	$/KW
	Replacement cost		500	$/KW
	O&M		0.030	$/op.h
	Lifetime		15000	h

- Constraints

  - Economic Constraints: Given the recent instability in political and economic conditions across the region, the authors have opted to set both the inflation rate and discount rate to zero. Additionally, the project lifetime is established at 25 years. The electricity tariff for the government sector remains at 0.098 USD/kWh, inclusive of Value Added Tax (VAT) [64].
  - Power Reliability Constraints: The reliability of the proposed system is ensured by restricting the annual f_{cs} and the f_{ren}, as defined in the following expressions:

$$\max(f_{cs}) = 0\ \% \quad (3.15)$$

$$min(f_{ren}) = 0\ \% \quad (3.16)$$

Regarding the maximum capacity shortage, HOMER excludes configurations that fail to meet 100% of the electrical load demand. In terms of the renewable energy fraction constraint, HOMER evaluates and displays all feasible system configurations capable of supplying the entire electrical load, whether they incorporate renewable energy components or rely solely on conventional sources (e.g., with or without grid integration).

- BSS Constraints: Overcharging and over-discharging can significantly impact battery lifespan and performance. Therefore, the battery state of charge (SoC) is constrained within a maximum limit (, SoC_{max}) of 100% and a minimum limit (SoC_{min}) of 20% to ensure safe and efficient operation.
- The number of PV panels (N_{PV}):

$$N_{PV,min} \leq N_{PV} \leq N_{PV,max} \tag{3.17}$$

where $N_{PV,max}$ represents the maximum number of PV panels that can be accommodated based on the available roof area.

- Roof Area and Inter-Row Distance

For PV systems with limited space, determining the inter-row distance is essential to minimize or prevent shading between adjacent PV rows. To accurately evaluate shading effects throughout the year, it is necessary to track the sun's path at the system's location, with particular emphasis on December 21, the date when maximum potential shading occurs in the northern hemisphere [65].

The inter-row distance D is computed using the following equation:

$$\triangle H = L \sin \theta_{tilt} \tag{3.18}$$

$$D = \triangle H \frac{\cos \theta_{az}}{\tan \theta_{elev}} \tag{3.19}$$

where ΔH represents the height of the PV panel from its lower terminal, and L denotes the length of the PV panel. The parameters θ_{tilt}, θ_{az}, and θ_{elev} correspond to the PV array tilt angle, azimuth angle, and sun elevation angle, respectively, as depicted in Figure 3.9.

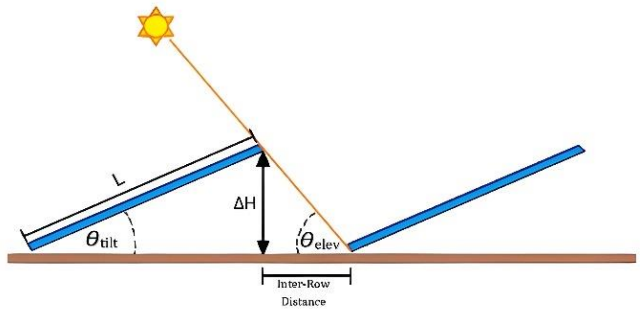

Figure 3.9 Schematic of the proposed system's calculated angles

3.6.2 Cases under Study

This study was conducted using the Cycle Charging (CC) strategy. Under this approach, the generator operates at a higher power level than the instantaneous demand, with the excess power utilized to charge the batteries until they reach their maximum state of charge (SoC_{max}) or become fully charged. A recent study analyzed tilt angles in Najran City across all seasons. The findings indicated that the optimal annual tilt angle for maximum solar energy capture was 20.97°. In this study, the system was assessed under various tilt angles, incorporating both the values derived frand the default values provided by HOMER software. Meanwhile, the azimuth angles were set at 0° and 50°.

The total available roof area at NSII was determined to be 12,000 m², after allocating 5–8% of each roof for maintenance purposes. Using this value, along with the inter-row distance equation, the maximum number of PV panels ($N_{PV,max}$)

for each scenario was computed relative to the total roof area. Table 3.4 presents the various cases analyzed, considering different tilt and azimuth angles, along with their corresponding $N_{PV,max}$ values.

Table 3.4 Cases under study based on tilt and azimuth angles

Case	Tilt	Azimuth	Panels maximum number	Tilt angle Reference
1	17.55	0	3,185	[33]HOMER default
2	0	0	3,878	[66] Summer
3	47.7	0	2,938	[66] Winter
4	47.7	50	2,938	
5	20.97	0	3,115	[66] Optimal
6	20.97	50	3,115	

3.6.3 Results

This section presents the simulation and optimization results obtained using HOMER software. To provide a comprehensive evaluation, the analysis was structured into three key assessments: economic, environmental, and reliability evaluations.

- The economic analysis focused on identifying the most cost-effective system configurations, using Net Present Cost (NPC) and Levelized Cost of Energy (LCOE) as the primary indicators.

- The environmental analysis ranked the optimal configurations based on CO_2 emissions and the renewable fraction (f_{ren}).

- The reliability assessment determined the most effective system setups by evaluating the extent of unserved electrical load.

Table 3.5 presents the economic analysis of the examined cases, demonstrating that all configurations achieved significant NPC savings compared to the existing grid-only system. The current system has an NPC of USD 7.02 million and an LCOE of 0.098 USD/kWh. Among the cases analyzed, Case 6 exhibited the lowest NPC and LCOE values, recorded at USD 3.18 million and 0.0442 USD/kWh, respectively. This result was 2% lower than the HOMER default case, which had an NPC of USD 3.2 million and an LCOE of 0.04523 USD/kWh.

For the environmental evaluation, particularly in assessing CO_2 emissions, a substantial reduction was observed in all hybrid system configurations compared to the grid-only system, which emits 1,812,134 kg/year of CO_2. Case 6 achieved the greatest reduction in emissions, cutting CO_2 output by 92%, with emissions reduced to 142,410 kg/year, supported by its high renewable fraction (f_{ren}) of 92.1%. In contrast, Case 3 had the lowest f_{ren} at 80.7%, leading to an 81% CO_2 reduction, with emissions reduced to 350,413 kg/year. Table 3.6 summarizes the environmental comparisons for all configurations relative to the existing grid-only system.

Table 3.5 Economic comparative optimization results based on the current system (grid-only)

Case	PV Unit	BSS Unit	Converter KW	DG KW	Grid KW	NPC $	LCOE $/KWh	Reduction %
6	3,030	65	985	0	225,333	3,184,478.00	0.0442	54.67%
1	3,168	80	952	0	249,364	3,242,472.00	0.04523	53.84%
5	3,106	75	1,004	0	269,390	3,266,806.00	0.04557	53.50%
2	3,273	86	1,000	0	237,826	3,268,012.00	0.04559	53.48%
4	2,924	99	888	0	296,852	3,347,622.00	0.0467	52.35%
3	2,892	79	924	0	554,452	3,673,245.00	0.05124	47.71%

Table 3.6 Environmental comparative optimization results based on the current system (grid-only)

Case	PV Unit	BSS Unit	Converter KW	DG KW	Grid KW	RF %	CO_2 Kg/yr	Reduction %
6	3,030	65	985	0	225,333	92.1	142,410	92%
2	3,273	86	1,000	0	237,826	91.7	150,306	92%
1	3,168	80	952	0	249,364	91.3	157,598	91%
5	3,106	75	1,004	0	269,390	90.6	170,255	91%
4	2,924	99	888	0	296,852	89.6	187,611	90%
3	2,892	79	924	0	554,452	80.7	350,413	81%

For the reliability assessment, the capacity shortage constraint (f_{cs}) results in the generation of excess energy. Excess energy refers to the portion of generated power that cannot be utilized or stored, leading to either its curtailment or reduction. This occurs when there is surplus electricity production, either from RESs or when the generator produces more electricity than required, and the batteries lack the capacity to absorb the surplus power. In all analyzed cases, the unmet load was zero; however, there was a substantial amount of surplus energy, which varied among the configurations. Since this study does not account for selling excess electricity back to the main grid, surplus generation is not considered an operational advantage in this analysis. The excess electricity fraction (f_{excess}) is defined as the ratio of total excess electricity to total produced electricity. Among the evaluated cases, Case 6 exhibited the highest surplus energy, while Case 3 recorded the lowest f_{excess}, as summarized in Table 3.7. Table 3.8 presents a summary of the optimal cases based on the three key assessment criteria.

Among all the analyzed cases, Case 6, featuring a 20.97° tilt angle and a 50° azimuth angle, demonstrated superior performance across economic, environmental, and reliability assessments when compared to the current system.

- Economic Performance: Case 6 achieved a lower Net Present Cost (NPC) of USD 3,184,478, representing a total cost reduction of 54.67%.

- Environmental Impact: In terms of emissions, Case 6 produced only 142,410 kg/year of CO_2, leading to a 92% reduction in emissions.

- Reliability Assessment: Although this study does not account for selling excess electricity to the main grid, Case 6 generated 1,154,073 kWh/year of surplus energy, which could potentially be monetized through integration with other energy systems.

Table 3.7 Reliability comparative optimization results

Case	**PV** Unit	**BSS** Unit	**Converter** KW	DG **KW**	Grid **KW**	Excess Electricity **KWh/yr**	f_{exess} **%**
6	3,030	65	985	0	225,333	1,154,073	27.4
1	3,168	80	952	0	249,364	1,088,189	26.3
5	3,106	75	1,004	0	269,390	1,037,577	25.4
2	3,273	86	1,000	0	237,826	1,032,197	25.3
4	2,924	99	888	0	296,852	1,016,520	24.9
3	2,892	79	924	0	554,452	806,489	21.1

Table 3.8 Comparative analysis based on economic, environmental, and reliability criteria

Case	**PV Unit**	**BSS Unit**	**Converter KW**	**DG KW**	**Grid KW**	**NPC Reduction**	**CO_2 Reduction**	f_{exess} **%**
6	3,030	65	985	0	225,333	54.67%	92%	27.4
1	3,168	80	952	0	249,364	53.84%	91%	26.3
5	3,106	75	1,004	0	269,390	53.50%	91%	25.4
2	3,273	86	1,000	0	237,826	53.48%	92%	25.3
4	2,924	99	888	0	296,852	52.35%	90%	24.9
3	2,892	79	924	0	554,452	47.71%	81%	21.1

3.6.4 Sensitivity

Resilience: On September 22, a day characterized by high electrical demand, every system component played an active role in continuously meeting the electrical load requirements for the entire 24-hour period. A comprehensive resilience evaluation was conducted based on four principal scenarios, which were applied to Case 6, as it was identified as the most effective configuration among all the analyzed cases. As shown in Table 3.9, the resilience scenarios included:

- Grid outage,
- Planned downtime for battery maintenance,
- Planned downtime for PV system maintenance, and
- A scenario where all these conditions occurred simultaneously.

Table 3.9 Resilience evaluation scenarios

Scenario	Outage	Duration
Scenario 1	Grid	24 hours
Scenario 2	BSS	24 hours
Scenario 3	PV	24 hours
Scenario 4	Grid, BSS, PV	24 hours

Figure 3.10 illustrates the engagement of various system components throughout the 24-hour period. Notably, the DG did not operate continuously over the entire day. Instead, the BSS managed the electrical load independently from 7 PM until the early morning hours. During the peak load period, which extended from 6 AM to 6

PM, all system components, except the DG, actively contributed to meeting the electricity demand.

The optimal system configuration, which ensures an optimal balance between economic efficiency and resilience, was identified through optimization. The optimization results were categorized based on the resilience assessment scenarios outlined in Table 3.10.

When comparing Case 6 (normal operation) with Scenarios 1, 2, and 3, the Net Present Cost (NPC) increased by approximately 0.2%, 0.16%, and 0.72%, respectively. However, Scenario 4, which accounted for simultaneous disruptions, exhibited a notable increase in NPC by 2.68% compared to the normal operation.

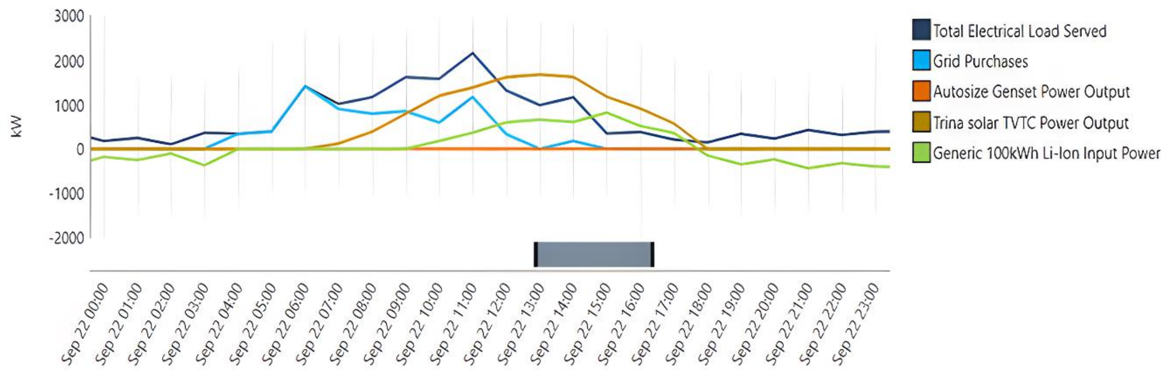

Figure 3.10 System components participation across 22 September

Table 3.10. The resilience assessment results

Scenario	**PV Unit**	**BSS Unit**	**Converter KW**	**DG KW**	**Grid KW**	**NPC $**	**LCOE $/KWh**	**Unmet Load KWh/yr**
Base case	3,030	65	985	0	225,333	3,184,478	0.0442	0
Scenario 1	3,108	70	1,000	2,400	195,303	$3,190,998	0.04452	0
Scenario 2	3,086	64	991	0	216,723	$3,189,468	0.04449	0
Scenario 3	3,030	65	985	0	236,002	$3,207,389	0.04474	0
Scenario 4	3,097	62	998	2,400	202,562	$3,269,805	0.04562	0

In Scenario 1, the DG functioned as a backup power source during grid outages, as illustrated in Figure 3.11. In Scenario 2, the grid compensated for the BSS when it was under maintenance, as shown in Figure 3.12. Scenario 3 addressed the absence of PV power by increasing electricity purchases from the grid. Additionally, Figure 3.13 confirms that the BSS did not draw any power from the grid in this scenario. Scenario 4 represents the worst-case scenario, where a complete energy shortfall occurred due to the simultaneous unavailability of the grid, PV system, and BSS supply. Despite this, during the comprehensive outage period, the DG demonstrated its ability to sustain the load demand for an entire day, as depicted in Figure 3.14. Furthermore, it is noteworthy that all scenarios successfully met the load demands, with an unmet load of 0 kWh/year, aligning with the operating conditions of the system.

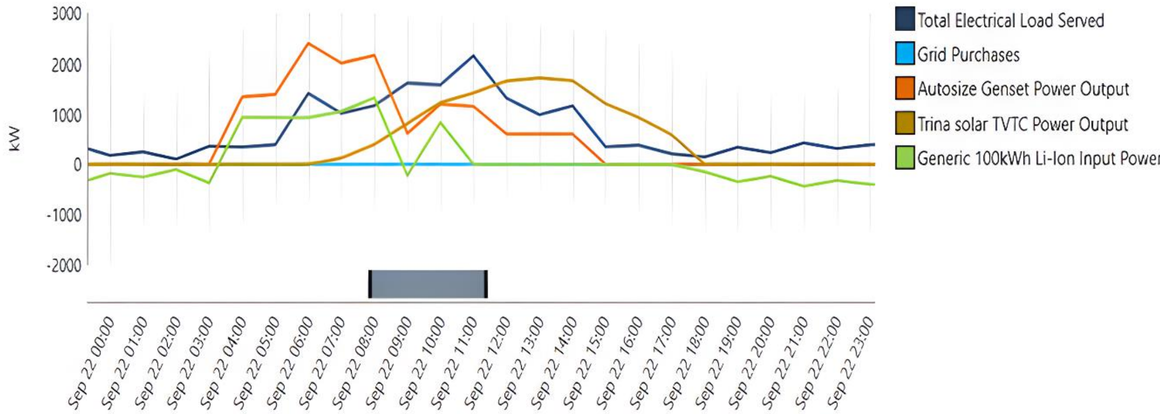

Figure 3.11 System performance during grid outage

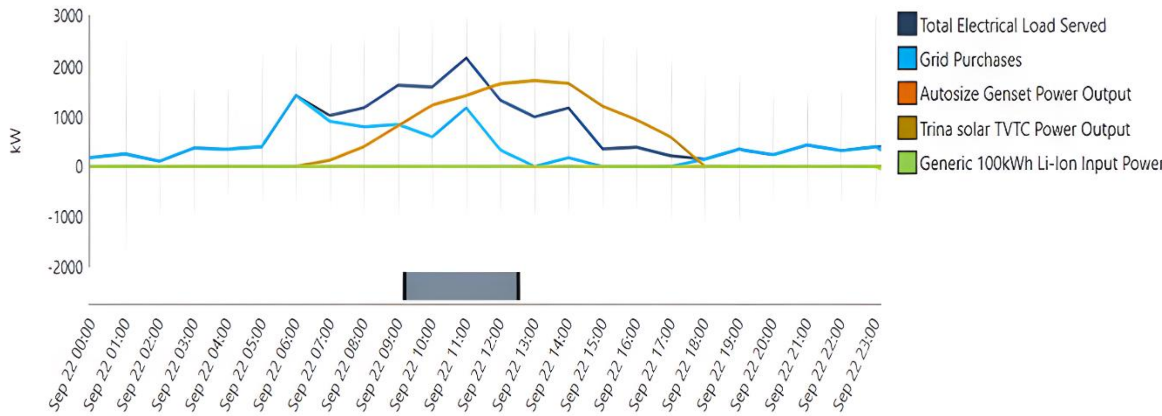

Figure 3.12 System performance on a BSS maintenance schedule

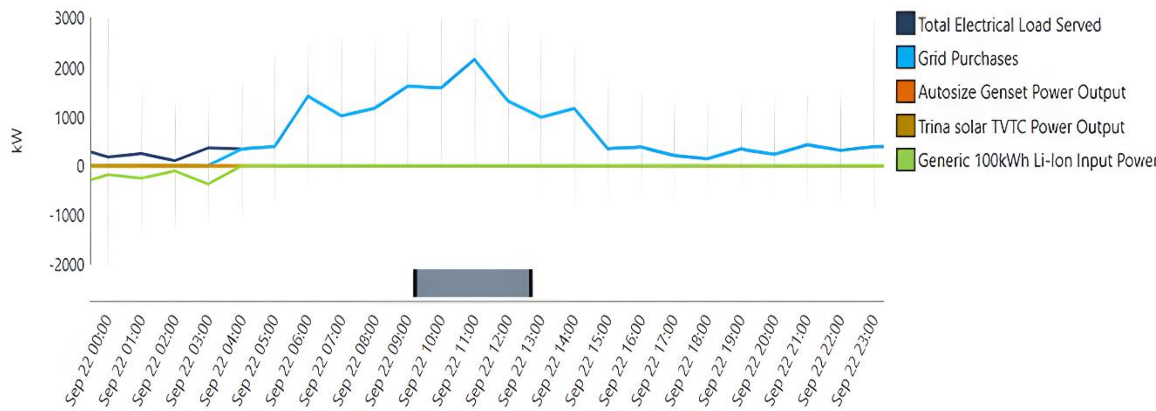

Figure 3.13 System performance on a PV maintenance schedule

Figure 3.14 System performance during a comprehensive outage

3.7 Conclusion

This study examined the implementation of a hybrid microgrid (MG) system at Najran Secondary Industrial Institute (NSII), located in Najran City, in the southern region of Saudi Arabia. The research focused on evaluating the system's economic, environmental, and reliability performance under varying tilt and azimuth angles. This work contributes to the advancement of renewable energy deployment in Najran, supporting the increasing demand for sustainable energy solutions across Saudi Arabia. A distinctive aspect of this study is its integrated approach, which combines innovative architectural design with optimized system management for the selected site. Additionally, it incorporates recent research findings to determine the optimal tilt and azimuth angles specific to this location, comparing them with the default values provided by HOMER software. The proposed microgrid model selects technically and economically viable configurations, considering environmental constraints while ensuring a stable and reliable power supply within the available rooftop area. Furthermore, an extensive sensitivity analysis was conducted, assessing the system's resilience under multiple operational scenarios.

Among the six evaluated cases, Case 6, with a tilt angle of 20.97° and an azimuth angle of 50°, was identified as the most optimal configuration in terms of economic feasibility, environmental sustainability, and system reliability. It demonstrated significant reductions in Net Present Cost (NPC) by 54.69% and carbon emissions (CO_2) by 92%, compared to the current grid-only system, while effectively meeting the entire electrical demand under all resilience scenarios.

In conclusion, this research builds upon recent studies and real-world input data to provide a comprehensive and well-supported evaluation of the proposed hybrid microgrid system. It underscores the renewable energy potential of the Najran region and emphasizes the need for further research and investment to accelerate the adoption of sustainable energy solutions in Saudi Arabia.

CHAPTER FOUR

OPTIMAL SIZING OF SOLAR OFF GRID MICROGRID USING MODIFIED FIREFLY ALGORITHM

4.1 Introduction

The growing need for reliable and sustainable energy solutions has heightened interest in off-grid microgrids powered by solar PV systems. These microgrids provide an effective alternative for supplying electricity to remote and underserved regions where access to the main power grid is either unavailable or extremely limited [67], [68]. However, designing and optimizing solar off-grid microgrids remains a complex task due to the intermittent nature of solar energy and the fluctuations in energy demand. Al-Shahri et al. [69] conducted a detailed review of the challenges and issues associated with PV system optimization. The process of optimizing PV system size comes with multiple challenges, including:

- Limited space availability, particularly in urban settings or on existing structures like rooftops, which can constrain the system size and complicate the optimization process.
- Accurate energy demand estimation is required, but demand varies seasonally, daily, and even hourly due to weather changes and energy usage patterns.
- As PV system size increases, the complexity of its design, installation, and maintenance also grows, necessitating advanced engineering and management solutions.

- Intermittent solar energy generation, caused by factors like cloud cover and shading, makes it difficult to predict the optimal system size to match energy consumption needs.
- Balancing the initial installation cost of a larger PV system against its long-term benefits, including increased energy output and financial savings, remains a challenge—especially considering financing options, incentives, and payback periods.
- PV technology efficiency and performance impose additional constraints on size optimization, as higher-efficiency panels or cutting-edge technologies may be costlier or less readily available.
- Larger PV systems require more frequent maintenance and operational monitoring to ensure peak performance, further adding to the complexity and cost of system optimization.

Ensuring optimal sizing of components such as solar panels, batteries, and inverters is critical to enhancing the cost-effectiveness, reliability, and efficiency of off-grid microgrid systems. Mathew, Mobi, et al. [31] provided an extensive review of the various sizing methods used in PV system design.

The optimized design of PV systems has a substantial impact on the development and implementation of sustainable energy solutions. It facilitates the wider adoption of solar-powered off-grid microgrids, making them a viable solution for electrifying remote and off-grid locations.

Ridha et al. [70] outlined the benefits of optimizing PV systems. An effectively optimized PV system offers multiple advantages, such as:

- Maximizing sunlight capture, ensuring the system generates the highest possible energy output based on the location's solar conditions.
- Enhancing system efficiency by fine-tuning design parameters such as panel orientation, tilt angle, and layout, which leads to improved performance.
- Reducing overall system costs by minimizing unnecessary components, optimizing material usage, and increasing energy production per unit cost.
- Boosting return on investment (ROI) through higher energy yields and lower costs, making PV systems a more attractive long-term investment.
- Maximizing space utilization, whether on rooftops, open land, or integrated into building structures, allowing for additional panels and increased energy generation.
- Enhancing system reliability and longevity by considering factors like weather conditions, shading, and layout to minimize performance degradation and failures.
- Ensuring scalability and adaptability, making PV systems flexible for various applications and sizes depending on specific energy needs and space constraints.
- Seamless integration with energy storage systems, leading to improved energy utilization and increased self-consumption, further enhancing the financial feasibility of solar energy solutions.

4.2 Literature Review

Researchers have introduced a variety of problem-solving methods to tackle complex engineering challenges. Broadly, these methods can be classified into two main categories: heuristics and metaheuristics. Heuristic approaches focus on quickly identifying satisfactory solutions when conducting an exhaustive search is impractical. They function as practical guidelines that aid decision-making by utilizing experience, intuition, or general principles instead of following a strictly algorithmic process. Heuristics are particularly beneficial in cases where determining an exact optimal solution is either computationally demanding or infeasible.

Metaheuristics, in contrast, serve as higher-level strategies designed to enhance heuristic methods [71]. These approaches provide a structured framework for exploring the solution space, often incorporating concepts inspired by natural processes, such as genetic algorithms, simulated annealing, or particle swarm optimization. Compared to heuristics, metaheuristics adopt a more methodical approach to problem-solving, allowing for efficient navigation of large solution spaces and facilitating the discovery of near-optimal solutions for complex problems [72]. Figure 4.1 below illustrates several well-established heuristic and metaheuristic techniques found in the literature.

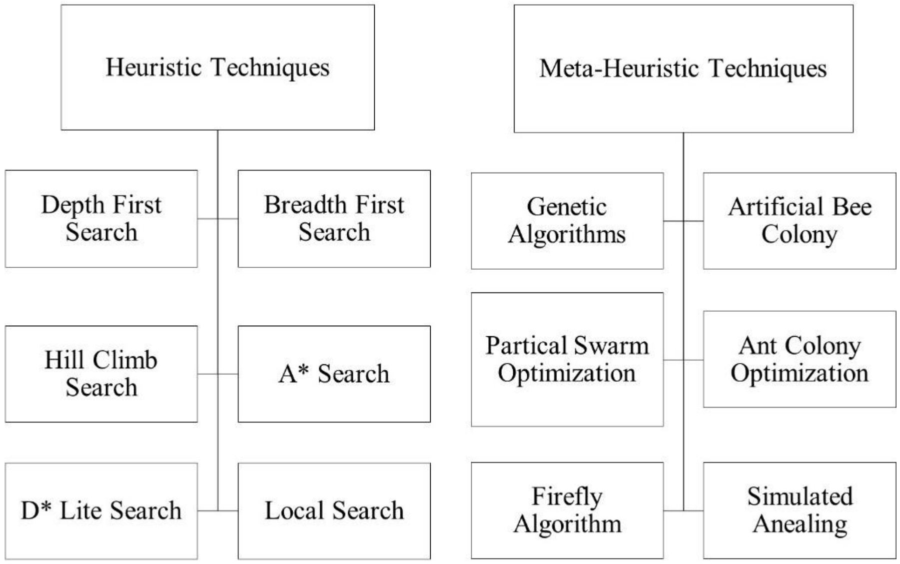

Figure 4.1 Problem solving techniques

Traditional approaches for determining the size of off-grid microgrids often depend on heuristic methods or simulation-based techniques. Fioriti, Davide, et al. [73] and Bektas, Zeynep, et al. [74] proposed heuristic methods for microgrid sizing while evaluating multiple design alternatives. However, these methods do not always lead to the most efficient or cost-effective solutions. To overcome this limitation, optimization algorithms have gained prominence as effective tools for identifying the optimal configuration of microgrid components.

Khan, Baseem, et al. [75] conducted a detailed analysis to determine the most suitable metaheuristic techniques for optimizing smart microgrids. Gao, Kaiye, et al. [76] provided an in-depth discussion on microgrid operation optimization, including its subcomponents. Their study also emphasized that genetic algorithms and simulated annealing algorithms are among the most widely applied optimization methods for microgrid operations. Leonori, Stefano, et al. [77] implemented a genetic algorithm to optimize energy management within a microgrid. Diab, Ahmed A. Zaki, et al. [78] proposed an approach aimed at reducing the cost of energy (COE) supplied by the system while enhancing its reliability and efficiency by addressing the loss of power supply probability (LPSP). In [78], a comparative analysis was conducted on various optimization techniques, including the Whale Optimization Algorithm (WOA), Water Cycle Algorithm (WCA), Moth-Flame Optimizer (MFO), and the Hybrid Particle Swarm-Gravitational Search Algorithm (PSOGSA), to achieve an optimized microgrid design.

Among various optimization algorithms, the Firefly Algorithm (FA) has gained recognition for its effectiveness in solving complex optimization problems, drawing inspiration from the flashing behavior of fireflies in nature. Vasanth, J. Deepak, et al. [79] applied the firefly algorithm to minimize the operational costs of a microgrid. Ibrahim, Ibrahim M., et al. [80] developed a hybrid approach by combining Particle Swarm Optimization (PSO) with the Firefly Algorithm (FA) to determine the optimal size of a microgrid system. The problem was implemented in MATLAB, with the primary objective of identifying the optimal microgrid size that minimizes both total costs and emissions. Yang, YuDe, et al. [81] introduced an enhanced metaheuristic optimization technique based on the firefly algorithm, known as the multidimensional firefly algorithm (MDFA), for addressing day-ahead scheduling optimization in a microgrid.

The literature review indicates that the firefly algorithm has gained significant attention from researchers for addressing various challenges related to microgrid parametric optimization. This study presents a novel approach for determining the optimal size of solar off-grid microgrids using a modified Firefly Algorithm. The proposed algorithm is specifically designed to tackle the complexities associated with off-grid microgrid design optimization, incorporating multiple objectives such as system cost, reliability, and performance. By utilizing the distinctive properties of the Firefly Algorithm and integrating modifications to enhance convergence speed and solution accuracy, the proposed approach aims to address the limitations of existing optimization methods and deliver more precise and efficient results.

This study conducts a detailed case analysis to illustrate the effectiveness of the modified Firefly Algorithm in optimizing the sizing of solar off-grid microgrids. A comparative assessment with other optimization techniques highlights the advantages of the proposed approach in achieving optimal solutions that align with the diverse requirements of off-grid electrification projects. The outcomes of this research hold significant relevance for the design and deployment of sustainable energy systems, contributing to the broader adoption of solar off-grid microgrids as a practical solution for electrifying remote and off-grid communities.

4.3 Problem Formulation

The formulation and modeling of a microgrid PV system for size optimization involves identifying key variables and constraints to achieve optimal performance while considering the various subsystems of the PV system [82]. These subsystems generally consist of photovoltaic panels, inverters, and batteries, with the possibility of incorporating backup generators [83]. Each subsystem presents specific parameters and constraints that must be incorporated into the optimization model. For example, factors such as the capacity and efficiency of photovoltaic panels, the efficiency and power rating of inverters, the storage capacity and efficiency of batteries, and restrictions on the operation of backup generators all play a role in shaping the overall system configuration. Achieving a well-balanced design requires careful analysis of the interaction between energy generation, storage, and distribution within the microgrid, with the objective of maximizing efficiency, reducing costs, and ensuring a reliable power supply under varying operational conditions [84]. The PV system is modeled using the following equations from [52].

The output power of a PV module is calculated using equation (4.1), which depends on the solar irradiation at time *t*, while the efficiency of the PV module is determined using equation (4.2).

$$P_{PV}(t) = \eta_{PV}.A_{PV}.G(t) \tag{4.1}$$

$$\eta_{PV} = \eta_{STC}.\eta_{MPPT}[1-\alpha(T_C - T_{ATC})] \tag{4.2}$$

where A_{PV} represents the area of a PV module in (m^2), *G(t)* is the hourly solar irradiance in (W/m^2), η_{PV} is the efficiency of the PV array, η_{STC} refers to the reference efficiency of the PV cell under standard temperature condition (STC), and η_{MPPT} represents the efficiency of the maximum power point tracker, T_C is the PV cell in temperature in degrees Celsius (˚C), and T_{STC} is the reference temperature of the PV cell at STC (25˚C), and α is a temperature coefficient of the PV cell typically ranges from 0.4%/˚C to 0.6%/˚C for silicon-based cells.

The energy storage system's discharging and charging energies at time *t* are determined using equations (4.3) and (4.4), respectively.

$$E_{ESS}^{d}(t) = E_{ESS}(t-1) - \frac{[E_{Load}(t) - E_{PV}(t) - E_{WT}(t)]}{\eta_d} \tag{4.3}$$

$$E_{ESS}^{c}(t) = E_{ESS}(t-1) + [E_{PV}(t) + E_{WT}(t) - E_{Load}(t)].\eta_c \quad (4.4)$$

where $E_{ESS}(t-1)$ represents the stored energy at time *t −1* in (kWh);

E_{PV}, E_{WT} , and E_{Load} correspond to the energy contributions from the PV system, wind turbine, and load, respectively. Additionally, η_d and η_c denote the discharge and charge efficiencies of ESS, respectively.

The loss of power supply, which occurs when energy demand surpasses the energy generated, is represented as:

$$LPS(t) = P_{Load}(t) - \left[P_{PV}(t) + P_{WT}(t) + P_{ESS}^{d}(t)\right].\eta_{inv} \quad (4.5)$$

where η_{inv} represents the inverter efficiency. The Loss of Power Supply Probability (LPSP) over a given time period *T* is defined as the ratio of the total *LPS (t)* values within that period to the sum of all load demands, as in equation (4.6)

$$LPSP = \frac{\sum_{t=0}^{T} LPS(t)}{\sum_{t=0}^{T} P_{Load}(t)} = \frac{\sum_{t=0}^{T} Power\ Failure\ Time}{T} \quad (4.6)$$

Following the modeling of PV systems, the firefly and modified firefly algorithm [85] have been applied to determine the optimal solution for the given problem. In the firefly algorithm, the primary update equation for any two fireflies *i* and *j* at positions x_i and x_j is expressed as:

$$x_i^{Itr+1} = x_i^{Itr} + \beta\left(x_i^{Itr} - x_j^{Itr}\right) + \alpha\epsilon_i^{Itr} \quad (4.7)$$

where α is a parameter regulates the step size, $\beta = \beta_0 e^{-\gamma r^2}$ defines the attractiveness, with β_0 representing the attractiveness at distance of $(r = 0)$ and γ denotes the light absorption coefficient. ϵ_i introduces randomness, where the vector of random variables is drawn from a probability distribution, such as the Gaussian distribution. The distance between any pair of fireflies i and j at positions x_i and x_j is given by the Cartesian distance r_{ij}. These equations indicate that FA relies on three adjustable parameters: α, γ and ϵ. Manually tuning these parameters is highly challenging. In the modified FA, these parameters are adaptively updated. In this approach, the tunable parameters can be computed using the following equations.

$$\alpha(Itr_i) = exp\left(1 - \left(\frac{Itr_{max}}{Itr_{max} - Itr_i}\right)^c \right) \tag{4.8}$$

$$\beta = \beta_0 e^{-\gamma r^2} \tag{4.9}$$

$$r = \left\| x_i - x_j \right\| \tag{4.10}$$

$$\gamma(Itr_i) = 1 - exp\left(1 - \left(\frac{Itr_{max}}{Itr_{max} - Itr_i}\right)^c \right) \tag{4.11}$$

Where c is an integer that defines the decay rate. During the search process, two update equations are described and selected randomly, as presented below:

$$x_{i+1} = \begin{cases} \beta(i)x_i + x_j(1 - \beta(i)) + \alpha(i)\epsilon_i & rand > 0.5 \\ \frac{NG-i}{NG}(1 - \delta)x_i + \delta x_{best} & Elsewhere \end{cases} \tag{4.12}$$

where δ denotes the gray coefficient and *NG* represents the total number of generations. Table 4.1, Table 4.2 and Table 4.3 represent the key parameters of PV panels, BSS and inverter in microgrid system.

Table 4.1 PV parameters

Parameter	Value	Units
Area of Panel	2.9094	m^2
Rated Capacity	0.66	KW
Temperature Coefficient	-0.34	% / C
Operating Temperature	43	C
Efficiency	0.2125	%
Panel Lifetime	25	Years
Capital Cost	147	$/KWh
Replacement Cost	110	$/KWh
Operational / Maintenance Cost	10	$/Year

Table 4.2 Inverter parameters

Parameter	Value	Units
Capacity	100	KWh
Lifetime	25	Year
Capital Cost	280	$
Replacement Cost	280	$
Operational / Maintenance Cost	10	$/KW
Loss of Power Supply Probability (LPSP)	1000	---

Table 4.3 BSS parameters

Parameter	Value	Units
Nominal Voltage	600	V
Nominal Power Capacity	100	KWh
Nominal Current Capacity	167	Ah
Round Trip Efficiency	90	%
Maximum Charge Current	167	A
Initial State of Charge	100	%
Minimum State of Charge	20	%
Maximum Discharge Current	500	A
Lifetime	5	Year
Capital Cost	100	$/KW
Replacement Cost	100	$/KW
Operational / Maintenance Cost	10	$/KW

4.4 Proposed Algorithm

The objective is to minimize the total cost of the microgrid configuration, which includes both initial investment and operational expenses while ensuring system reliability by maintaining a low Loss of Power Supply Probability (LPSP). Amara et al. [86], Azaza et al. [87], and Huang et al. [88] utilized LPSP as a technical reliability criterion in the optimization of microgrid sizing. The complexity of this problem arises from its nonlinear nature, influenced by fluctuating energy demand, variations in renewable energy supply, and multiple operational and technical constraints, as highlighted by Azeem et al. [89], Saeed et al. [90], and Choudhury et al. [91].

The FA replicates the attraction behavior of fireflies, where each firefly represents a candidate solution, moving toward brighter fireflies that indicate more optimal solutions [92]. The algorithm’s simplicity is counterbalanced by its innovative search mechanism, where attractiveness is determined based on the inverse of the objective function, which in this case is the total cost [93].

Khan et al. [93], Kumar et al. [94], and Tilahun et al. [95] provided a comprehensive review of the firefly algorithm and its modified versions proposed by researchers to enhance FA performance. The modified firefly algorithm (MFA) improves upon the standard FA by incorporating additional techniques, such as local search mechanisms, to enhance solution quality and accelerate convergence. This modification aims to overcome the limitations of the FA, including premature convergence and inefficiencies in exploration. Figure 4.2 presents the flowchart of the standard FA alongside the proposed MFA.

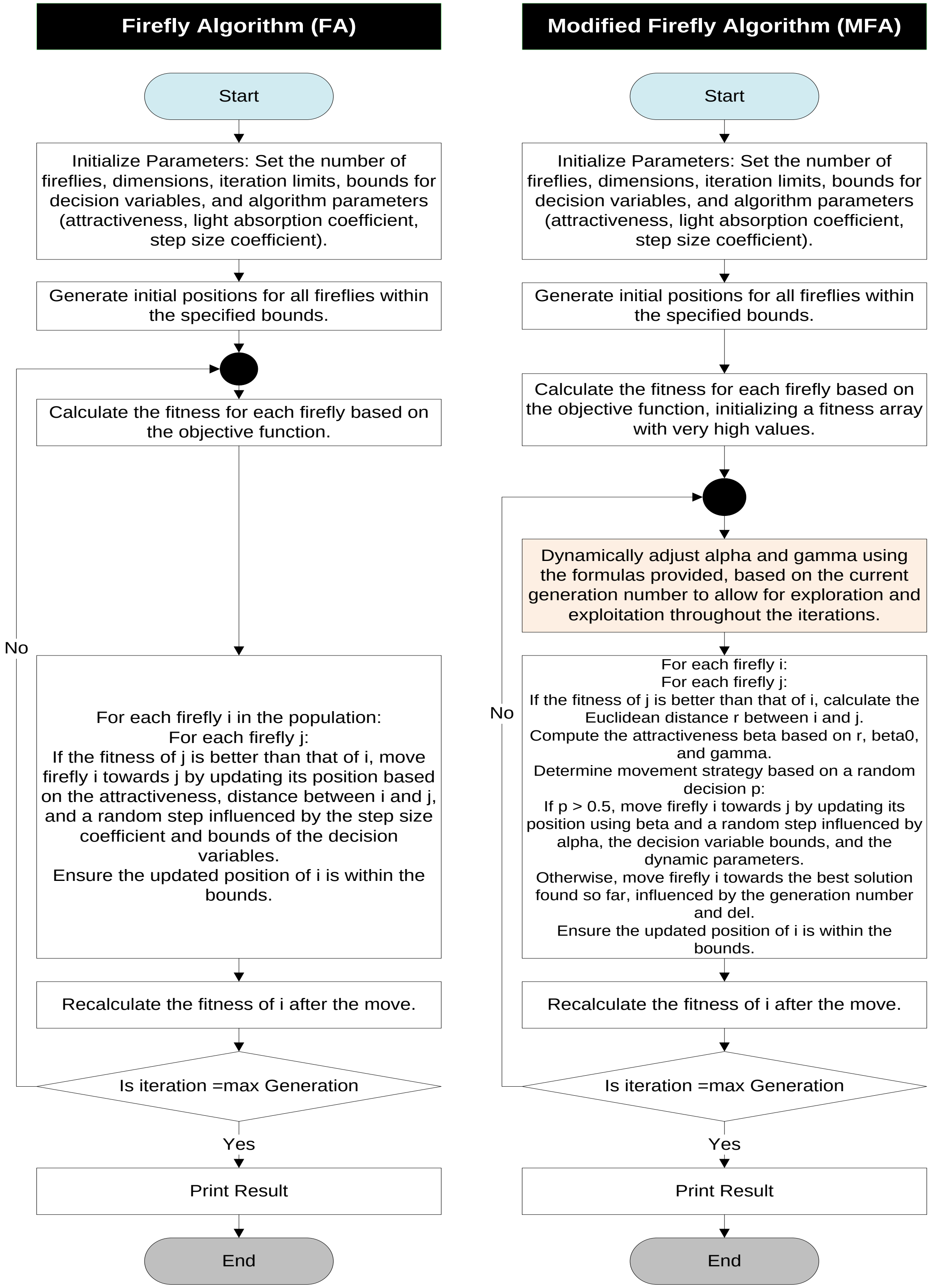

Figure 4.2 FA and proposed MFA

4.5 Result and Discussion

The performance of the firefly algorithm is influenced by multiple parameters, each of which plays a vital role in defining its efficiency and overall effectiveness. The light absorption coefficient (γ) controls the level of attractiveness between fireflies, affecting their movement toward brighter fireflies within the search space. The level of attractiveness can be modified to regulate exploration and exploitation, ensuring a balance between discovering new regions and refining promising solutions. The step size coefficient (α) determines the extent of randomness in the movement of fireflies, facilitating a trade-off between exploration and exploitation. Moreover, the population size and the maximum number of iterations are key parameters that influence the algorithm's convergence rate and computational efficiency. Proper tuning of these parameters is critical for achieving optimal performance across different optimization problems. Figure 4.3 depicts the system configuration where FA and MFA were utilized to optimize the system using load and meteorological data derived from prior research [10].

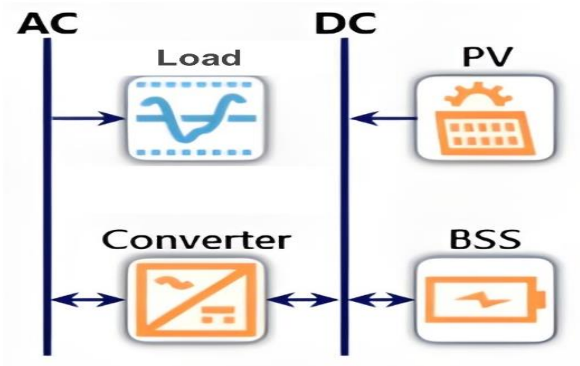

Figure 4.3 System configuration

This study examined two scenarios based on LPSP values of 0.01 and 0.1. Both scenarios were implemented using the same initial algorithm settings, including the number of fireflies, problem dimensions, and the maximum number of generations, as outlined in Table 4.4.

The key difference is that the MFA incorporates a local search phase after movement, which is designed to refine solutions and enhance the algorithm's ability to escape local optima. A similar approach, integrating harmony search with the firefly algorithm, was applied by Satapathy et al. [96] to address an optimization problem within the microgrid domain.

Table 4.4 Algorithm parameters

Parameter	Value
Number of Fireflies	20
Problem Dimensionality	2
Maximum Generations	30
Lower Bound of Decision Variable	1
Upper Bound of Decision Variable	6000
Attractiveness at r=0 ($\boldsymbol{\beta_0}$)	1
Light Absorption Coefficient ($\boldsymbol{\gamma}$)	0.1
Step Size Coefficient ($\boldsymbol{\alpha}$)	0.2
C	1
Del	0.5

The performance of the microgrid, optimized using the FA and MFA for both scenarios with LPSP values of 0.01 and 0.1, is illustrated in Figure 4.4, Figure 4.5, Figure 4.6, and Figure 4.7, respectively. These figures demonstrate the relationship between photovoltaic generation, energy demand, and battery storage over time. The trend appears relatively stable, with some fluctuations reflecting peak usage periods or variations in load within the microgrid. The battery status, represented by the green line, indicates the amount of energy stored in the system's batteries. The charging and discharging cycles are clearly visible, with energy levels decreasing during periods of high demand or low PV generation and increasing when surplus energy is available.

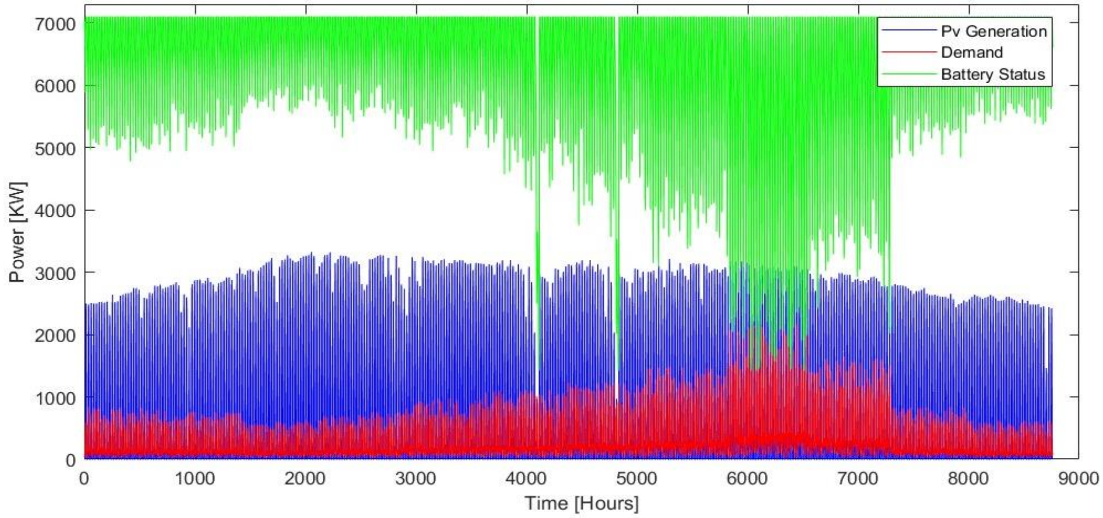

Figure 4.4 System performance of Standard FA with LPSP = 0.01

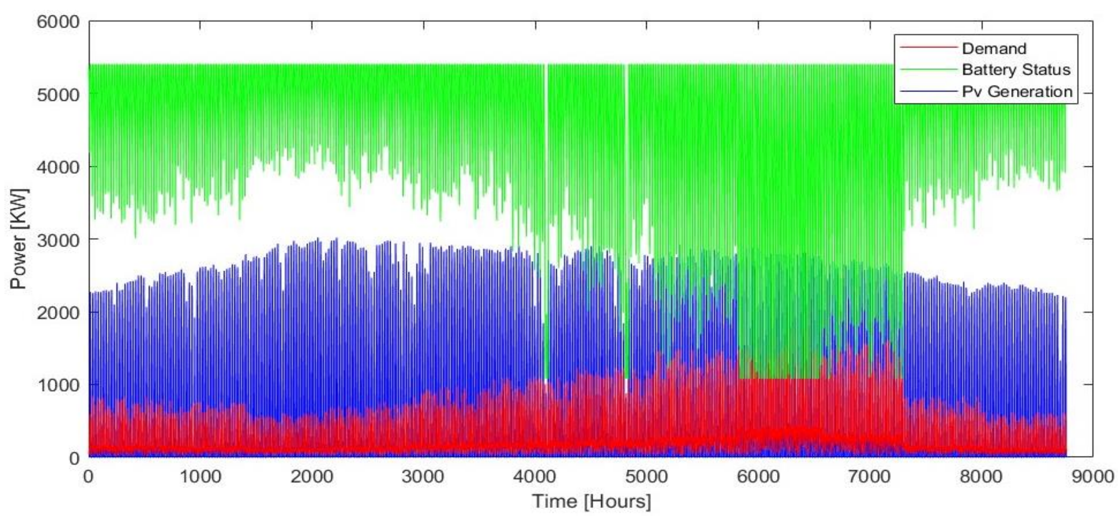

Figure 4.5 System performance of MFA with LPSP = 0.01

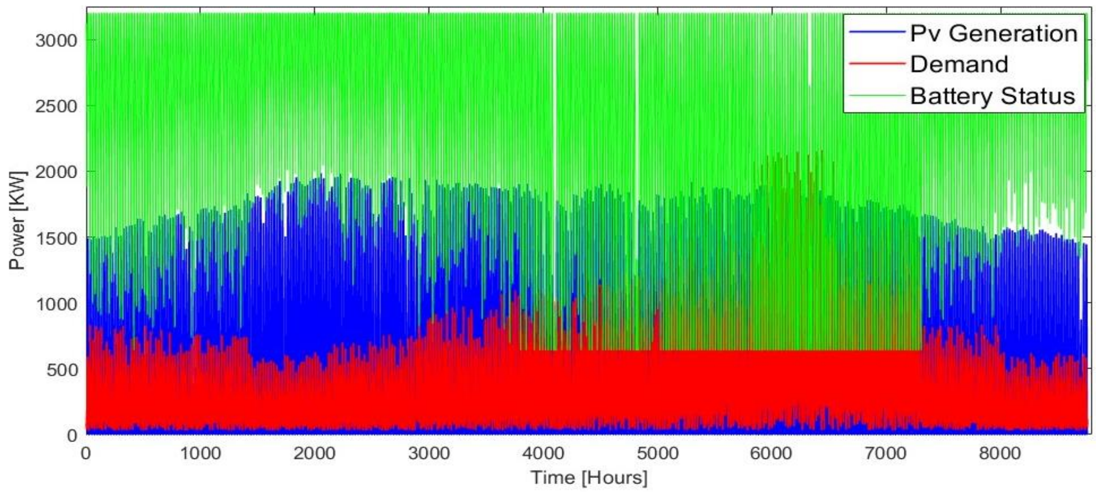

Figure 4.6 System performance of Standard FA with LPSP = 0.1

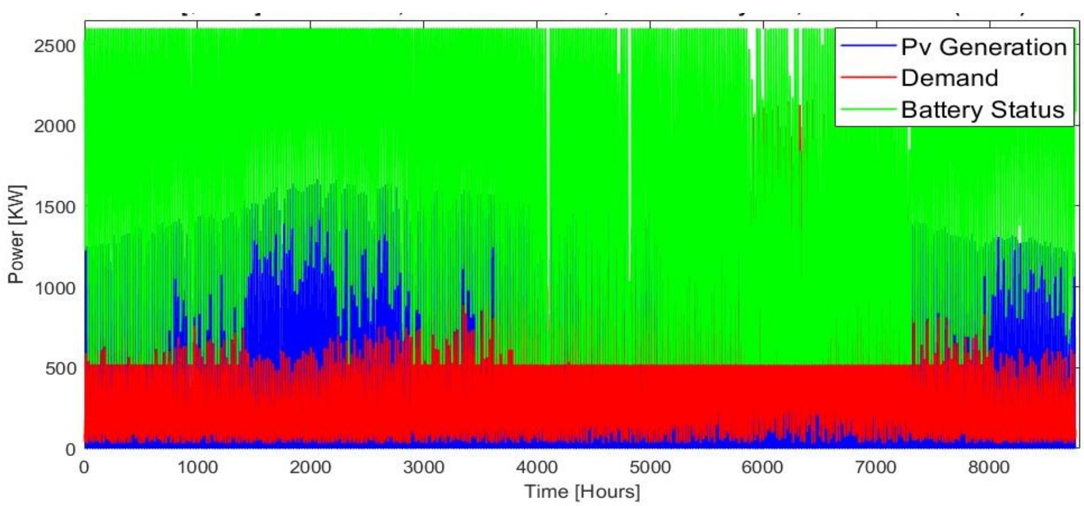

Figure 4.7 System performance of MFA with LPSP = 0.1

Table 4.5 presents a comparative analysis of the FA and MFA performance in optimizing a solar off-grid microgrid system under two different scenarios based on LPSP values. It highlights key metrics for each scenario and algorithm, including the number of PV units, BSS units, converters, total cost, and the number of iterations required to achieve the optimal solution.

Table 4.5 Performance results

Scenario	LPSP	Algorithm	PV (Unit)	BSS (Unit)	Converter (Unit)	Cost ($)	Iteration
Case 1	0.01	Standard FA	4634	71	10185	4208461	18
		Modified FA	4211	54	8179	3917511	15
Case 2	0.1	Standard FA	2765	32	5025	2468980	28
		Modified FA	2321	26	4131	2360733	4

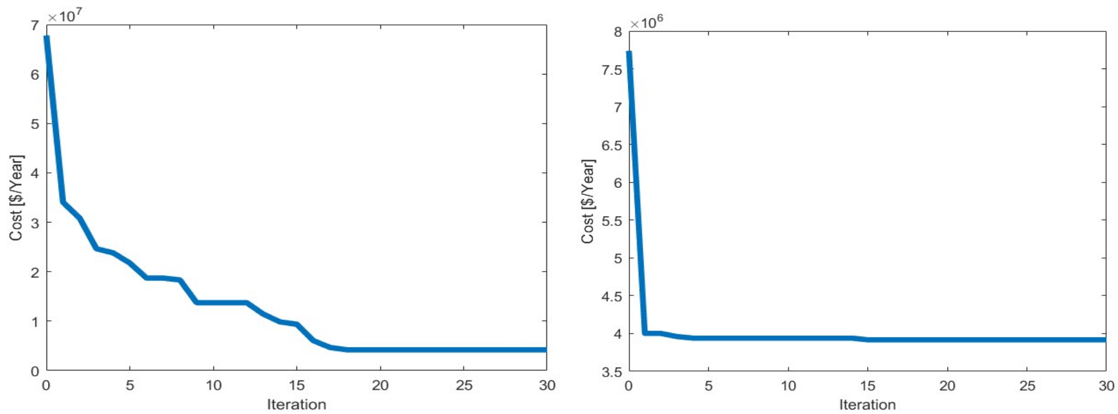

(a) (b)

Figure 4.8 Convergence comparison of Standard FA (a) and MFA (b) systems with LPSP=0.01

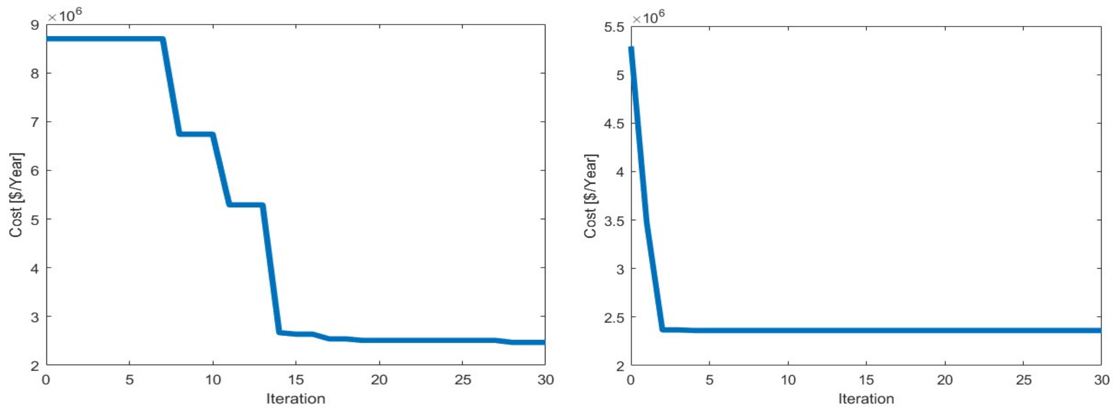

(a) (b)

Figure 4.9 Convergence comparison of Standard FA (a) and MFA (b) systems with LPSP=0.1

In Case 1, where the LPSP was set at 0.01, the MFA required fewer photovoltaic units, battery storage units, and converters, leading to a lower total cost of $3,917,511 and achieving convergence in 15 iterations, outperforming the standard FA. Similarly, in Case 2, with an LPSP of 0.1, the MFA again demonstrated superior performance over the standard FA, achieving cost savings of $2,360,733 and improving efficiency by utilizing fewer components and requiring fewer iterations. These findings highlight the effectiveness of MFA in optimizing microgrid configurations. Figure 4.8 and Figure 4.9 illustrate the iteration process for both cases, showing that the MFA consistently outperformed the standard FA in identifying lower-cost microgrid configurations.

Key observations include:

- Enhanced Exploration and Exploitation: The hybrid structure of MFA facilitated a more extensive exploration of the search space while effectively exploiting promising regions.

- Diversity Preservation: The inclusion of local search mechanisms enabled MFA to maintain solution diversity, thereby reducing the likelihood of premature convergence.
- Adaptability: The flexibility of MFA to integrate problem-specific insights or additional optimization techniques proved beneficial in navigating the complex optimization challenges associated with microgrid systems.

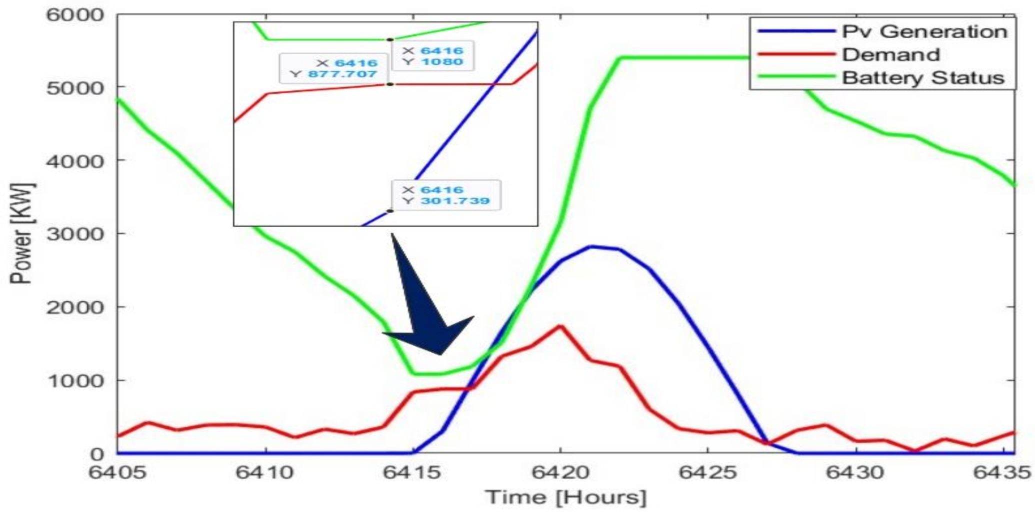

Figure 4.10 24-hour performance of the MFA with LPSP = 0.1

Figure 4.10 illustrates the 24-hour performance of the MFA. Over this period, the graphs depict the diurnal cycle of PV generation, which starts and ends at low levels, peaking around midday. In contrast, energy demand appears to have minimal fluctuations, while the battery status reflects charging during periods of excess generation and discharging during high demand or low generation. The solar generation, represented by the blue line, contributes energy to the grid only between 08:00 AM and 06:00 PM. During this period, both the demand and battery charging are supported by solar energy, as indicated by the red and green lines, respectively. In the absence of solar energy, the demand is met by the battery, which can be observed as the green line declines, indicating battery discharge.

The microgrid's performance throughout the analyzed period provides a fundamental understanding of the system's dynamics, offering valuable insights for future improvements in optimization and scalability. The implementation of the FFA has been effective in establishing an initial configuration; however, further refinement of algorithm parameters may enhance cost efficiency and power reliability.

The results indicate that the MFA successfully converged on a solution that required fewer PV units, fewer batteries, and resulted in a lower overall cost compared to the FA when applied under the same input conditions.

4.6 Conclusion

This comparative study underscores the effectiveness of modified optimization strategies, particularly the Modified Firefly Algorithm (MFA), in enhancing the optimization of microgrid configurations. By integrating fundamental principles of the standard Firefly Algorithm (FA) with additional optimization mechanisms, the MFA improves solution quality and accelerates convergence, making it a promising approach for designing cost-effective and reliable microgrids.

The results demonstrate that the MFA identifies the optimal solution in fewer iterations compared to the standard FA, showcasing its efficiency in computational performance. Looking ahead, future research directions could focus on further refining modification strategies and expanding their application to broader energy system optimization challenges. This could include incorporating dynamic operational constraints and enhancing the integration of renewable energy sources, ensuring greater flexibility and adaptability in microgrid optimization.

CHAPTER FIVE

MAXIMUM POWER POINT TRACKING BASED ON MODIFIED FIREFLY ALGORITHM FOR PV SYSTEM UNDER PARTIAL SHADING CONDITIONS

5.1 Introduction

Electrical energy has become a fundamental necessity worldwide, significantly contributing to improved living standards. It is an essential element in sustaining various aspects of modern civilization. However, reliance on conventional energy sources such as coal and oil has led to increased fossil fuel costs, adverse environmental impacts, and negative health effects. To mitigate these issues, researchers are continuously exploring viable alternatives to minimize fossil fuel consumption. Numerous options exist for generating electricity without causing pollution, primarily through sustainable energy sources. These sources, including solar, wind, biomass, fuel cells, and hydropower, are naturally abundant, clean, and inexhaustible. Among them, solar energy is the most widely adopted for electricity generation due to its minimal operational and maintenance costs. The increasing focus on solar energy harvesting has gained considerable attention in recent years, particularly for both stand-alone and grid-connected systems [97], [98].

The output power of photovoltaic (PV) systems exhibits a nonlinear response to variations in solar irradiance and ambient temperature. Conventional methods for maximum power point tracking (MPPT) include fractional open-circuit voltage (FOCV), fractional short-circuit current (FSCC), incremental conductance (INC), and perturb and observe (P&O). However, under partial shading conditions (PSC), the most shaded cell in a series-connected string can restrict the current flow, leading to performance limitations. This scenario can trigger a hot-spot issue, where the heavily shaded cell becomes reverse-biased by the adjacent cells, potentially resulting in excessive heating and damage. To mitigate this, bypass diodes are typically installed in parallel with clusters of cells. While effective in preventing hot-spot damage, these diodes introduce multiple local maximum power points (LMPPs) in the power-voltage (P-V) curve and lead to stepped variations in the string's current-voltage (I-V) characteristics. As a consequence, conventional MPPT algorithms often struggle to differentiate the global maximum power point (GMPP) from the numerous LMPPs, hindering the PV system's ability to achieve optimal performance [99]. Therefore, selecting an appropriate control strategy is essential for accurately tracking the global maximum power point (GMPP). Various soft computing-based techniques, including fuzzy logic, neural networks (NNs), normal harmonic search (NHS), and Cauchy and Gaussian sine cosine optimization (CGSCO), have been successfully implemented to identify optimal operating points for PV systems under partial shading conditions (PSCs). Additionally, several nature-inspired optimization algorithms have demonstrated effective performance in MPPT applications under PSCs, such as the firefly algorithm (FA), genetic algorithm (GA), differential evolution (DE), grey wolf optimization (GWO), intelligent monkey king evolution algorithm (IMKE), and particle swarm optimization (PSO) [100].

Moreover, hybrid nature-inspired techniques, including combinations such as GA with FA, GWO integrated with P&O, hybrid Jaya with DE (JayaDE), and whale optimization with DE (WODE), have been observed to yield superior tracking accuracy and response times compared to their standalone counterparts. Compared to traditional

MPPT methods used in PSC scenarios, these meta-heuristic algorithms provide several advantages, including automatic identification of shading patterns, effective GMPP searching capabilities, and simplified computational structure [101], [102]. To further improve tracking efficiency, some studies have recently explored enhanced MPPT techniques, such as modified perturb and observe (P&O). While these improved methods demonstrate the ability to track the GMPP, they vary in terms of accuracy, speed, and complexity. Despite their capability to track the global peak, these approaches often exhibit slower convergence rates [103].

The authors in [104] implemented the dividing rectangles algorithm for MPPT under partial shading conditions (PSC). This method ensures that the P-V characteristic curve of the PV module conforms to the Lipschitz function, allowing for the identification of the maximum power point. In [105], an adaptive neuro-fuzzy inference system-based MPPT tracker was introduced for PV modules. However, this approach struggled to track the global MPP in PSC scenarios when the system operated under uniform irradiance conditions. Another study in [106] proposed an adaptive neuro-fuzzy inference system (ANFIS) as an MPPT technique for PV systems. The ANFIS model was trained using the incremental conductance (INC) method based on the uniform irradiance approach. Additionally, in [107], a hybrid MPPT technique was employed. This method initially utilizes the ant colony optimization (ACO) algorithm to approach the MPP, followed by the perturb and observe (P&O) technique to ensure accurate tracking.

In [108], the author applied the artificial bee colony (ABC) algorithm for maximum power point tracking (MPPT). A boost converter was utilized to align the PV system with the output load. The proposed approach demonstrated a higher tracking speed compared to the improved perturb and observe (P&O) and particle swarm optimization (PSO) methods. To further enhance the search capability, the differential evolution (DE) algorithm was integrated with PSO [109]. In this hybrid PSO-DE approach, the PSO algorithm executes half of the iterations, after which the DE algorithm takes over for the remaining iterations. This alternating process continues until the termination criterion is met. According to the simulation results, the PSO-DE hybrid method surpasses incremental conductance (INC), fuzzy logic controller (FLC), and standalone PSO techniques in terms of efficiency, tracking speed, simplicity, and minimizing oscillations around the maximum power point (MPP).

This chapter presents the performance evaluation and comparative analysis of various maximum power point tracking (MPPT) algorithms, including Perturb and Observe (P&O), Particle Swarm Optimization (PSO), the Firefly Algorithm (FA), and the Modified Firefly Algorithm (MFA), in a photovoltaic (PV) system under different partial shading conditions (PSCs). The primary objective of this study is to assess the effectiveness of MFA in MPPT applications under PSCs. To validate the findings, a comparative analysis has been conducted, demonstrating the superiority of MFA over other algorithms in terms of tracking efficiency. Additionally, the influence of load resistance on MFA performance has been examined. The entire analysis has been carried out using MATLAB/Simulink software, ensuring a comprehensive evaluation of the proposed approach.

5.2 Characteristic of Solar Cells

A photovoltaic cell can vary its short-circuit current from milliamperes to several amperes, while the voltage it generates is approximately half of the nominal light intensity. The nominal power generation capacity of the cell is determined by multiplying the open-circuit voltage with the short-circuit current, which provides the maximum possible power output of the cell. Generally, the power output of a single cell ranges from a few milliwatts to several watts [110].

$$I = I_{pv} - I_0\left[exp\left(\frac{V+R_S I}{V_t a}\right) - 1\right] - \frac{V+R_S I}{R_{sh}} \tag{5.1}$$

The produced current of the photovoltaic module is denoted as I_{pv}, while I_0 represents the reverse saturation current. The thermal voltage of the PV array is given by $V_t = \frac{N_S KT}{q}$, where N_s is the number of series-connected cells, q is the electron charge (q = 1.6e^{-19}c), and T is the temperature of the cell in Kelvin. The constant K refers to the Boltzmann factor (K=1.3805e^{-23} $\frac{j}{k}$), and " a " represents the diode's ideality factor. The equivalent circuit of the solar PV module is illustrated in Figure 5.1.

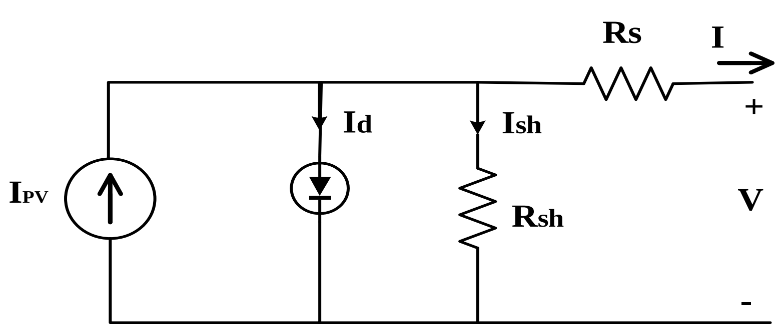

Figure 5.1 Electrical model of solar PV module

5.3 Characteristics of PV Module under PSC

Solar photovoltaic (PV) systems are among the most promising renewable energy technologies, offering several advantages over other power generation methods. However, one of the key challenges associated with PV systems is their low conversion efficiency, as a significant portion of the solar irradiance received by PV panels is not effectively converted into usable electrical power. The challenge becomes even more pronounced when certain panels receive reduced sunlight due to obstructions, a phenomenon known as partial shading conditions (PSC). Under PSC, multiple local maximum power points (LMPPs) emerge in the power-voltage (P-V) curve, particularly in arrays with long series-connected chains, leading to more complex P-V characteristics [111], [112]. In such conditions, the power output of PV modules can be significantly diminished, as conventional maximum power point tracking (MPPT) techniques may struggle to differentiate between LMPPs and the global maximum power point (GMPP), potentially resulting in the algorithm becoming trapped at a local peak. Furthermore, rapid fluctuations in solar irradiance can cause continuous shifts in the location of the GMPP and changes in the shape of the P-V curve. Therefore, for optimal system performance, an MPPT algorithm must be capable of quickly and accurately identifying the GMPP among multiple LMPPs under PSCs [113].

The P-V and P-I characteristics of the photovoltaic system under both uniform and variable irradiance conditions are illustrated in Figure 5.2.

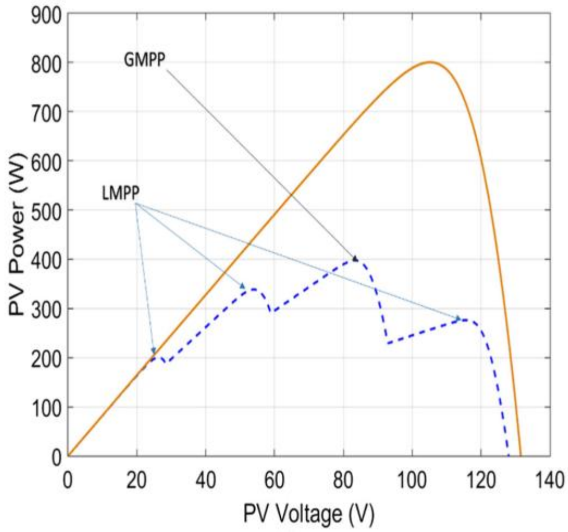

(a)

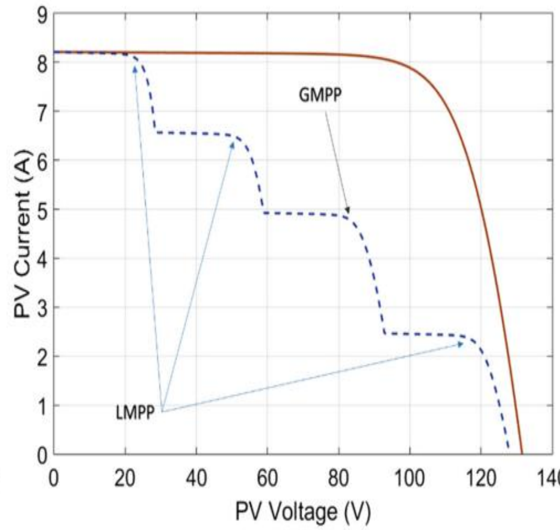

(b)

Figure 5.2 (a) P-V curve, (b) I-V curve under PSC and uniform irradiance [114]

<u>Irradiation patterns:</u>

This study analyzes three distinct partial shading scenarios: middle peak, left peak, and right peak. Each scenario represents a different shading pattern that influences the power-voltage (P-V) characteristics of the photovoltaic system. The subsequent figures illustrate the variations in power output under these shading conditions.

- Middle Peak :

In this scenario, the three PV panels receive different irradiance levels: 1000 W/m² for PV-1, 700 W/m² for PV-2, and 300 W/m² for PV-3. This variation in irradiance creates three distinct peaks at different operating points in the P-V curve. Among these peaks, the Global Maximum Power Point (GMPP) occurs at the middle peak, as illustrated in the following figure. This phenomenon results from the combined effect of partial shading, where multiple Local Maximum Power Points (LMPPs) appear due to the bypass diodes' activation, leading to a complex P-V characteristic curve.

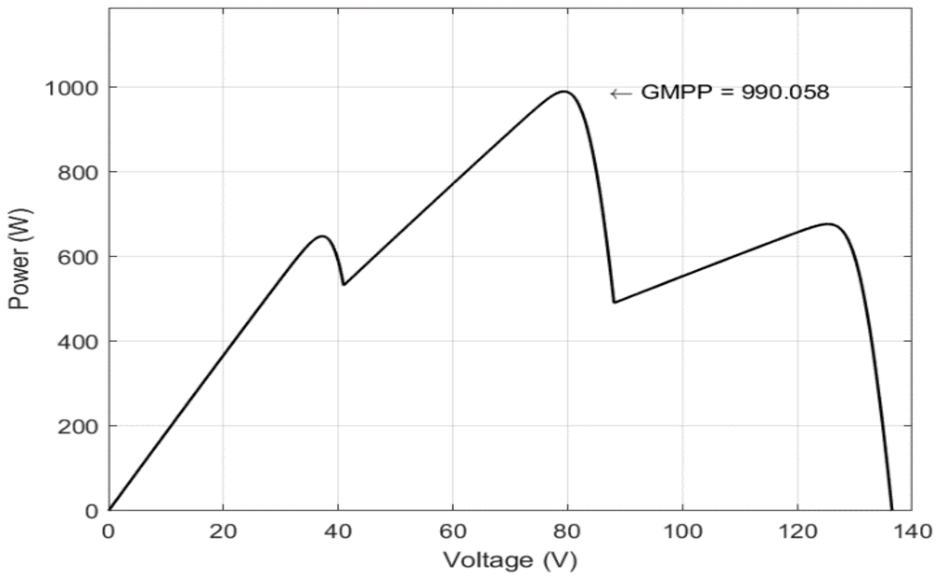

Figure 5.3 Middle peak irradiation pattern

- Left Peak:

In the left peak scenario, the irradiance falling on PV-1, PV-2, and PV-3 is 800, 300, and 200 W/m², respectively. Such a condition results in the formation of three peaks, similar to the previous case, but in this scenario, the global maximum power point occurs at the left-most of those three points. For the specific values of solar irradiation used in this simulation, the maximum power that can be generated is approximately 521.802 W, as depicted below.

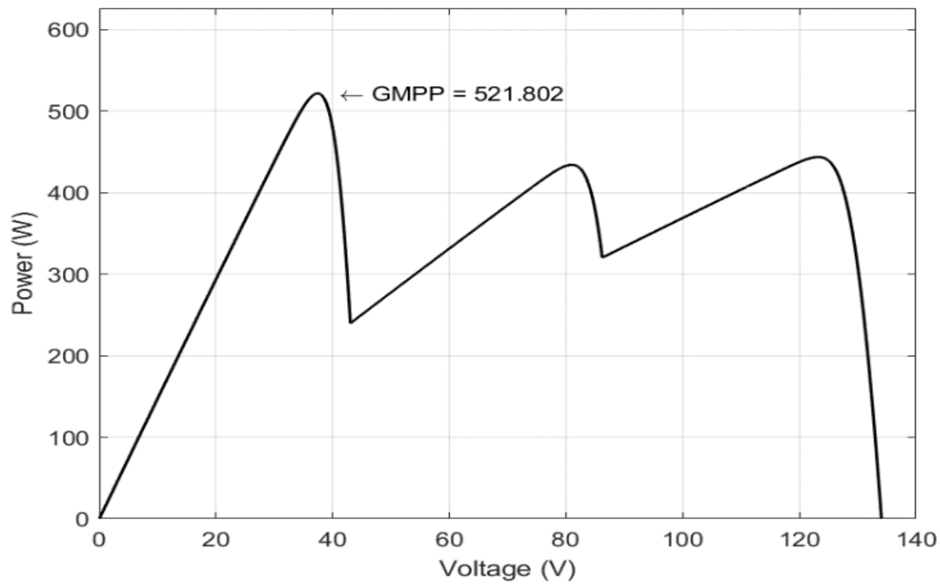

Figure 5.4 Left peak irradiation pattern

- Right Peak:

In the third case, where the global maximum power point (GMPP) is positioned on the right, the solar irradiation values applied to the PV panels are 500 W/m² for PV-1, 700 W/m² for PV-2, and 900 W/m² for PV-3. The power versus voltage curve illustrated in the figure below confirms that the GMPP is indeed located towards the right side, highlighting the impact of varying irradiation levels on the positioning of the maximum power point.

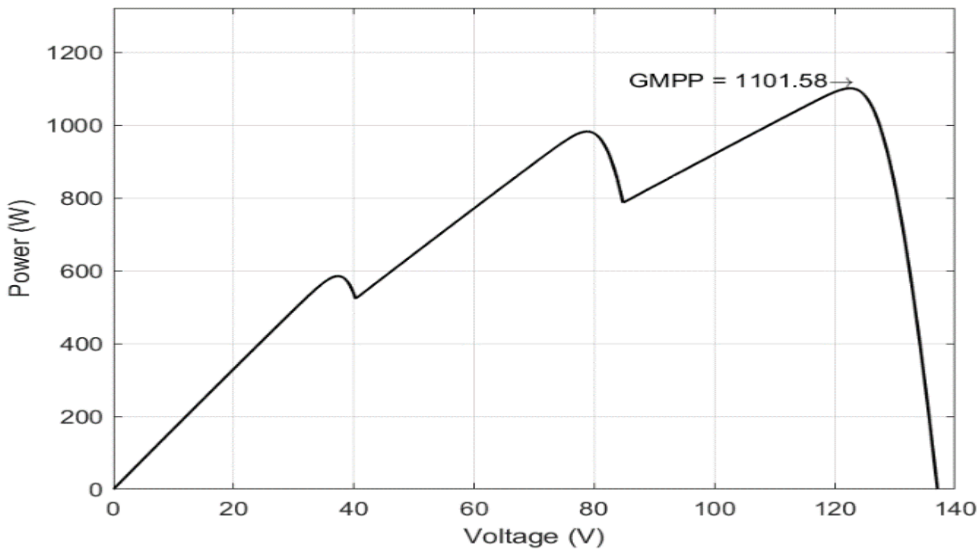

Figure 5.5 Right peak irradiation pattern

5.4 Perturbation and Observation Algorithm (P&O)

The P&O algorithm is the most widely used MPPT technique, primarily due to its balance between simplicity and acceptable performance [115]. This method tracks the MPP by perturbing a single parameter, typically the voltage. By adjusting the duty cycle of the PV system, the operating voltage is modified, which in turn influences the generated power. If the power output increases after a perturbation, it indicates that the system is moving toward the MPP, and the perturbation continues in the same direction. Conversely, if the power output decreases, the system is diverging from the MPP, requiring a reversal in the direction of the perturbation [116], [117].

Despite its simplicity, the effectiveness of P&O largely depends on its convergence speed. One of its primary limitations is the oscillation around the MPP, which results in energy losses due to its inability to precisely stabilize at the exact MPP. Furthermore, the performance of P&O degrades under rapidly changing environmental conditions, such as cloudy weather, where fluctuations in irradiance can mislead the algorithm. This issue becomes more critical under PSC, as P&O struggles to differentiate between local and global MPPs, often getting trapped at a local peak instead of tracking the actual GMPP [118], [119], [120].

5.5 Particle Swarm Optimization (PSO) Algorithm

PSO is a population-based evolutionary search algorithm that maintains a swarm of particles, where each particle represents a potential solution within the swarm [110], [121]. This method determines the optimal parameters that maximize or minimize the objective function within a defined search space. Each particle possesses a current position, a velocity, and a personal best position within the search space. The personal best position, $pbest_i$, corresponds to the location where the particle achieved the highest value as determined by the objective function F, considering a maximization problem. Additionally, the highest value obtained among all personal bests within the swarm is referred to as the global best position, denoted as $gbest_i$ [122].

Once optimal solutions are identified, the particles update their velocities and positions according to the equations provided below.

$$V_i^{k+1} = WV_i^k + C_1 rand_1^k\left(pbest_i^k - X_i^k\right) + C_2 rand_2^k\left(gbest_i^k - X_i^k\right) \tag{5.2}$$

$$X_i^{k+1} = X_i^k + V_i^{k+1} \tag{5.3}$$

where V_i^k represents the velocity of particle i after k iterations, W is the inertia weight that balances exploration and exploitation, and C_1 and C_2 are the acceleration coefficients that control the influence of the personal best ($pbest$) and the global best ($gbest$)

positions, respectively. The terms $rand_1$ and $rand_2$ are random numbers uniformly distributed between 0 and 1, ensuring stochastic behavior in the search process. These parameters collectively guide the movement of each particle toward the optimal solution while maintaining a balance between local and global search capabilities.

5.6 Firefly Algorithm

FA is a metaheuristic optimization algorithm inspired by the collective behavior of fireflies, developed by Yang in 2008 [101]. It is an intelligence-based algorithm that mimics the flashing behavior of fireflies, which they use to attract mating partners and potential prey, commonly observed in tropical and temperate regions. The fundamental principle behind the algorithm is the attractiveness of fireflies—where a less bright firefly is drawn toward a brighter one [113].

The FA operates based on three key assumptions derived from the natural behavior of fireflies:

- Fireflies are not gender-specific, meaning that each firefly is attracted to the brighter and more attractive companion regardless of gender.
- The attractiveness of a firefly is proportional to its brightness, which decreases as the distance between individuals increases. If no brighter firefly exists in its vicinity, it moves randomly.
- The brightness or attractiveness of a firefly is determined by the objective function's value, meaning that better solutions in the search space correspond to higher brightness levels.

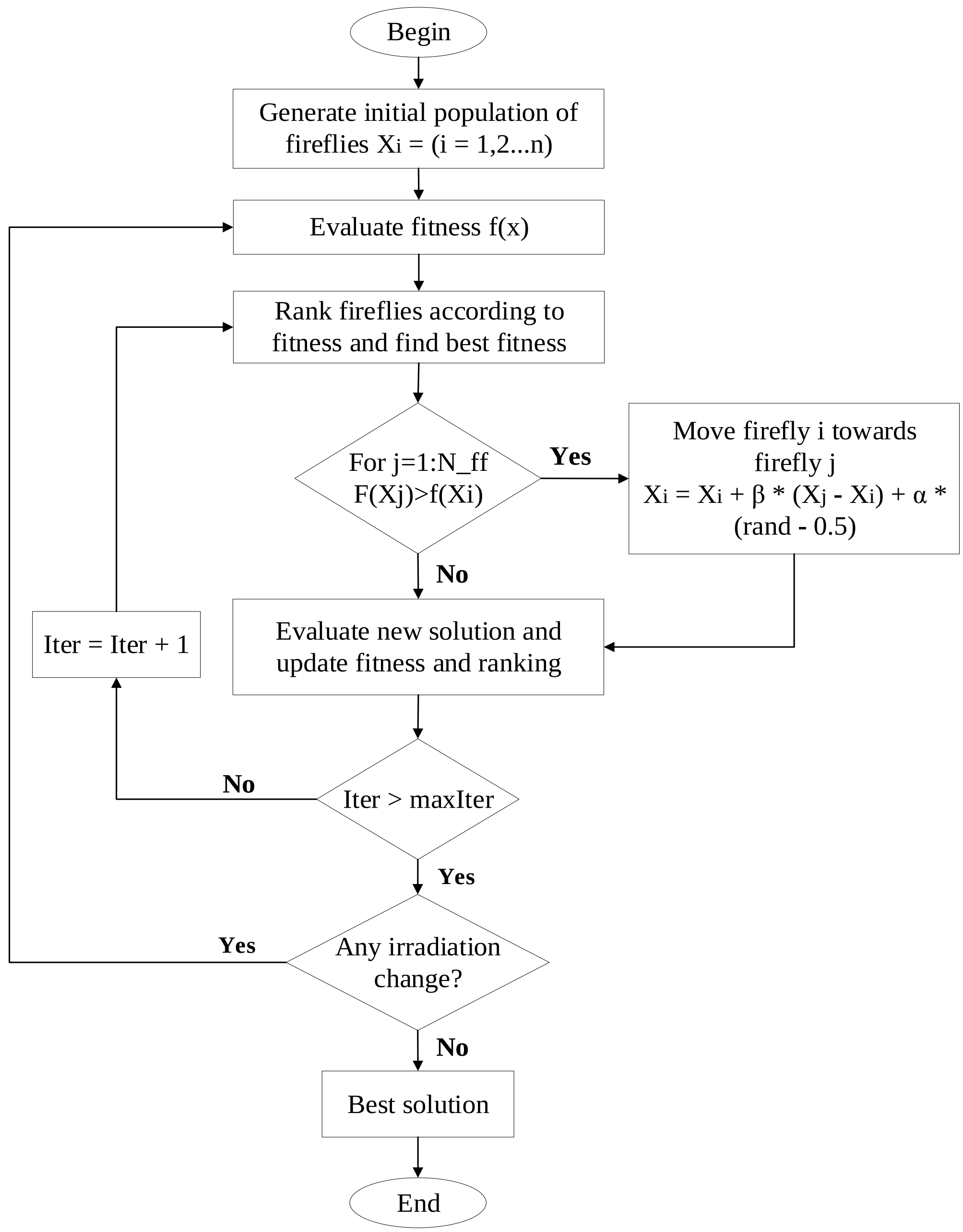

Figure 5.6 Flowchart for the FA

Following these three principles, the FA is applied to MPPT in PV systems, as illustrated in Figure 5.6. The attraction between fireflies is directly proportional to the light intensity perceived by nearby ones. Thus, the attractiveness parameter β is mathematically defined as follows:

$$\beta = \beta_0 e^{-\gamma r^2} \tag{5.4}$$

Where γ is the light absorption coefficient, determining how quickly the attractiveness decreases with distance. β_0 represents the attractiveness at $r = 0$, meaning the maximum attraction when there is no distance between fireflies. The distance between two fireflies i and j, located at positions Xi and Xj, respectively, is determined using the Euclidean distance formula, which is expressed as:

$$r_{ij} = \left\|X_i - X_j\right\| = \sqrt{\sum_{K=1}^{d}\left(X_{i,k} - X_{j,k}\right)^2} \tag{5.5}$$

Where $X_{i,k}$ represents the K_{th} component of the position vector X_i associated with firefly i. This means that each firefly's position is defined in a multi-dimensional search space, where each dimension corresponds to a specific parameter in the optimization problem. The movement of firefly i towards a more attractive firefly j is governed by the following equation:

$$X_i^{t+1} = X_i^t + \beta_0 e^{-\gamma r^2}\left(X_j - X_i\right) + \alpha\varepsilon_i \tag{5.6}$$

Where the first term X_i^t represents the current position of the firefly i, while the second term represents the attraction between fireflies, ensuring that the less bright firefly moves towards the brighter one. The strength of this attraction is controlled by β, which depends on the light intensity and the distance between fireflies. The third term, $\alpha\varepsilon_i$, introduces a randomization factor, which helps maintain diversity in the search space and prevents the algorithm from getting stuck in local optima. Here, α is the randomization coefficient that determines the magnitude of the random step and ε_i is a random vector, where each component is drawn from either a Gaussian distribution or a uniform distribution.

5.7 Modified Firefly Algorithm (MFA)

Owing to its efficiency, rapid execution time, and high stability, the FA offers an effective solution for complex non-linear optimization problems. However, it has certain drawbacks. One major limitation is that all algorithm coefficients remain constant throughout each iteration, preventing adjustments over time or across iterations. Additionally, FA lacks a mechanism to store historical data, which could be valuable for optimization. These constraints necessitate the development of an enhanced version, known as the Modified Firefly Algorithm (MFA).

MFA is designed to address FA's limitations and shortcomings. One approach to improving the algorithm's performance involves enhancing the balance between exploration and exploitation by adjusting the fixed parameter values. In the original FA, many parameters in the movement update equation are pre-set and remain unchanged. However, in the proposed MFA, the randomization and attractiveness parameters are initialized at the beginning and dynamically updated throughout the optimization process. The goal of these modifications is to refine local searches, improve accuracy near local optima, and enhance performance in the final optimization stages while preventing random fluctuations. These adjustments ensure a more structured and efficient search process, reducing the likelihood of stagnation. Another advantage of MFA is its ability to accelerate convergence towards the optimal solution. The primary improvement in MFA lies in the enhancement of firefly movement. The mathematical representation used to improve firefly movement is given as [85]:

$$x_i^{Itr+1} = x_i^{Itr} + \beta\left(x_i^{Itr} - x_j^{Itr}\right) + \alpha\epsilon_i^{Itr} \tag{5.7}$$

The parameters in conventional FA may result in varying performances when solving optimization problems. However, it is hard to manually tune the parameters by looking at various problems with distinguish characteristics. A new strategy has been employed in the MFA to avoid premature convergence of classical FA. This strategy is vital for the selection of the parameter of randomization. Accordingly, the randomness coefficient α equation can be expressed as [85]:

$$\alpha(Itr_i) = exp\left(1 - \left(\frac{Itr_{max}}{Itr_{max} - Itr_i}\right)^c\right) \tag{5.8}$$

Where c denotes an integer that determines the rate at which randomness decays, Itr_{max} represents the maximum number of iterations, and Itr_i signifies the current iteration number.

Additionally, the parameter γ plays a crucial role in defining the variation in convergence speed and attractiveness, as expressed in [85]:

$$\gamma(Itr_i) = 1 - exp\left(1 - \left(\frac{Itr_{max}}{Itr_{max} - Itr_i}\right)^c\right) \tag{5.9}$$

With this adjustment, the proposed firefly algorithm avoids becoming trapped in local extrema and enhances its convergence speed, leading to a more optimal solution by maintaining a balance between local and global search.

Heterogeneous adaptation is incorporated into the updating rule using Gray Relational Analysis (GRA), which serves as a measurement technique for finite sequences with incomplete information, as proposed in previous studies. This approach is implemented to improve the search capabilities of fireflies. During the search process, two updating equations are defined and selected randomly, as presented in Equation [85].

$$x_{i+1} = \begin{cases} \beta(i)x_i + x_j(1-\beta(i)) + \alpha(i)\epsilon_i & rand > 0.5 \\ \frac{NG-i}{NG}(1-\delta)x_i + \delta x_{best} & Elsewhere \end{cases} \tag{5.10}$$

Here, δ denotes the gray coefficient, which influences the adaptation process, while NG represents the total number of generations in the optimization procedure. The execution process of the MFA for MPPT in a PV system, incorporating the modifications discussed earlier, is illustrated in Figure 5.7. This process integrates adaptive parameter tuning and an enhanced movement strategy to improve tracking efficiency and convergence speed, ensuring accurate identification of the GMPP under varying PSCs.

5.8 Application of MFA to MPPT

The application of the MFA for tracking the MPP PSC is elaborated in this section. The execution process of the algorithm and the block diagram of the MPPT scheme utilizing the MFA approach within a PV system are presented in Figure 5.7 and Figure 5.8, respectively. The system configuration consists of three photovoltaic modules connected in series, forming the primary power generation unit. Additionally, a DC-DC boost converter is employed to interface the PV system with the load, ensuring efficient power transfer and voltage regulation.

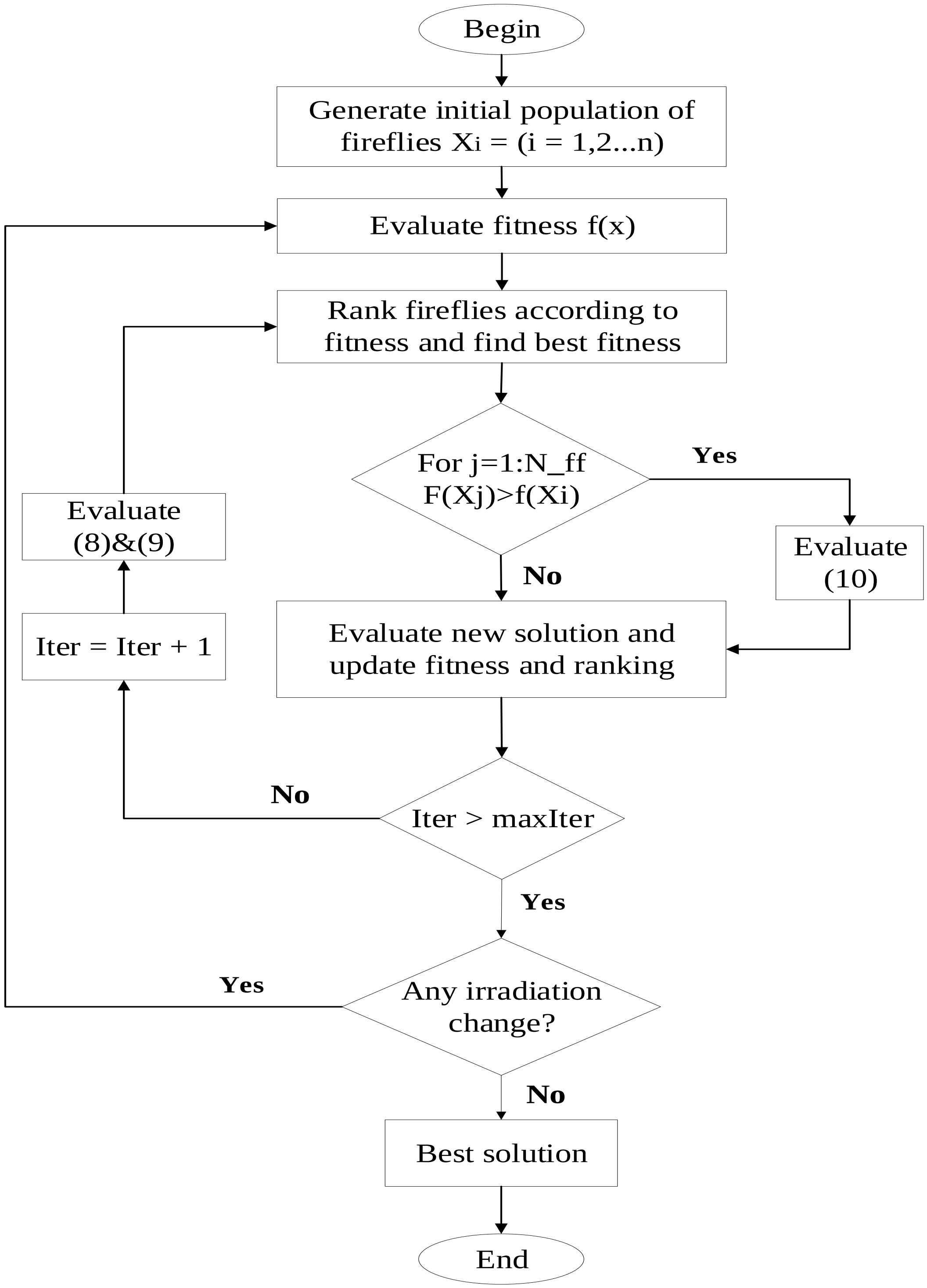

Figure 5.7 Flowchart for the MFA

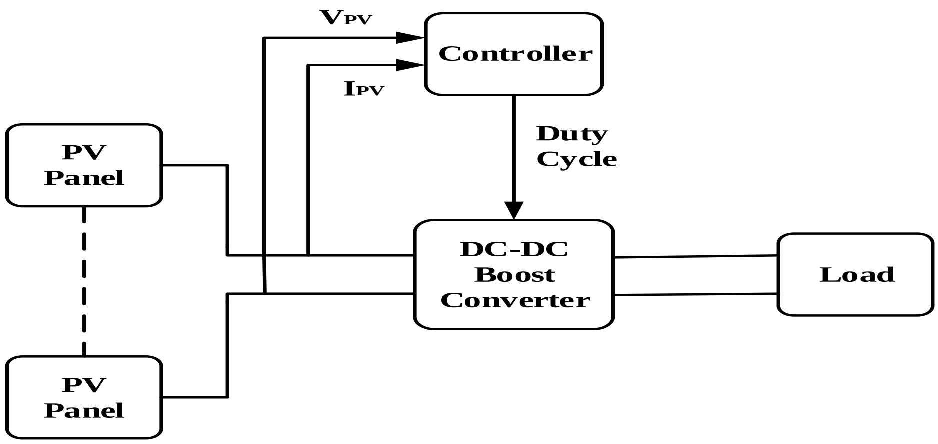

Figure 5.8 Block diagram of the tracking scheme based on PSO, FA, and MFA methods

The operational steps of the MFA algorithm for MPPT are systematically described in the following steps.

Step 1: Parameter Initialization: Define the key MFA parameters, including the attraction factor (β), mutation factor (δ), adaptation control (c), step size coefficient (α) light absorption coefficient (γ), maximum iterations (Itr_{max}), and firefly population size (N_{ff}). Firefly positions represent duty cycle values, and their brightness corresponds to power output.

Step 2: Firefly Position Initialization: Randomly distribute fireflies within the allowable duty cycle range ($d = 0.1$ to $d = 0.9$) Each firefly's intensity (power output) is computed, and an initial best firefly position is assigned.

Step 3: Firefly Brightness Evaluation: Each firefly's assigned duty cycle is applied to the PV system, and the corresponding power output is measured. The brightness (fitness) of each firefly is determined based on its power output. The iteration counter is incremented.

Step 4: Firefly Position Update: Fireflies adjust their positions using Equation (10), moving toward the brightest firefly in the swarm. Parameters (α) and (γ) are also updated dynamically using Equations (8) and (9) to enhance convergence and avoid local optima.

Step 5: Ranking and Best Solution Identification: Fireflies are ranked according to their brightness levels. The firefly with the highest brightness is identified as the best solution (X_{best}), and its duty cycle is stored as the optimal candidate.

Step 6: Stopping Condition Check: If the predefined iteration limit (Itr_{max}) is reached, the process terminates, and the best duty cycle is recorded as the final solution. Otherwise, the algorithm proceeds to the next step.

Step 7: Adaptive Parameter Update: If the stopping condition is not met, the parameters (α) and (γ) are adaptively updated using Equations (8) and (9) to refine firefly movement and improve optimization accuracy.

Step 8: Irradiance Change Detection: Before the next iteration, the algorithm verifies if a change in irradiance has occurred. If an irradiance change is detected, fireflies are reinitialized, and the process returns to *Step 2*. If no change is detected, the algorithm proceeds to *Step 3*.

Step 9: Iteration Process: The algorithm continues iterating, updating firefly positions, and refining solutions until the stopping condition is reached.

Step 10: Record the Optimal MPP: Once the stopping criterion is satisfied, the best duty cycle and corresponding maximum power output are recorded, and the algorithm terminates.

The components of the simulation model, along with their corresponding parameter values utilized in this study, are presented in Table 5.1.

Table 5.1 System model and controller parameters

System	Parameter	Description	Value
PV module	N_{cell}	Cells per module	60
	V_{oc} (V)	Open circuit voltage	45.7
	I_{sc} (A)	Short circuit current	18.53
	P_{max} (W)	Maximum power	660.366
	V_{mp} (V)	Voltage at MPP	37.8
	I_{mp} (A)	Current at MPP	17.47
P&O	d_{max}	Maximum duty ratio	0.9
	d_{min}	Minimum duty ratio	0.1
	ΔD	Change in duty	$5*10^{-7}$
PSO	ω	inertia	0.1
	$C1$	Self-adjustment weight	2
	$C2$	Social-adjustment weight	0.4
	Np	Number of particles	5
	lb	Lower bound	0.1
	ub	Upper bound	0.9
	$Iter_{max}$	Maximum number of iterations	20
FA	α	Coefficient of randomizer	0.9
	β_0	Attractiveness coefficient	1.9
	γ	Light absorption coefficient	1.9
	N_ff	Number of fireflies	100
	lb	Lower bound	0.1
	ub	Upper bound	0.9
	$Iter_{max}$	Maximum number of iterations	20

Table 5.1 System model and controller parameters (continued)

System	Parameter	Description	Value
MFA	α	Coefficient of randomizer	0.9
	β_0	Attractiveness coefficient	1.9
	γ	Light absorption coefficient	1.9
	C	Speed of decaying of the randomness	1.0
	δ	Gray coefficient	0.8
	N_ff	Number of fireflies	100
	lb	Lower bound	0.1
	ub	Upper bound	0.9
	$Iter_{max}$	Maximum number of iterations	20
Boost Converter	$L(mH)$	Inductance	0.9
	C_{in} (μF)	Input capacitance	1.9
	C_{out} (μF)	Output capacitance	1.9
Simulation	Ts (μs)	Sampling time	1.0
	fs (kHz)	Switching frequency	0.8

5.9 Simulation Results

The simulation model designed to evaluate the performance of the algorithms is configured as illustrated in Figure 5.9. It comprises three solar PV panels connected in series, each receiving distinct solar irradiance levels to emulate partial shading conditions. Additionally, the system includes a boost DC-DC converter, a resistive load, and an MPPT controller capable of operating with P&O, PSO, FA, and MFA algorithms. The controller generates the duty ratio, which is then fed into a PWM generator to regulate the IGBT of the boost converter.

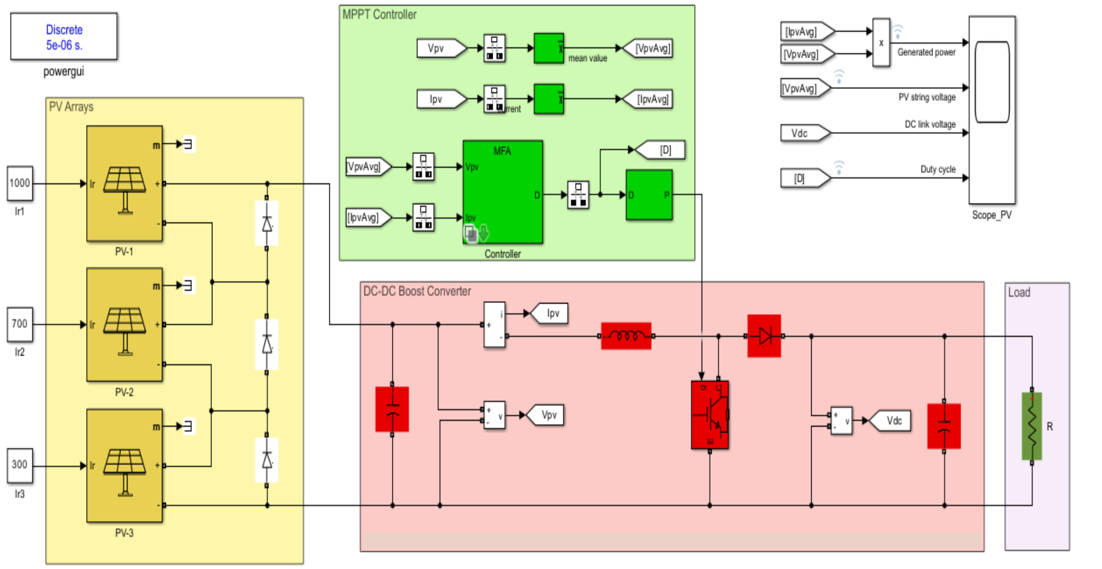

Figure 5.9 MATLAB/Simulink simulation of the P&O, PSO, FA, and MFA based MPPT system

5.9.1 Effect of PSCs

- Middle Peak.

Under the previously discussed middle peak condition (PV-1 at 1000 W/m², PV-2 at 700 W/m², and PV-3 at 300 W/m²), four MPPT algorithms were evaluated for a load resistance of 20 Ω. Figure 5.10 illustrates the simulation scenario where the three PV panels operate under middle peak conditions with the P&O MPPT controller. As shown in Figure 5.10 (a), the P&O algorithm successfully reaches the maximum power point at 939.73 W and maintains stability for the remainder of the simulation.

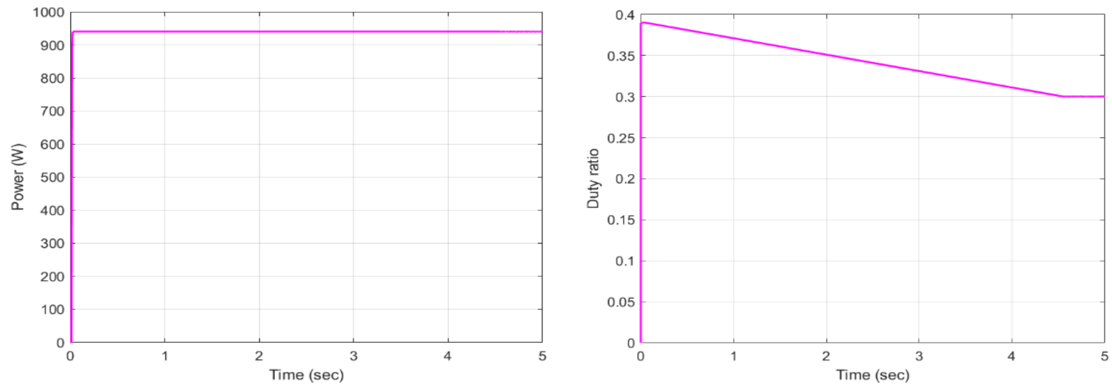

(a) PV power output (b) PWM duty ratio

Figure 5.10 Middle-peak P&O performance

The performance of the PSO algorithm in tracking the maximum power is presented in Figure 5.11. Figure 5.11 (b) indicates that the algorithm searches for the optimal duty ratio for approximately the first 2 seconds (equivalent to 20 iterations) before settling at a duty ratio of approximately D = 0.31, yielding an output power of around 940.29 W. In Figure 5.12, the power output of the PV system, Figure 5.12 (a), and the duty cycle, Figure 512 (b), under the FA algorithm are illustrated. In this case, the power generated is 829.89 W, with a duty cycle settling around D = 0.45, demonstrating that FA fails to effectively track the GMPP.

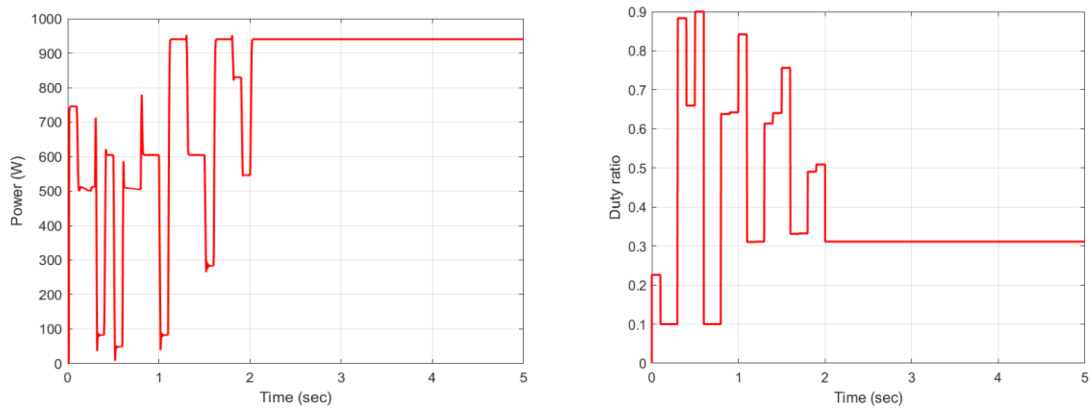

(a) PV power output (b) PWM duty ratio

Figure 5.11 Middle-peak PSO performance

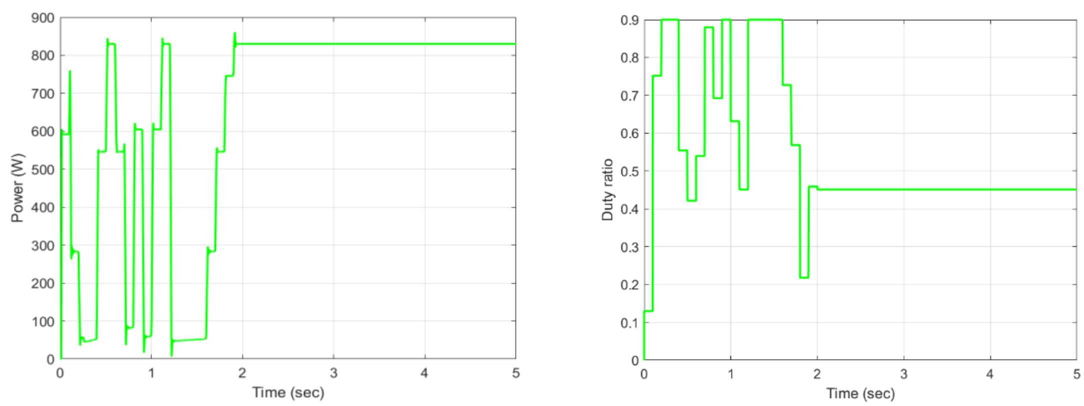

(a) PV power output (b) PWM duty ratio

Figure 5.12 Middle-peak FA performance

The power output and the corresponding duty ratio for the MFA algorithm are displayed in Figure 5.13. Once the maximum iteration count is reached, the duty ratio stabilizes at D = 0.39, and the power output achieves approximately 940.29 W, which matches the results obtained using PSO.

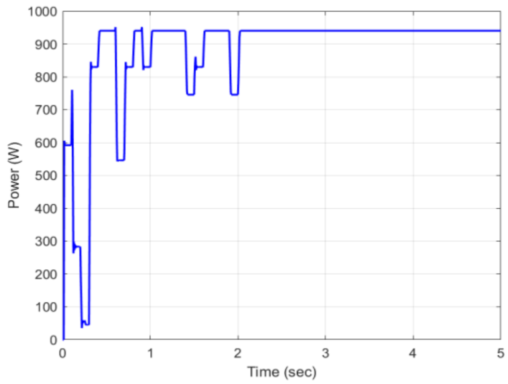

(a) PV power output

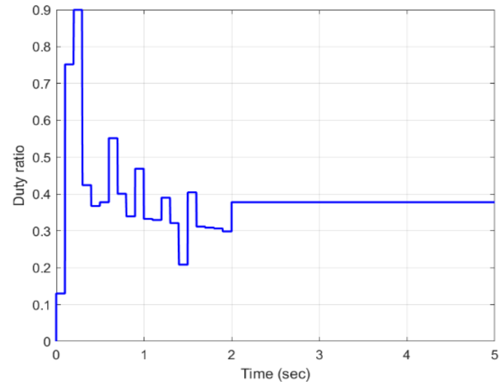

(b) PWM duty ratio

Figure 5.13 Middle-peak MFA performance

For comparative analysis, the power output curves for all four algorithms under the middle peak shading condition are plotted together in Figure 5.14. The results indicate that PSO and MFA demonstrate superior MPPT tracking capabilities compared to P&O and FA. Regarding convergence speed, MFA reaches the peak power level faster than PSO. Among the remaining algorithms, P&O exhibits better tracking performance than FA. Notably, all heuristic algorithms PSO, FA, and MFA were configured with a maximum iteration limit of 20. Since these algorithms update their solutions at intervals of 0.1 seconds, they cease searching for improved solutions after 2 seconds of simulation time.

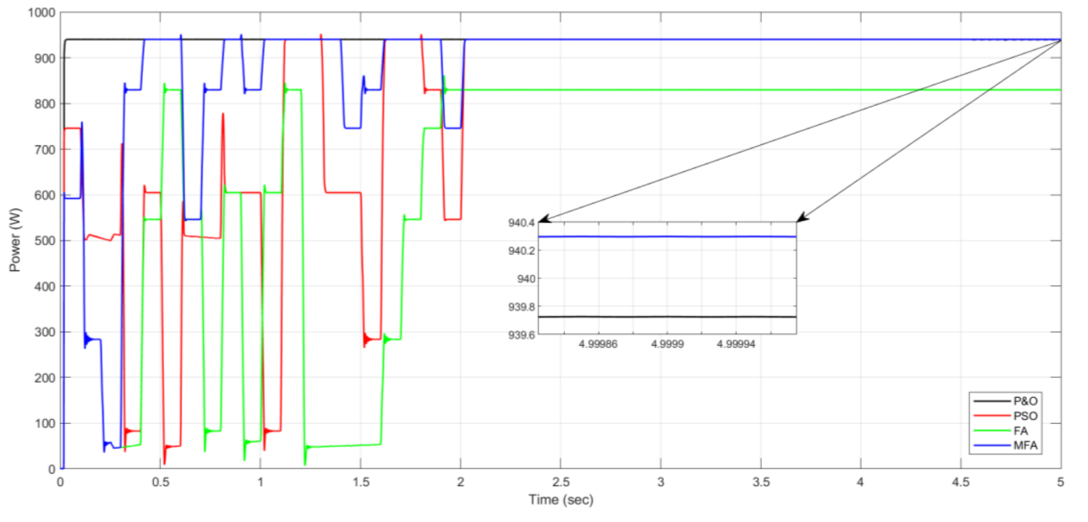

Figure 5.14 Comparison of algorithms for middle peak

- Left Peak.

In this case, the left peak occurs when the GMPP is positioned at the left-most peak among the three possible peaks. Similar to the middle peak scenario, the three PV panels experience different levels of solar irradiation, simulating partial shading conditions. The irradiation levels are set as follows: PV-1 at 800 W/m², PV-2 at 300 W/m², and PV-3 at 200 W/m². By running simulations for the four MPPT algorithms, the results obtained are presented in the following figures.

Figure 5.15 illustrates the simulation results under left peak conditions, where the MPPT controller is P&O. In Figure 5.15 (a), it can be observed that the P&O algorithm converges to the maximum power 348.67 W within approximately 0.5 seconds and remains stable for the rest of the simulation.

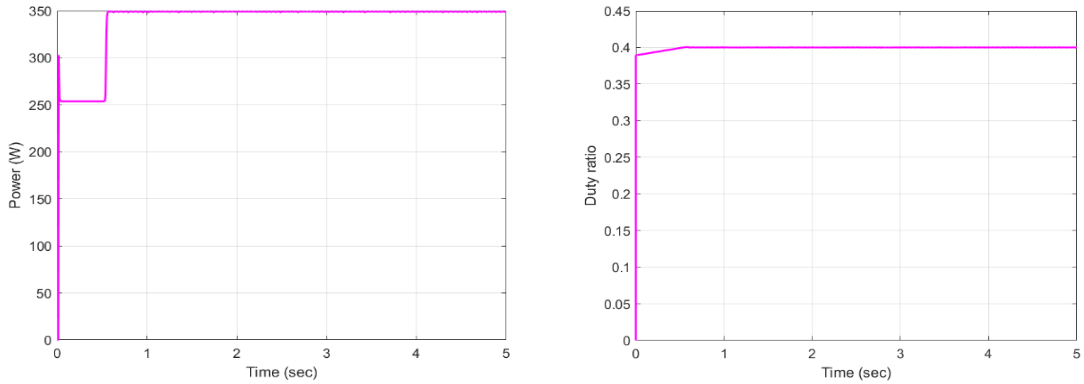

(a) PV power output (b) PWM duty ratio

Figure 5.15 Left-peak P&O performance

The performance of the PSO algorithm in tracking the maximum power is depicted in Figure 5.16 (b), where the algorithm searches for the optimal duty ratio corresponding to maximum power during the initial phase of 20 iterations over 2 seconds before stabilizing at d = 0.1, yielding an output power of 433.78 W. Similarly, Figure 5.17 illustrates the power output of the PV system and the duty ratio using the FA controller. It shows that the generated power reaches 487.53 W, with the duty ratio remaining around d = 0.45.

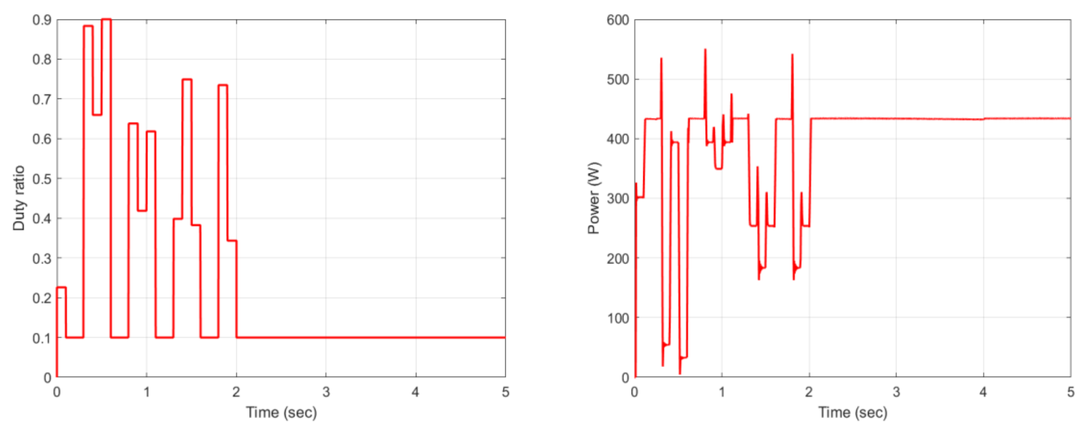

(a) PV power output (b) PWM duty ratio

Figure 5.16 Left-peak PSO performance

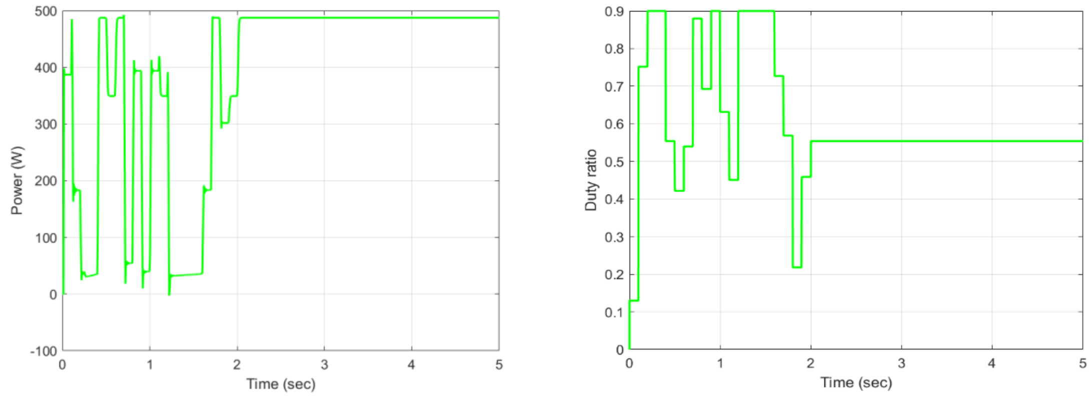

(a) PV power output (b) PWM duty ratio

Figure 5.17 Left-peak FA performance

Figure 5.18 illustrates the power output of the PVs and the duty ratio of the MFA, showing a performance similar to the FA, where the generated power reaches 487.53 W and the duty ratio for the MFA remains around 0.54. Figure 5.19 presents a comparison of the four algorithms under the left peak shading pattern, demonstrating that the FA and MFA algorithms achieve superior MPP tracking performance compared to the other two methods. Additionally, the MFA exhibits a faster convergence to the optimal duty cycle than the other algorithms.

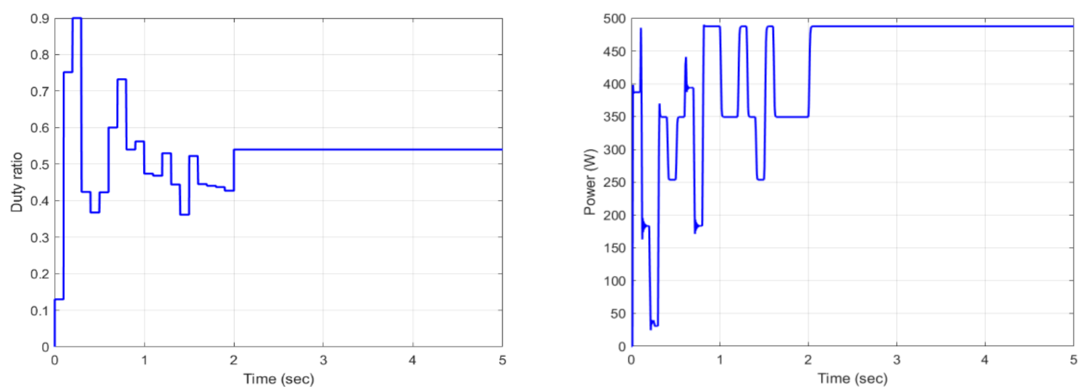

(a) PV power output (b) PWM duty ratio

Figure 5.18 Left-peak MFA performance

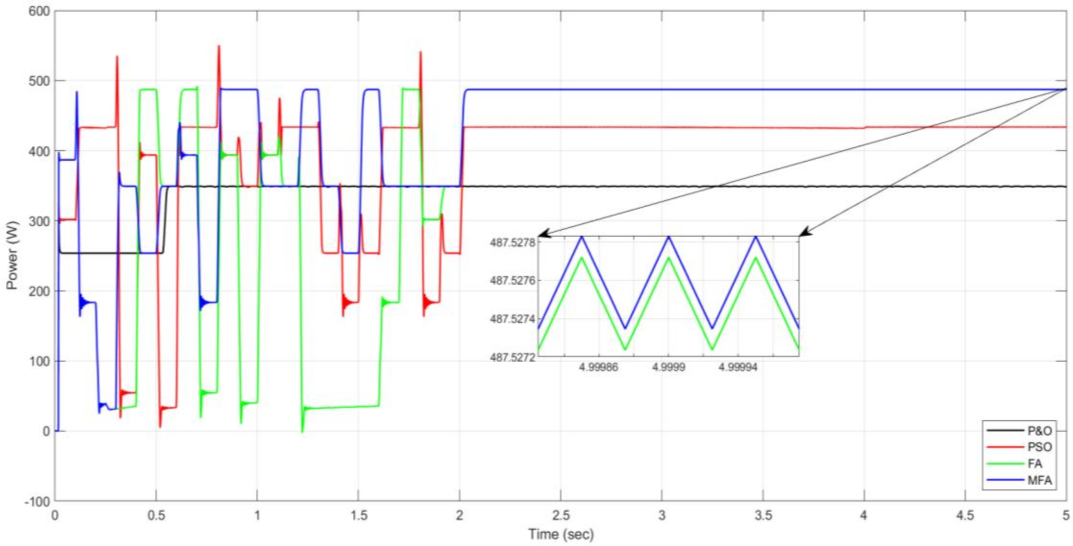

Figure 5.19 Comparison of algorithms for left peak

- Right Peak.

Under the right peak condition, the simulation results for the four MPPT algorithms are analyzed. Figure 5.20 presents the performance of the P&O algorithm, where the three PVs operate under the right peak condition. As seen in Figure 5.20 (a), the P&O algorithm successfully tracks the maximum power at 931.45 W and maintains this value throughout the simulation. Figure 5.21 illustrates the performance of the PSO algorithm in tracking maximum power, demonstrating that the algorithm searches for the optimal duty ratio corresponding to maximum power for the first two seconds, stabilizing at d = 0.1 and generating an output power of 1.051 kW.

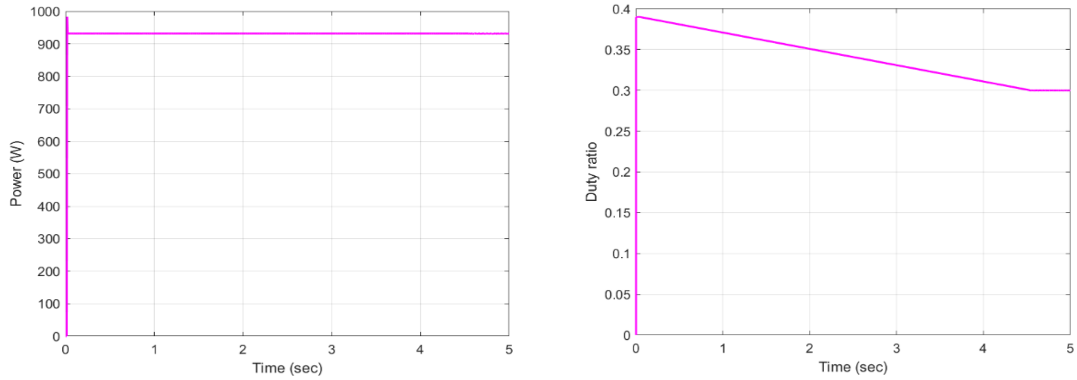

(a) PV power output (b) PWM duty ratio

Figure 5.20 Right-peak P&O performance

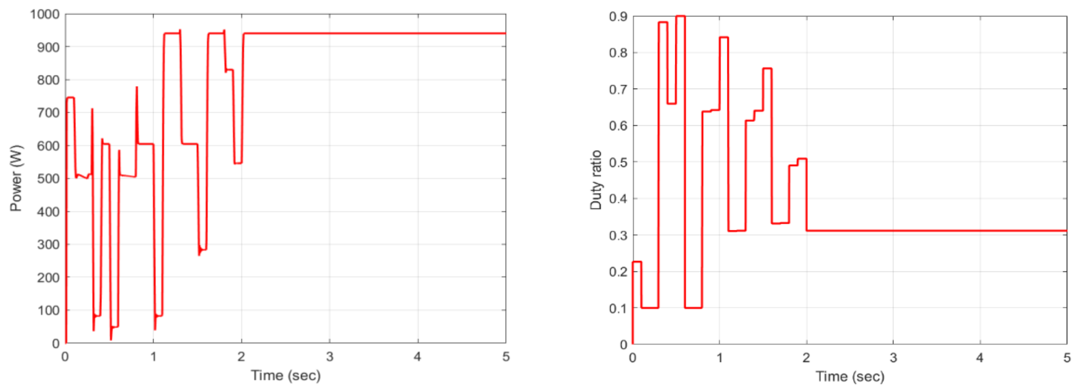

(a) PV power output (b) PWM duty ratio

Figure 5.21 Right-peak PSO performance

Figure 5.22 displays the power output of the PV system and the duty ratio for FA, revealing that the generated power reaches 841.25 W with a duty cycle of approximately 0.21. However, it is evident that the algorithm does not efficiently track the GMPP. Figure 5.23 presents the power output and duty ratio for MFA, showing a performance similar to FA, with power generation reaching 1.067 kW and a duty ratio of approximately 0.15.

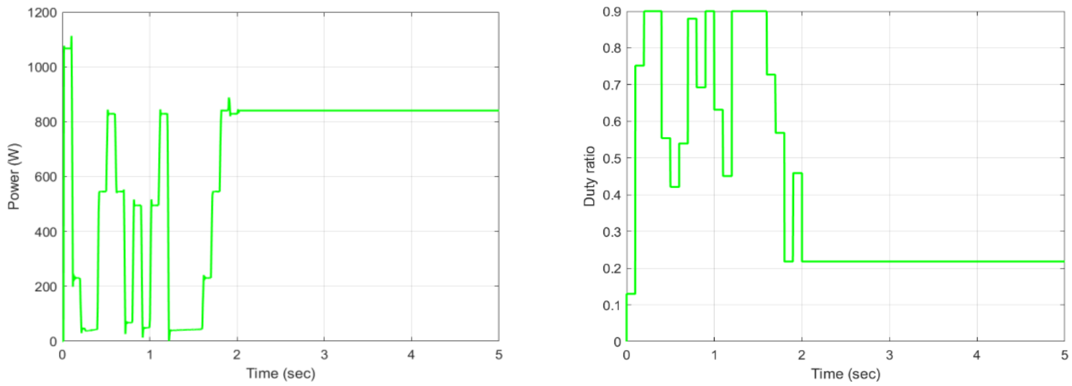

(a) PV power output (b) PWM duty ratio

Figure 5.22 Right-peak FA performance

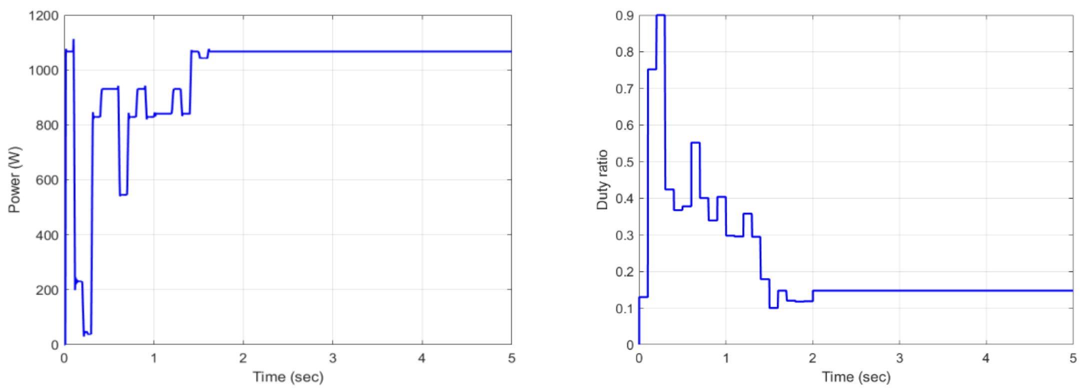

(a) PV power output (b) PWM duty ratio

Figure 5.23 Right-peak MFA performance

For comparative analysis, Figure 5.24 illustrates the power output of the PVs for all four algorithms. From these results, it is evident that MFA and PSO exhibit superior performance compared to the other two algorithms, with MFA emerging as the most effective due to its faster and more consistent convergence to the optimal duty ratio.

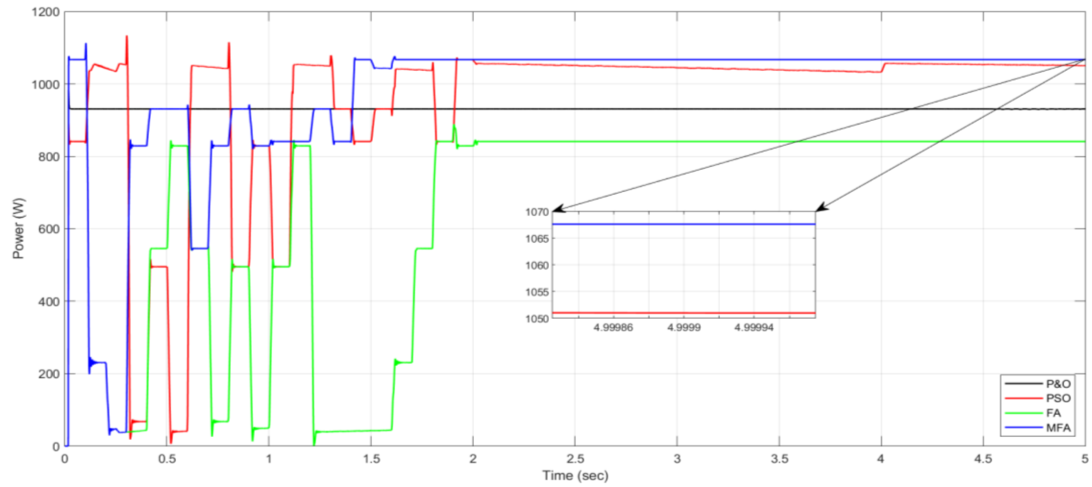

Figure 5.24 Comparison of algorithms for left peak

A quantitative comparison of the four algorithms under the three partial shading conditions is provided in Table 5.2, where efficiency is calculated based on the behavior of the solar PV system. The GMPP for each specific shading pattern was identified, and the power output obtained from each algorithm was determined through simulation. Efficiency was then computed as the ratio of the power output achieved by each controller to the ideal GMPP, as formulated in Equation 11.

$$Efficiency\ (\eta) = \frac{P_{Algorithm}}{P_{GMPP}} * 100\% \qquad (11)$$

where $P_{Algorithm}$ represents the power output achieved by the MPPT algorithms, and P_{GMPP} denotes the ideal maximum power generated by the PV system.

Table 5.2 Performance of P&O, PSO FA, and MFA under different shading conditions

Shading pattern	**Techniques**	**Power (W)**	**Global power (W)**	**Efficiency (%)**
Middle Peak	P&O	939.73	990.05	94.92
	PSO	940.29		94.97
	FA	828.89		83.72
	MFA	940.29		94.97
Left Peak	P&O	348.67	521.80	66.82
	PSO	433.78		83.13
	FA	487.53		93.43
	MFA	487.53		93.43
Right Peak	P&O	931.45	1101.58	84.56
	PSO	1051		95.40
	FA	841.25		76.37
	MFA	1067		96.86

5.9.2 Effect of Load Resistance

The effectiveness of MPPT heuristic algorithms under varying load resistance conditions plays a crucial role in assessing their adaptability for real-world applications. To systematically evaluate the overall performance of the implemented algorithms, the mean efficiency η_{mean} is computed across all resistance values for each peak condition. The mean efficiency is determined using Equation 12:

$$\eta_{mean} = \frac{1}{N}\sum_{i=1}^{N}(\eta_i) \tag{12}$$

where *N* denotes the total number of resistance values analyzed, and η_i represents the efficiency of the algorithm at a specific resistance R_i .

- Resistance variation under middle peak condition.

The MPPT performance under varying resistance values for the middle peak condition is illustrated in the figures below. Figure 5.25 demonstrates the performance of PSO, while Figure 5.26 and Figure 5.27 depict the performance of FA and MFA, respectively. For this condition, the calculated mean efficiency values were 85.85% for PSO, 92.39% for FA, and 94.26% for MFA. The PSO algorithm exhibited significant fluctuations in efficiency, reaching a low of 61.66% at R=40Ω before recovering at higher resistances. FA displayed a more stable performance, maintaining efficiency values consistently above 83.72% and achieving a peak efficiency of 99.90% at R=70Ω. MFA demonstrated the highest mean efficiency among the three algorithms, sustaining values above 88.31% across all resistance variations and peaking at 99.90% for R=70Ω. These results affirm MFA's superior adaptability in tracking the maximum power under the middle peak shading condition. The impact of different load resistances on MPPT performance for this condition is summarized in Table 5.3.

Table 5.3 Resistance variation under middle peak condition

R_i (Ω)	PSO		FA		MFA	
	P (W)	η_i	**P (W)**	η_i	**P (W)**	η_i
20	940.29	94.97%	828.89	83.72%	940.29	94.97%
30	916.05	92.53%	916.05	92.53%	916.05	92.53%
40	610.46	61.66%	988.64	99.86%	988.64	99.86%
50	752.51	76.01%	874.27	88.31%	874.27	88.31%
60	891.13	90.01%	891.13	90.01%	891.13	90.01%
70	989.06	99.90%	989.06	99.90%	989.06	99.90%
η_{mean}	85.85%		92.39%		94.26%	

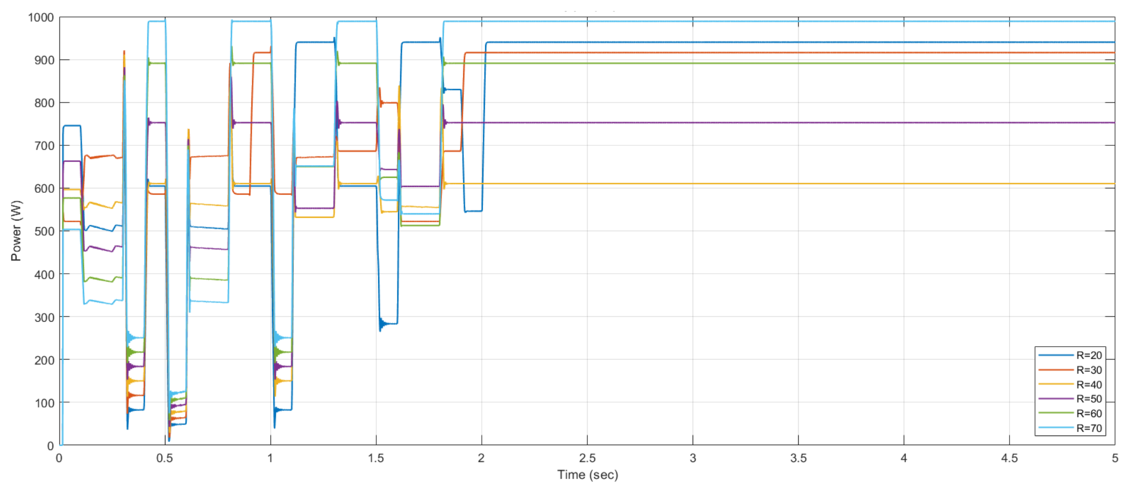

Figure 5.25 PSO algorithm for different values of R under the middle peak condition

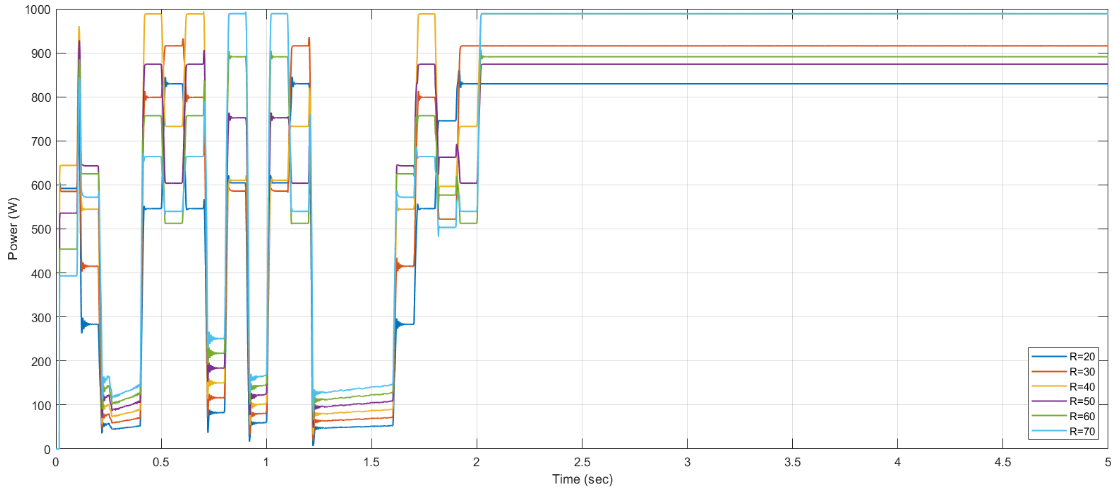

Figure 5.26 FA algorithm for different values of R under the middle peak condition

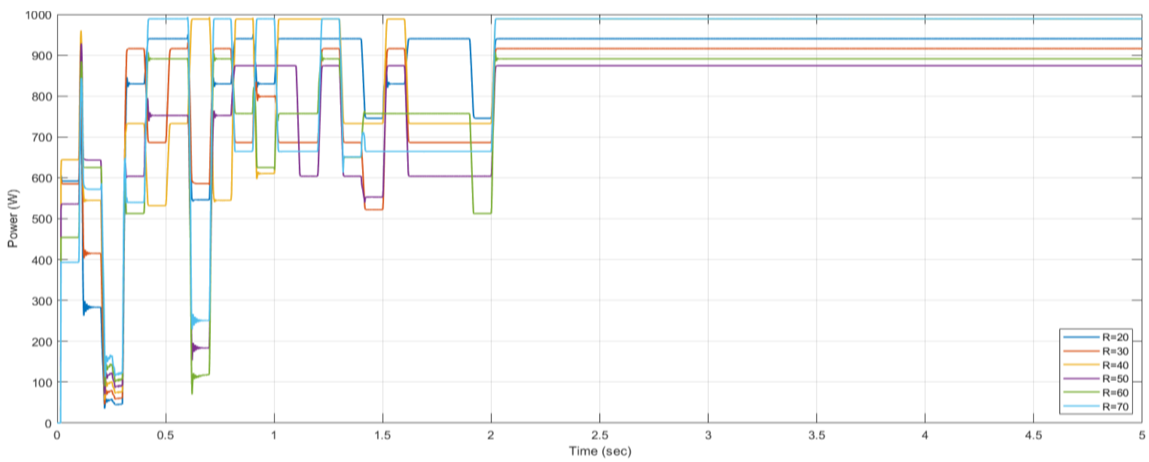

Figure 5.27 MFA algorithm for different values of R under the middle peak condition

- Resistance variation under left peak condition

The MPPT performance under varying resistance values for the left peak condition is illustrated in the figures below. Figure 5.28 shows the performance of PSO, while Figure 5.29 and Figure 5.30 present the performance of FA and MFA, respectively. For this condition, the calculated mean efficiency values were 85.57% for PSO, 93.26% for FA, and 93.26% for MFA. The PSO algorithm exhibited noticeable fluctuations, with efficiency dropping to 77.30% at R=70Ω, indicating its sensitivity to changes in load resistance. In contrast, FA and MFA displayed significantly better tracking performance, maintaining efficiency values consistently above 93% across most resistances and reaching a peak efficiency of 99.83% at R=30Ω. The similar performance of FA and MFA under this condition suggests that both algorithms are well-suited for tracking the MPP when shading patterns result in left-dominant peaks in the P-V curve. The impact of different load resistances on MPPT performance for the left peak condition is summarized in Table 5.4.

Table 5.4 Resistance variation under left peak condition

Ri (Ω)	**PSO**		**FA**		**MFA**	
	P (W)	**ηi**	**P (W)**	**ηi**	**P (W)**	**ηi**
20	433.78	83.13%	487.53	93.43%	487.53	93.43%
30	520.92	99.83%	520.92	99.83%	520.92	99.83%
40	451.44	86.52%	451.44	86.52%	451.43	86.51%
50	435.50	83.46%	435.50	83.46%	435.50	83.46%
60	434.14	83.20%	507.24	97.21%	507.24	97.21%
70	403.33	77.30%	517.19	99.12%	517.19	99.12%
η_{mean}	85.57%		93.26%		93.26%	

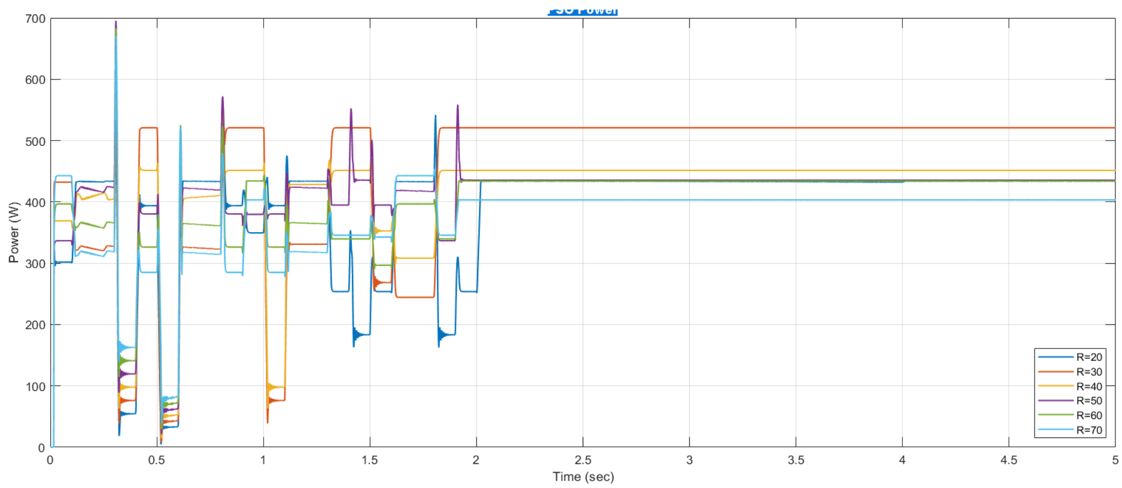

Figure 5.28 PSO algorithm for different values of R under the left peak condition

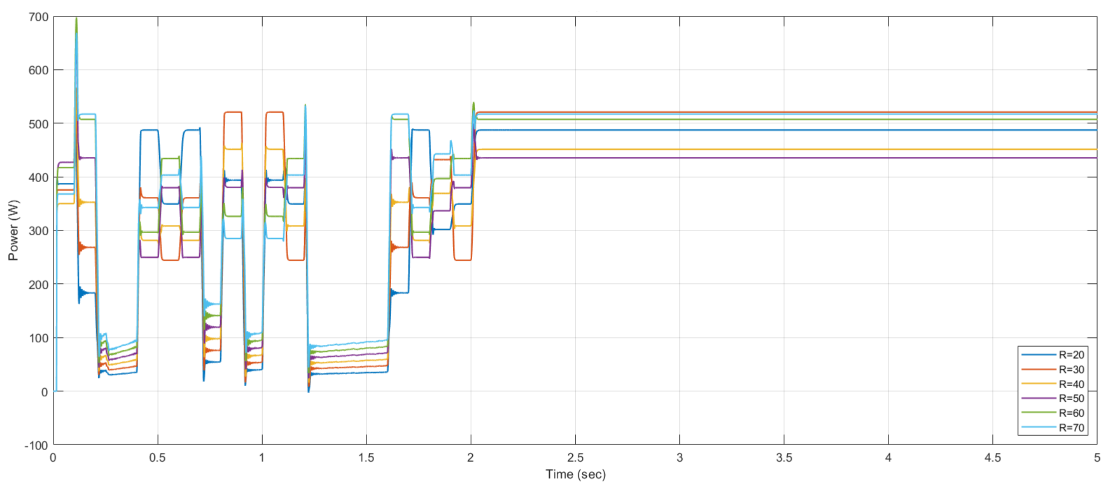

Figure 5.29 FA algorithm for different values of R under the left peak condition

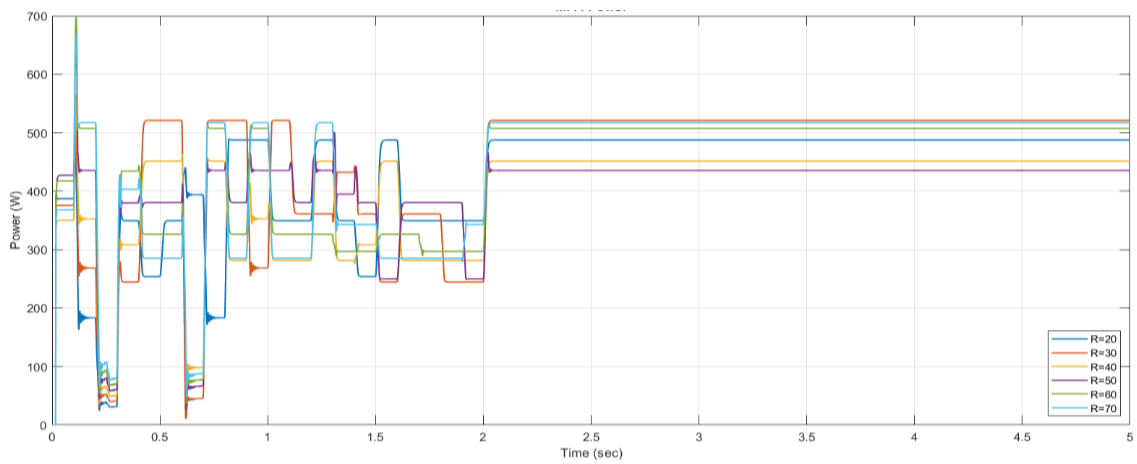

Figure 5.30 MFA algorithm for different values of R under the left peak condition

- Resistance variation under right peak condition

The MPPT performance under varying resistance values for the right peak condition is illustrated in the figures below. Figure 5.31 presents the performance of PSO, while Figure 5.32 and Figure 5.33 show the performance of FA and MFA, respectively. For this condition, the mean efficiency values were 88.39% for PSO, 90.41% for FA, and 95.35% for MFA. The PSO algorithm demonstrated high efficiency at R=40Ω, achieving 98.13%, but exhibited notable drops at lower and higher resistances, such as 83.43% at R=30Ω and 80.84% at R=60Ω, highlighting its sensitivity to resistance variations. FA showed improved consistency across the range, particularly at moderate resistances, peaking at 97.02% at R=30Ω while maintaining efficiency values above 89%. MFA outperformed both algorithms, achieving the highest mean efficiency among the three. It maintained efficiency above 95% for most resistances, reaching 98.13% at R=40Ω and 95.84% at R=60Ω, demonstrating its robustness and superior ability to accurately track the GMPP.

The impact of different load resistances on MPPT performance for the right peak condition is summarized in Table 5.5.

Table 5.5 Resistance variation under right peak condition

Ri (Ω)	**PSO**		**FA**		**MFA**	
	P (W)	**ηi**	**P (W)**	**ηi**	**P (W)**	**ηi**
20	1051.00	95.41%	841.25	76.37%	1067.00	96.86%
30	919.04	83.43%	1068.80	97.02%	1068.80	97.02%
40	1081.00	98.13%	980.40	89.00%	1081.00	98.13%
50	919.01	83.43%	1048.10	95.15%	1048.10	95.15%
60	890.53	80.84%	1055.80	95.84%	1055.80	95.84%
70	981.58	89.11%	981.58	89.11%	981.58	89.11%
η_{mean}	88.39%		90.41%		95.35%	

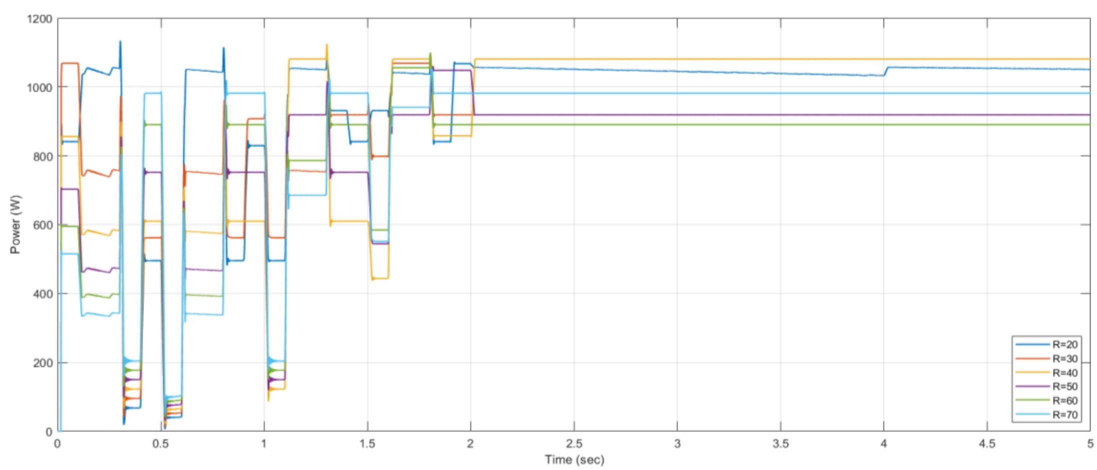

Figure 5.31 PSO algorithm for different values of R under the right peak condition

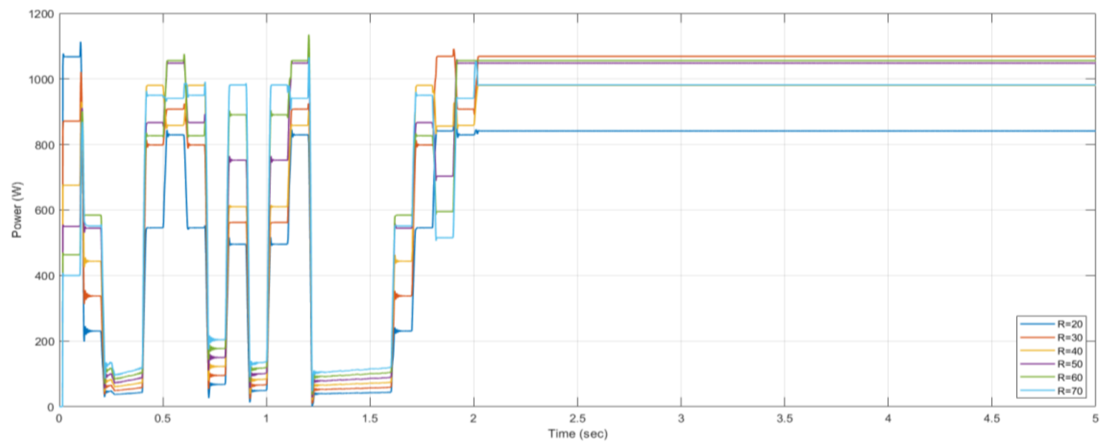

Figure 5.32 FA algorithm for different values of R under the right peak condition

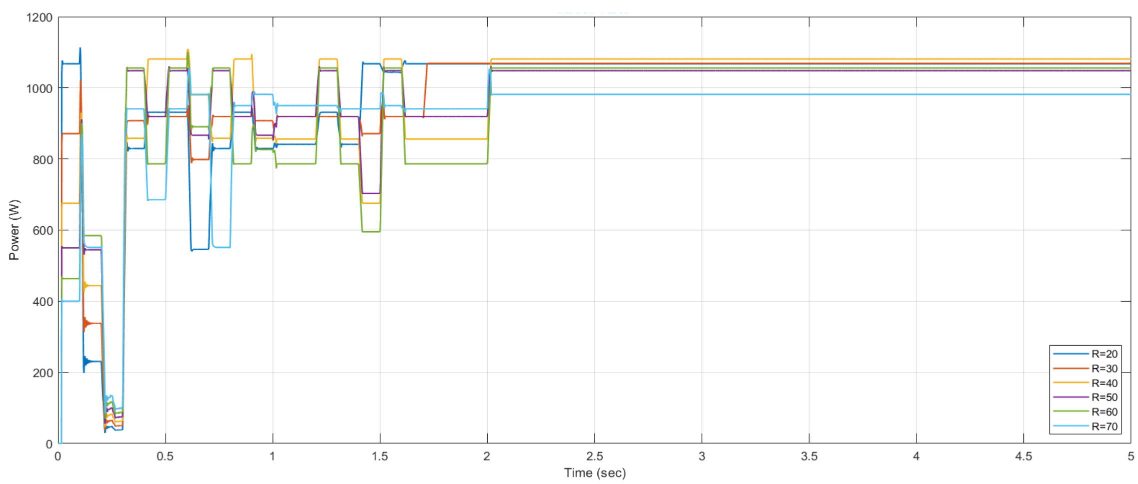

Figure 5.33 MFA algorithm for different values of R under the right peak condition

5.10 Conclusion

The comparative analysis in this study underscores the effectiveness of the Modified Firefly Algorithm (MFA) in tracking the Maximum Power Point (MPP) under Partial Shading Conditions (PSC) in photovoltaic (PV) systems. Extensive simulations confirmed that MFA consistently outperformed Particle Swarm Optimization (PSO) and the standard Firefly Algorithm (FA) across all tested shading scenarios. While FA demonstrated stable tracking capabilities, MFA's adaptive parameter tuning enabled it to achieve higher mean efficiency, especially in cases where PSO exhibited efficiency drops due to variations in load resistance.

Additionally, MFA showcased exceptional consistency in maintaining high efficiency while adapting to different resistances, affirming its robustness and adaptability in dynamic environmental conditions. The results indicate that although PSO and FA occasionally approached MFA's performance under certain conditions, they failed to sustain the same level of efficiency across all scenarios. MFA's ability to efficiently track the global MPP while minimizing fluctuations makes it the most reliable MPPT algorithm among the tested methods.

In conclusion, the findings of this study confirm that MFA is the most efficient and adaptive algorithm for optimizing power extraction in PV systems under varying shading and load conditions. Its superior tracking accuracy, faster convergence, and consistent high efficiency highlight its potential as a leading solution for enhancing the reliability and performance of solar energy systems.

CHAPTER SIX

CONCLUSION AND FUTURE WORK

6.1 Conclusion

This dissertation has explored the optimization, reliability, and performance enhancement of microgrid systems in Saudi Arabia's southern region, with a particular focus on photovoltaic (PV)-based microgrids. Three comprehensive studies were conducted, addressing both grid-connected and off-grid microgrid configurations, along with the development of an advanced maximum power point tracking (MPPT) strategy under partial shading conditions (PSCs). The findings of these studies significantly contribute to the field of renewable energy integration and microgrid optimization, providing practical solutions for enhancing energy efficiency and reliability.

The first study investigated a grid-connected hybrid microgrid for the Najran Secondary Industrial Institute (NSII) using HOMER software. The system incorporated photovoltage (PV), a battery storage system (BSS), a diesel generator (DG), and grid. The analysis showed that the proposed system significantly reduced the Net Present Cost (NPC) and carbon emissions, while ensuring an uninterrupted power supply with zero Loss of Power Supply Probability (LPSP). This study demonstrated the feasibility of hybrid microgrids in improving energy security and sustainability while balancing economic and environmental factors.

The second study extended the research to off-grid microgrid optimization, proposing a Modified Firefly Algorithm (MFA) for optimal system sizing. The MFA was designed to overcome the limitations of conventional optimization techniques by improving convergence speed and solution accuracy. The study compared the MFA with the standard Firefly Algorithm (FA) and found that it achieved superior results in determining the most efficient microgrid configurations. Additionally, reliability analysis was performed under two LPSP scenarios (0.01 and 0.1), confirming that the MFA-based design provides a cost-effective and resilient energy solution for off-grid regions.

The third study focused on the MPPT problem under PSCs. A detailed comparative analysis of four MPPT algorithms, Perturb and Observe (P&O), Particle Swarm Optimization (PSO), FA, and MFA was conducted to evaluate their efficiency in tracking the global maximum power point (GMPP). The results demonstrated that MFA outperformed the other algorithms by achieving faster convergence, higher accuracy, and more consistent MPP tracking under various shading patterns. Furthermore, the effect of load resistance variations on the performance of MPPT algorithms was examined, and MFA exhibited the highest adaptability.

Overall, this dissertation highlights the effectiveness of advanced optimization techniques in microgrid system design and MPPT strategies. By integrating HOMER, MATLAB-based optimization, and novel algorithmic enhancements, the research presents a scalable and efficient approach for deploying renewable energy systems in Saudi Arabia's underutilized southern region. These findings align with Vision 2030, supporting the country's transition toward a diversified and sustainable energy future.

6.2 Future Work

While this research has significantly contributed to the design, optimization, and performance analysis of microgrid systems, several potential areas warrant further investigation to enhance the adaptability and scalability of these systems.

- Hybrid Optimization Techniques.

  Future studies can explore hybrid metaheuristic algorithms that combine the Modified Firefly Algorithm (MFA) with other nature-inspired techniques, such as Genetic Algorithm (GA), Grey Wolf Optimization (GWO), and Artificial Bee Colony (ABC). This can further enhance the performance of microgrid optimization by achieving faster convergence and more accurate system sizing.

- Real-Time MPPT Implementation.

  The simulation-based analysis of MPPT under PSCs provides strong theoretical validation, but future work should involve real-time hardware implementation of the MFA-based MPPT controller in a physical microgrid setup. This would validate the algorithm's practical efficiency, robustness, and computational feasibility in real-world conditions.

- Incorporation of Hybrid Energy Sources.

  While this research primarily focused on solar PV-based microgrids, future studies could integrate additional renewable sources such as wind and biomass energy, particularly in regions with significant wind energy potential. Areas with consistent wind resources can benefit from a hybrid solar-wind microgrid, ensuring more stable power generation by compensating for solar energy fluctuations, especially during nighttime or cloudy conditions. A multi-source renewable energy microgrid would enhance system resilience, improve energy diversity, and reduce dependence on a single energy source, making it a more sustainable and reliable solution for off-grid and remote locations.

- Economic Feasibility Studies for Large-Scale Deployment.

  While the case studies focused on a specific region (Najran), large-scale feasibility studies should be conducted to assess the viability of deploying MFA-optimized microgrids across multiple regions in Saudi Arabia. This would help determine the economic benefits and policy implications of integrating advanced optimization techniques into the national energy strategy.

- Exploration of Energy Trading and Grid Interaction.

  With advancements in blockchain and smart grid technologies, future research could examine the possibility of peer-to-peer (P2P) energy trading within microgrid networks. Implementing an intelligent energy-sharing platform would allow independent microgrids to sell excess energy or exchange power with the main grid, enhancing overall energy efficiency.

- Adaptive MPPT Strategies for Highly Fluctuating Conditions.

  While MFA has shown superior performance under PSCs, further research can explore adaptive MPPT strategies that dynamically adjust optimization parameters based on weather forecasting models and predictive control algorithms. This would improve MPP tracking in environments with rapidly changing solar conditions.

- Resilience Studies Under Extreme Weather Events.

  Climate-related uncertainties such as sandstorms, heatwaves, and seasonal variations can significantly impact microgrid performance. Future work should analyze the long-term resilience of optimized microgrid systems under extreme weather scenarios and develop fault-tolerant energy management strategies.

By addressing these areas, future research can further enhance the efficiency, adaptability, and reliability of microgrid systems. The continued development of hybrid optimization algorithms, real-time MPPT techniques, and smart energy management solutions will play a vital role in the widespread adoption of sustainable microgrid technologies in Saudi Arabia and beyond.

Mono Multi Solutions

Vertex

BACKSHEET MONOCRYSTALLINE MODULE

PRODUCT: TSM-DE21

POWER RANGE: 645-670W

670W	0~+5W	21.6%
MAXIMUM POWER OUTPUT	POSITIVE POWER TOLERANCE	MAXIMUM EFFICIENCY

High customer value

- Lower LCOE (Levelized Cost Of Energy), reduced BOS (Balance of System) cost, shorter payback time
- Lowest guaranteed first year and annual degradation;
- Designed for compatibility with existing mainstream system components

High power up to 670W

- Up to 21.6% module efficiency with high density interconnect technology
- Multi-busbar technology for better light trapping effect, lower series resistance and improved current collection

High reliability

- Minimized micro-cracks with innovative non-destructive cutting technology
- Ensured PID resistance through cell process and module material control
- Resistant to harsh environments such as salt, ammonia, sand, high temperature and high humidity areas
- Mechanical performance up to 5400 Pa positive load and 2400 Pa negative load

High energy yield

- Excellent IAM (Incident Angle Modifier) and low irradiation performance, validated by 3rd party certifications
- The unique design provides optimized energy production under inter-row shading conditions
- Lower temperature coefficient (-0.34%) and operating temperature

Trina Solar's Backsheet Performance Warranty

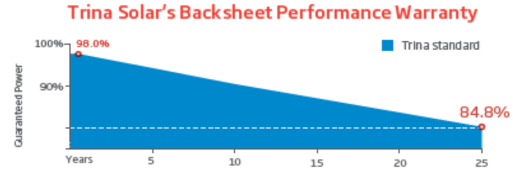

Comprehensive Products and System Certificates

IEC61215/IEC61730/IEC61701/IEC62716
ISO 9001: Quality Management System
ISO 14001: Environmental Management System
ISO14064: Greenhouse Gases Emissions Verification
ISO45001: Occupational Health and Safety Management System

Trinasolar

Vertex BACKSHEET MONOCRYSTALLINE MODULE

DIMENSIONS OF PV MODULE(mm)

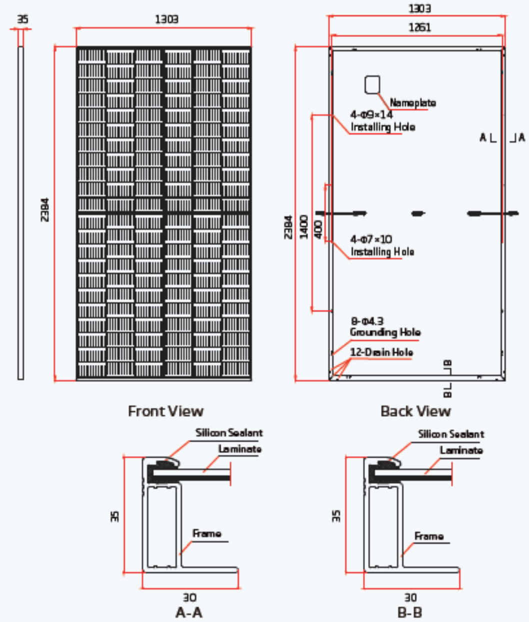

I-V CURVES OF PV MODULE(650 W)

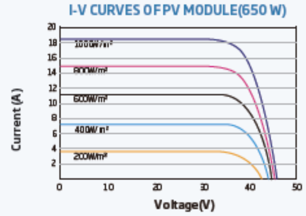

P-V CURVES OF PV MODULE(650W)

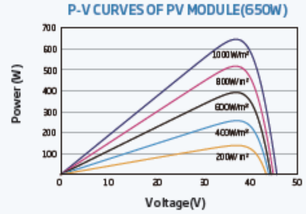

I-V CURVES OF PV MODULE(650 W)

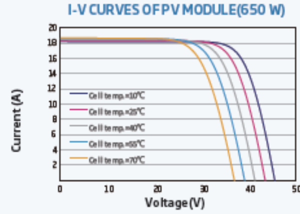

ELECTRICAL DATA (STC)

Peak Power Watts-PMAX (Wp)*	645	650	655	660	665	670
Power Tolerance-PMAX (W)	0~+5					
Maximum Power Voltage-VMPP (V)	37.2	37.4	37.6	37.8	38.0	38.2
Maximum Power Current-IMPP (A)	17.35	17.39	17.43	17.47	17.51	17.55
Open Circuit Voltage-VOC (V)	45.1	45.3	45.5	45.7	45.9	46.1
Short Circuit Current-ISC (A)	18.39	18.44	18.48	18.53	18.57	18.62
Module Efficiency η m (%)	20.8	20.9	21.1	21.2	21.4	21.6

STC: Irradiance 1000W/m2, Cell Temperature 25°C, Air Mass AM1.5. *Measuring tolerance: ±3%.

ELECTRICAL DATA (NOCT)

Maximum Power-PMAX (Wp)	488	492	496	500	504	508
Maximum Power Voltage-VMPP (V)	34.8	34.9	35.1	35.3	35.4	35.6
Maximum Power Current-IMPP (A)	14.05	14.09	14.13	14.17	14.22	14.26
Open Circuit Voltage-VOC (V)	42.5	42.7	42.9	43.0	43.2	43.4
Short Circuit Current-ISC (A)	14.82	14.86	14.89	14.93	14.96	15.01

NOCT: Irradiance at 800W/m², Ambient Temperature 20°C, Wind Speed 1m/s.

MECHANICAL DATA

Solar Cells	Monocrystalline
No. of cells	132 cells
Module Dimensions	2384×1303×35 mm (93.86×51.30×1.38 inches)
Weight	33.6 kg (74.1 lb)
Glass	3.2 mm (0.13 inches), High Transmission, AR Coated Heat Strengthened Glass
Encapsulant material	EVA
Backsheet	White
Frame	35mm(1.38 inches) Anodized Aluminium Alloy
J-Box	IP 68 rated
Cables	Photovoltaic Technology Cable 4.0mm² (0.006 inches²), Portrait: 280/280 mm(11.02/11.02 inches) Length can be customized
Connector	MC4 EVO2 / TS4*

*Please refer to regional datasheet for specified connector.

TEMPERATURE RATINGS

NOCT (Nominal Operating Cell Temperature)	43°C (±2°C)
Temperature Coefficient of PMAX	- 0.34%/°C
Temperature Coefficient of VOC	- 0.25%/°C
Temperature Coefficient of ISC	0.04%/°C

MAXIMUM RATINGS

Operational Temperature	-40~+85°C
Maximum System Voltage	1500V DC (IEC)
	1500V DC (UL)
Max Series Fuse Rating	30A

WARRANTY

12 year Product Workmanship Warranty
25 year Power Warranty
2% first year degradation
0.55% Annual Power Attenuation

(Please refer to product warranty for details)

PACKAGING CONFIGUREATION

Modules per box: 31 pieces
Modules per 40' container: 558 pieces

Trinasolar

CAUTION: READ SAFETY AND INSTALLATION INSTRUCTIONS BEFORE USING THE PRODUCT.

Version number: TSM_EN_2021_A

www.trinasolar.com

REFERENCES

[1] H. Mahmood, T. T. Y. Alkhateeb, M. M. Z. Al-Qahtani, Z. Allam, N. Ahmad, and M. Furqa, "URBANIZATION, OIL PRICE AND POLLUTION IN SAUDI ARABIA," *IJEEP*, vol. 10, no. 2, pp. 477–482, Jan. 2020, doi: 10.32479/ijeep.8914.

[2] F. E. M. Suliman, "Solar- and Wind-Energy Utilization in the Kingdom of Saudi Arabia: A Comprehensive Review," *Energies*, vol. 17, no. 8, p. 1894, Apr. 2024, doi: 10.3390/en17081894.

[3] G. Brumana, G. Franchini, E. Ghirardi, and A. Perdichizzi, "Techno-economic optimization of hybrid power generation systems: A renewables community case study," *Energy*, vol. 246, p. 123427, May 2022, doi: 10.1016/j.energy.2022.123427.

[4] Y. Z. Alharthi, M. K. Siddiki, and G. M. Chaudhry, "Resource Assessment and Techno-Economic Analysis of a Grid-Connected Solar PV-Wind Hybrid System for Different Locations in Saudi Arabia," *Sustainability*, vol. 10, no. 10, p. 3690, Oct. 2018, doi: 10.3390/su10103690.

[5] A. A. Mas'ud and H. Z. Al-Garni, "Optimum Configuration of a Renewable Energy System Using Multi-Year Parameters and Advanced Battery Storage Modules: A Case Study in Northern Saudi Arabia," *Sustainability*, vol. 13, no. 9, p. 5123, May 2021, doi: 10.3390/su13095123.

[6] N. Alshammari, M. M. Samy, and J. Asumadu, "Optimal Economic Analysis Study for Renewable Energy Systems to Electrify Remote Region in Kingdom of Saudi Arabia," in *2018 Twentieth International Middle East Power Systems Conference (MEPCON)*, Cairo, Egypt: IEEE, Dec. 2018, pp. 1040–1045. doi: 10.1109/MEPCON.2018.8635287.

[7] M. Kharrich *et al.*, "Optimal Design of an Isolated Hybrid Microgrid for Enhanced Deployment of Renewable Energy Sources in Saudi Arabia," *Sustainability*, vol. 13, no. 9, p. 4708, Apr. 2021, doi: 10.3390/su13094708.

[8] A. AlAhmed, G. M. Chaudhry, and M. K. Siddiki, "Modelling, Simulation, and Performance Analysis of a Microgrid with Photovoltaic Energy for Eastern Region of Saudi Arabia," in *2019 IEEE 46th Photovoltaic Specialists Conference (PVSC)*, Chicago, IL, USA: IEEE, Jun. 2019, pp. 1663–1668. doi: 10.1109/PVSC40753.2019.8981325.

[9] the United Nations, "The Sustainable Development Goals Report 2024," statics, Jun. 2024. [Online]. Available: https://unstats.un.org/sdgs/report/2024.

[10] M. Abusaq and M. A. Zohdy, "Optimizing Renewable Energy Integration through Innovative Hybrid Microgrid Design: A Case Study of Najran Secondary Industrial Institute in Saudi Arabia," *Clean Technol.*, vol. 6, no. 2, pp. 397–417, Mar. 2024, doi: 10.3390/cleantechnol6020020.

[11] M. Abusaq and M. A. Zohdy, "Optimal Sizing of Solar Off Grid Microgrid Using Modified Firefly Algorithm," vol. 8, no. 8, [Online]. Available: https://ijses.com/wp-content/uploads/2024/08/30-IJSES-V8N8.pdf

[12] M. Abusaq and M. A. Zohdy, "Maximum Power Point Tracking Based on Modified Firefly Algorithm for PV System under Partial Shading Conditions," vol.

9, no. 3, [Online]. Available: https://ijses.com/wp-content/uploads/2025/03/131-IJSES-V9N2.pdf

[13] M. Uddin, H. Mo, D. Dong, S. Elsawah, J. Zhu, and J. M. Guerrero, "Microgrids: A review, outstanding issues and future trends," *Energy Strategy Reviews*, vol. 49, p. 101127, Sep. 2023, doi: 10.1016/j.esr.2023.101127.

[14] M. Najafzadeh, R. Ahmadiahangar, O. Husev, I. Roasto, T. Jalakas, and A. Blinov, "Recent Contributions, Future Prospects and Limitations of Interlinking Converter Control in Hybrid AC/DC Microgrids," *IEEE Access*, vol. 9, pp. 7960–7984, 2021, doi: 10.1109/ACCESS.2020.3049023.

[15] W. Inam, D. Strawser, K. K. Afridi, R. J. Ram, and D. J. Perreault, "Architecture and system analysis of microgrids with peer-to-peer electricity sharing to create a marketplace which enables energy access," in *2015 9th International Conference on Power Electronics and ECCE Asia (ICPE-ECCE Asia)*, Seoul, South Korea: IEEE, Jun. 2015, pp. 464–469. doi: 10.1109/ICPE.2015.7167826.

[16] D. Rekioua and E. Matagne, *Optimization of Photovoltaic Power Systems: Modelization, Simulation and Control*. in Green Energy and Technology. London: Springer London, 2012. doi: 10.1007/978-1-4471-2403-0.

[17] A. A. Kebede *et al.*, "Techno-economic analysis of lithium-ion and lead-acid batteries in stationary energy storage application," *Journal of Energy Storage*, vol. 40, p. 102748, Aug. 2021, doi: 10.1016/j.est.2021.102748.

[18] K. Xu, Y. Guo, G. Lei, and J. Zhu, "A Review of Flywheel Energy Storage System Technologies," *Energies*, vol. 16, no. 18, p. 6462, Sep. 2023, doi: 10.3390/en16186462.

[19] M. Şahin, F. Blaabjerg, and A. Sangwongwanich, "A Comprehensive Review on Supercapacitor Applications and Developments," *Energies*, vol. 15, no. 3, p. 674, Jan. 2022, doi: 10.3390/en15030674.

[20] K. Mollah, N. K. C. Nair, and R. K. Rayudu, "Demand Response an Alternative Solution to Prevent Load Shedding Triggering," *EAI Endorsed Transactions on Energy Web*, vol. 1, no. 3, p. e2, Dec. 2014, doi: 10.4108/ew.1.3.e2.

[21] N. Kondrath, "Bidirectional DC-DC converter topologies and control strategies for interfacing energy storage systems in microgrids: An overview," in *2017 IEEE International Conference on Smart Energy Grid Engineering (SEGE)*, Oshawa, ON, Canada: IEEE, Aug. 2017, pp. 341–345. doi: 10.1109/SEGE.2017.8052822.

[22] S. M. Malik, X. Ai, Y. Sun, C. Zhengqi, and Z. Shupeng, "Voltage and frequency control strategies of hybrid AC/DC microgrid: a review," *IET Generation, Transmission & Distribution*, vol. 11, no. 2, pp. 303–313, Jan. 2017, doi: 10.1049/iet-gtd.2016.0791.

[23] E. M. Sandhu and D. T. Thakur, "Issues, Challenges, Causes, Impacts and Utilization of Renewable Energy Sources - Grid Integration," vol. 4, no. 3, 2014.

[24] L. Alhafadhi and J. Teh, "Advances in reduction of total harmonic distortion in solar photovoltaic systems: A literature review," *Int J Energy Res*, vol. 44, no. 4, pp. 2455–2470, Mar. 2020, doi: 10.1002/er.5075.

[25] A. Akinpelu, M. S. Alam, M. Shafiullah, S. M. Rahman, and F. S. Al-Ismail, "Greenhouse Gas Emission Dynamics of Saudi Arabia: Potential of Hydrogen Fuel

for Emission Footprint Reduction," *Sustainability*, vol. 15, no. 7, p. 5639, Mar. 2023, doi: 10.3390/su15075639.
[26] W. Ahmad, I. Ahmad, and A. M. Abdurraqeeb, "Renewable Energy in Kingdom of Saudi Arabia: Opportunities and Prospects," in *2017 9th IEEE-GCC Conference and Exhibition (GCCCE)*, Manama, Bahrain: IEEE, May 2017, pp. 1–9. doi: 10.1109/IEEEGCC.2017.8448157.
[27] "Saudi Vision 2030." Accessed: Oct. 30, 2023. [Online]. Available: http://www.vision2030.gov.sa/en/
[28] U.S. Energy Information Administration, "Country Analysis Brief: Saudi Arabia," *Saudi Arabia*, 2023, [Online]. Available: www.eia.gov
[29] GENERAL AUTHORITY FOR STATISTICS, "Renewable Energy Statistics 2020," 2020. [Online]. Available: https://www.stats.gov.sa/en/1081
[30] The U.S. Energy Information Administration (EIA), "Country Analysis Brief: Saudi Arabia," Country Analysis Brief: Saudi Arabia, Oct. 2023. [Online]. Available: https://www.eia.gov/international/analysis/country/SAU
[31] M. Mathew, M. S. Hossain, S. Saha, S. Mondal, and M. E. Haque, "Sizing approaches for solar photovoltaic-based microgrids: A comprehensive review," *IET Energy Syst Integration*, vol. 4, no. 1, pp. 1–27, Mar. 2022, doi: 10.1049/esi2.12048.
[32] E. Y. Alhawsawi, H. M. D. Habbi, M. Hawsawi, and M. A. Zohdy, "Optimal Design and Operation of Hybrid Renewable Energy Systems for Oakland University," *Energies*, vol. 16, no. 15, p. 5830, Aug. 2023, doi: 10.3390/en16155830.
[33] A. AlKassem, A. Draou, A. Alamri, and H. Alharbi, "Design Analysis of an Optimal Microgrid System for the Integration of Renewable Energy Sources at a University Campus," *Sustainability*, vol. 14, no. 7, p. 4175, Mar. 2022, doi: 10.3390/su14074175.
[34] O. Ekren, C. Hakan Canbaz, and Ç. B. Güvel, "Sizing of a solar-wind hybrid electric vehicle charging station by using HOMER software," *Journal of Cleaner Production*, vol. 279, p. 123615, Jan. 2021, doi: 10.1016/j.jclepro.2020.123615.
[35] A. M. Aly, A. M. Kassem, K. Sayed, and I. Aboelhassan, "Design of Microgrid with Flywheel Energy Storage System Using HOMER Software for Case Study," in *2019 International Conference on Innovative Trends in Computer Engineering (ITCE)*, Aswan, Egypt: IEEE, Feb. 2019, pp. 485–491. doi: 10.1109/ITCE.2019.8646441.
[36] A. T. Dahiru and C. W. Tan, "Optimal sizing and techno-economic analysis of grid-connected nanogrid for tropical climates of the Savannah," *Sustainable Cities and Society*, vol. 52, p. 101824, Jan. 2020, doi: 10.1016/j.scs.2019.101824.
[37] M. S. Islam, B. K. Das, P. Das, and M. H. Rahaman, "Techno-economic optimization of a zero emission energy system for a coastal community in Newfoundland, Canada," *Energy*, vol. 220, p. 119709, Apr. 2021, doi: 10.1016/j.energy.2020.119709.
[38] D. N. Luta and A. K. Raji, "Optimal sizing of hybrid fuel cell-supercapacitor storage system for off-grid renewable applications," *Energy*, vol. 166, pp. 530–540, Jan. 2019, doi: 10.1016/j.energy.2018.10.070.

[39] S. Mandal, B. K. Das, and N. Hoque, "Optimum sizing of a stand-alone hybrid energy system for rural electrification in Bangladesh," *Journal of Cleaner Production*, vol. 200, pp. 12–27, Nov. 2018, doi: 10.1016/j.jclepro.2018.07.257.
[40] H. Elsaraf, M. Jamil, and B. Pandey, "Techno-Economic Design of a Combined Heat and Power Microgrid for a Remote Community in Newfoundland Canada," *IEEE Access*, vol. 9, pp. 91548–91563, 2021, doi: 10.1109/ACCESS.2021.3091738.
[41] D. Groppi, D. Astiaso Garcia, G. Lo Basso, F. Cumo, and L. De Santoli, "Analysing economic and environmental sustainability related to the use of battery and hydrogen energy storages for increasing the energy independence of small islands," *Energy Conversion and Management*, vol. 177, pp. 64–76, Dec. 2018, doi: 10.1016/j.enconman.2018.09.063.
[42] M. S. Islam, "A techno-economic feasibility analysis of hybrid renewable energy supply options for a grid-connected large office building in southeastern part of France," *Sustainable Cities and Society*, vol. 38, pp. 492–508, Apr. 2018, doi: 10.1016/j.scs.2018.01.022.
[43] J. Kumar, B. V. Suryakiran, A. Verma, and T. S. Bhatti, "Analysis of techno-economic viability with demand response strategy of a grid-connected microgrid model for enhanced rural electrification in Uttar Pradesh state, India," *Energy*, vol. 178, pp. 176–185, Jul. 2019, doi: 10.1016/j.energy.2019.04.105.
[44] C. Li, D. Zhou, and Y. Zheng, "Techno-economic comparative study of grid-connected PV power systems in five climate zones, China," *Energy*, vol. 165, pp. 1352–1369, Dec. 2018, doi: 10.1016/j.energy.2018.10.062.
[45] J. Liu, L. Jian, W. Wang, Z. Qiu, J. Zhang, and P. Dastbaz, "The role of energy storage systems in resilience enhancement of health care centers with critical loads," *Journal of Energy Storage*, vol. 33, p. 102086, Jan. 2021, doi: 10.1016/j.est.2020.102086.
[46] H. Masrur, H. O. R. Howlader, M. Elsayed Lotfy, K. R. Khan, J. M. Guerrero, and T. Senjyu, "Analysis of Techno-Economic-Environmental Suitability of an Isolated Microgrid System Located in a Remote Island of Bangladesh," *Sustainability*, vol. 12, no. 7, p. 2880, Apr. 2020, doi: 10.3390/su12072880.
[47] Y. Sawle, S. Jain, S. Babu, A. R. Nair, and B. Khan, "Prefeasibility Economic and Sensitivity Assessment of Hybrid Renewable Energy System," *IEEE Access*, vol. 9, pp. 28260–28271, 2021, doi: 10.1109/ACCESS.2021.3058517.
[48] A. Mohammad Bagher, "Types of Solar Cells and Application," *AJOP*, vol. 3, no. 5, p. 94, 2015, doi: 10.11648/j.ajop.20150305.17.
[49] A. Joseph and M. Shahidehpour, "Battery storage systems in electric power systems," in *2006 IEEE Power Engineering Society General Meeting*, Montreal, Que., Canada: IEEE, 2006, p. 8 pp. doi: 10.1109/PES.2006.1709235.
[50] N. Yimen, O. Hamandjoda, L. Meva'a, B. Ndzana, and J. Nganhou, "Analyzing of a Photovoltaic/Wind/Biogas/Pumped-Hydro Off-Grid Hybrid System for Rural Electrification in Sub-Saharan Africa—Case study of Djoundé in Northern Cameroon," *Energies*, vol. 11, no. 10, p. 2644, Oct. 2018, doi: 10.3390/en11102644.

[51] J. Li, P. Liu, and Z. Li, “Optimal design and techno-economic analysis of a solar-wind-biomass off-grid hybrid power system for remote rural electrification: A case study of west China,” *Energy*, vol. 208, p. 118387, Oct. 2020, doi: 10.1016/j.energy.2020.118387.
[52] A. Traoré, H. Elgothamy, and M. A. Zohdy, “Optimal Sizing of Solar/Wind Hybrid Off-Grid Microgrids Using an Enhanced Genetic Algorithm,” *JPEE*, vol. 06, no. 05, pp. 64–77, 2018, doi: 10.4236/jpee.2018.65004.
[53] J. Faraji, M. Babaei, N. Bayati, and M. A.Hejazi, “A Comparative Study between Traditional Backup Generator Systems and Renewable Energy Based Microgrids for Power Resilience Enhancement of a Local Clinic,” *Electronics*, vol. 8, no. 12, p. 1485, Dec. 2019, doi: 10.3390/electronics8121485.
[54] A. M. Eltamaly and M. A. Mohamed, “A Novel Design and Optimization Software for Autonomous PV/Wind/Battery Hybrid Power Systems,” *Mathematical Problems in Engineering*, vol. 2014, pp. 1–16, 2014, doi: 10.1155/2014/637174.
[55] R. Atia and N. Yamada, “Sizing and Analysis of Renewable Energy and Battery Systems in Residential Microgrids,” *IEEE Trans. Smart Grid*, vol. 7, no. 3, pp. 1204–1213, May 2016, doi: 10.1109/TSG.2016.2519541.
[56] *HOMER Pro*. (2017). National Renewable Energy Laboratory. [Online]. Available: https://www.homerenergy.com/
[57] L. H. S. Santos, J. A. A. Silva, J. C. Lopez, N. B. Arias, M. J. Rider, and L. C. P. Da Silva, “Integrated Optimal Sizing and Dispatch Strategy for Microgrids Using HOMER Pro,” in *2021 IEEE PES Innovative Smart Grid Technologies Conference - Latin America (ISGT Latin America)*, Lima, Peru: IEEE, Sep. 2021, pp. 1–5. doi: 10.1109/ISGTLatinAmerica52371.2021.9543015.
[58] H. Cristian, N. Bizon, and B. Alexandru, “Design of hybrid power systems using HOMER simulator for different renewable energy sources,” in *2017 9th International Conference on Electronics, Computers and Artificial Intelligence (ECAI)*, Targoviste: IEEE, Jun. 2017, pp. 1–7. doi: 10.1109/ECAI.2017.8166507.
[59] S. Bracco, F. Delfino, P. Laiolo, L. Pagnini, and G. Piazza, “Evaluating LCOE in sustainable microgrids for smart city applications,” *E3S Web Conf.*, vol. 113, p. 03006, 2019, doi: 10.1051/e3sconf/201911303006.
[60] E. Niringiyimana, S. Wanquan, G. Dushimimana, and J. B. Niyigena, “Hybrid Renewable Energy System Design and Optimization for Developing Countries Using HOMER Pro: Case of Rwanda,” in *2023 7th International Conference on Green Energy and Applications (ICGEA)*, Singapore, Singapore: IEEE, Mar. 2023, pp. 72–76. doi: 10.1109/ICGEA57077.2023.10125739.
[61] J. Mustafa, S. Alqaed, F. A. Almehmadi, and B. Jamil, “Development and comparison of parametric models to predict global solar radiation: a case study for the southern region of Saudi Arabia,” *J Therm Anal Calorim*, vol. 147, no. 17, pp. 9559–9589, Sep. 2022, doi: 10.1007/s10973-022-11209-7.
[62] “Global Solar Atlas, Saudi Arabia,” Solargis, statistic 1, Nov. 2023. [Online]. Available: https://globalsolaratlas.info/
[63] APICORP, “Saudi energy price reform getting serious,” APICORP ENERGY RESEARCH, Report Vol. 03 No. 05, Feb. 2018.

[64] J. Mikayilov, “How Have Electricity Tariffs Evolved in Saudi Arabia Over the Last Half Century (1974 - 2023)?,” KAPSARC, Data Insight, Sep. 2023. [Online]. Available: https://www.kapsarc.org/research/publications/how-have-electricity-tariffs-evolved-in-saudi-arabia-over-the-last-half-century-1974-2023/

[65] A. Al-Quraan, M. Al-Mahmodi, K. Alzaareer, C. El-Bayeh, and U. Eicker, “Minimizing the Utilized Area of PV Systems by Generating the Optimal Inter-Row Spacing Factor,” *Sustainability*, vol. 14, no. 10, p. 6077, May 2022, doi: 10.3390/su14106077.

[66] S. Alqaed, J. Mustafa, F. A. Almehmadi, and B. Jamil, “Estimation of ideal tilt angle for solar-PV panel surfaces facing south: a case study for Najran City, Saudi Arabia,” *J Therm Anal Calorim*, vol. 148, no. 16, pp. 8641–8654, Aug. 2023, doi: 10.1007/s10973-022-11812-8.

[67] M. Ali *et al.*, “Renewable energy sources-based hybrid microgrid system for off-grid electricity solution for rural communities,” *Energy Science & Engineering*, vol. 11, no. 10, pp. 3486–3499, Oct. 2023, doi: 10.1002/ese3.1535.

[68] S. Feron, “Sustainability of Off-Grid Photovoltaic Systems for Rural Electrification in Developing Countries: A Review,” *Sustainability*, vol. 8, no. 12, p. 1326, Dec. 2016, doi: 10.3390/su8121326.

[69] O. A. Al-Shahri *et al.*, “Solar photovoltaic energy optimization methods, challenges and issues: A comprehensive review,” *Journal of Cleaner Production*, vol. 284, p. 125465, Feb. 2021, doi: 10.1016/j.jclepro.2020.125465.

[70] H. M. Ridha, C. Gomes, H. Hizam, M. Ahmadipour, A. A. Heidari, and H. Chen, “Multi-objective optimization and multi-criteria decision-making methods for optimal design of standalone photovoltaic system: A comprehensive review,” *Renewable and Sustainable Energy Reviews*, vol. 135, p. 110202, Jan. 2021, doi: 10.1016/j.rser.2020.110202.

[71] M. Abdel-Basset, L. Abdel-Fatah, and A. K. Sangaiah, “Metaheuristic Algorithms: A Comprehensive Review,” in *Computational Intelligence for Multimedia Big Data on the Cloud with Engineering Applications*, Elsevier, 2018, pp. 185–231. doi: 10.1016/B978-0-12-813314-9.00010-4.

[72] O. Bozorg-Haddad, M. Solgi, and H. A. Loáiciga, *Meta-Heuristic and Evolutionary Algorithms for Engineering Optimization*, 1st ed. Wiley, 2017. doi: 10.1002/9781119387053.

[73] D. Fioriti, G. Lutzemberger, D. Poli, P. Duenas-Martinez, and A. Micangeli, “Heuristic approaches to size microgrids: a methodology to compile multiple design options,” in *2020 IEEE International Conference on Environment and Electrical Engineering and 2020 IEEE Industrial and Commercial Power Systems Europe (EEEIC / I&CPS Europe)*, Madrid, Spain: IEEE, Jun. 2020, pp. 1–6. doi: 10.1109/EEEIC/ICPSEurope49358.2020.9160842.

[74] Z. Bektas, M. O. Kayalıca, and G. Kayakutlu, “A hybrid heuristic algorithm for optimal energy scheduling of grid-connected micro grids,” *Energy Systems*, vol. 12, no. 4, pp. 877–893, Nov. 2021, doi: 10.1007/s12667-020-00380-1.

[75] B. Khan and P. Singh, “Selecting a Meta-Heuristic Technique for Smart Micro-Grid Optimization Problem: A Comprehensive Analysis,” *IEEE Access*, vol. 5, pp. 13951–13977, 2017, doi: 10.1109/ACCESS.2017.2728683.

[76] K. Gao, T. Wang, C. Han, J. Xie, Y. Ma, and R. Peng, “A Review of Optimization of Microgrid Operation,” *Energies*, vol. 14, no. 10, p. 2842, May 2021, doi: 10.3390/en14102842.
[77] S. Leonori, M. Paschero, F. M. Frattale Mascioli, and A. Rizzi, “Optimization strategies for Microgrid energy management systems by Genetic Algorithms,” *Applied Soft Computing*, vol. 86, p. 105903, Jan. 2020, doi: 10.1016/j.asoc.2019.105903.
[78] A. A. Z. Diab, H. M. Sultan, I. S. Mohamed, O. N. Kuznetsov, and T. D. Do, “Application of Different Optimization Algorithms for Optimal Sizing of PV/Wind/Diesel/Battery Storage Stand-Alone Hybrid Microgrid,” *IEEE Access*, vol. 7, pp. 119223–119245, 2019, doi: 10.1109/ACCESS.2019.2936656.
[79] J. D. Vasanth, N. Kumarappan, R. Arulraj, and T. Vigneysh, “Minimization of operation cost of a microgrid using firefly algorithm,” in *2017 IEEE International Conference on Intelligent Techniques in Control, Optimization and Signal Processing (INCOS)*, Srivilliputhur: IEEE, Mar. 2017, pp. 1–6. doi: 10.1109/ITCOSP.2017.8303149.
[80] I. M. Ibrahim, W. A. Omran, and A. Y. Abdelaziz, “Optimal Sizing of Microgrid System Using Hybrid Firefly and Particle Swarm Optimization Algorithm,” in *2021 22nd International Middle East Power Systems Conference (MEPCON)*, Assiut, Egypt: IEEE, Dec. 2021, pp. 287–293. doi: 10.1109/MEPCON50283.2021.9686271.
[81] Y. Yang, J. Qiu, and Z. Qin, “Multidimensional Firefly Algorithm for Solving Day-Ahead Scheduling Optimization in Microgrid,” *Journal of Electrical Engineering & Technology*, vol. 16, no. 4, pp. 1755–1768, Jul. 2021, doi: 10.1007/s42835-021-00707-7.
[82] A. Alzahrani, M. Ferdowsi, P. Shamsi, and C. H. Dagli, “Modeling and Simulation of Microgrid,” *Procedia Computer Science*, vol. 114, pp. 392–400, 2017, doi: 10.1016/j.procs.2017.09.053.
[83] A. K. Raji and D. N. Luta, “Modeling and Optimization of a Community Microgrid Components,” *Energy Procedia*, vol. 156, pp. 406–411, Jan. 2019, doi: 10.1016/j.egypro.2018.11.103.
[84] M. Farrokhabadi, S. Konig, C. A. Canizares, K. Bhattacharya, and T. Leibfried, “Battery Energy Storage System Models for Microgrid Stability Analysis and Dynamic Simulation,” *IEEE Trans. Power Syst.*, vol. 33, no. 2, pp. 2301–2312, Mar. 2018, doi: 10.1109/TPWRS.2017.2740163.
[85] M. Sababha, M. Zohdy, and M. Kafafy, “The Enhanced Firefly Algorithm Based on Modified Exploitation and Exploration Mechanism,” *Electronics*, vol. 7, no. 8, p. 132, Jul. 2018, doi: 10.3390/electronics7080132.
[86] S. Amara, S. Toumi, and C. B. Salah, “Comparative Study of Optimal Sizing Approaches for Microgrid Systems”.
[87] M. Azaza and F. Wallin, “Multi objective particle swarm optimization of hybrid micro-grid system: A case study in Sweden,” *Energy*, vol. 123, pp. 108–118, Mar. 2017, doi: 10.1016/j.energy.2017.01.149.
[88] M. Huang, L. Fu, Y. Zhang, and X. Gao, “Optimal design of an island microgrid with considering scheduling optimization,” in *2017 International Smart Cities*

Conference (ISC2), Wuxi, China: IEEE, Sep. 2017, pp. 1–6. doi: 10.1109/ISC2.2017.8090809.
[89] O. Azeem *et al.*, “A Comprehensive Review on Integration Challenges, Optimization Techniques and Control Strategies of Hybrid AC/DC Microgrid,” *Applied Sciences*, vol. 11, no. 14, p. 6242, Jul. 2021, doi: 10.3390/app11146242.
[90] M. H. Saeed, W. Fangzong, B. A. Kalwar, and S. Iqbal, “A Review on Microgrids’ Challenges & Perspectives,” *IEEE Access*, vol. 9, pp. 166502–166517, 2021, doi: 10.1109/ACCESS.2021.3135083.
[91] S. Choudhury, “A comprehensive review on issues, investigations, control and protection trends, technical challenges and future directions for Microgrid technology,” *Int Trans Electr Energ Syst*, vol. 30, no. 9, Sep. 2020, doi: 10.1002/2050-7038.12446.
[92] X. Yang, *Engineering Optimization: An Introduction with Metaheuristic Applications*, 1st ed. Wiley, 2010. doi: 10.1002/9780470640425.
[93] W. A. Khan, N. N. Hamadneh, S. L. Tilahun, and J. M. T. Ngnotchouye, “A Review and Comparative Study of Firefly Algorithm and its Modified Versions,” in *Optimization Algorithms - Methods and Applications*, O. Baskan, Ed., InTech, 2016. doi: 10.5772/62472.
[94] V. Kumar and D. Kumar, “A Systematic Review on Firefly Algorithm: Past, Present, and Future,” *Arch Computat Methods Eng*, vol. 28, no. 4, pp. 3269–3291, Jun. 2021, doi: 10.1007/s11831-020-09498-y.
[95] S. L. Tilahun, J. M. T. Ngnotchouye, and N. N. Hamadneh, “Continuous versions of firefly algorithm: a review,” *Artif Intell Rev*, vol. 51, no. 3, pp. 445–492, Mar. 2019, doi: 10.1007/s10462-017-9568-0.
[96] P. Satapathy, S. Dhar, and P. K. Dash, “Stability improvement of PV-BESS diesel generator-based microgrid with a new modified harmony search-based hybrid firefly algorithm,” *IET Renewable Power Generation*, vol. 11, no. 5, pp. 566–577, Apr. 2017, doi: 10.1049/iet-rpg.2016.0116.
[97] M. Sameeullah and A. Swarup, “MPPT Schemes for PV System under Normal and Partial Shading Condition: A Review,” *Int. J. Renew. Energy Dev.*, vol. 5, no. 2, pp. 79–94, Jul. 2016, doi: 10.14710/ijred.5.2.79-94.
[98] T. T. Yetayew, T. R. Jyothsna, and G. Kusuma, “Evaluation of Incremental conductance and Firefly algorithm for PV MPPT application under partial shade condition,” in *2016 IEEE 6th International Conference on Power Systems (ICPS)*, New Delhi, India: IEEE, Mar. 2016, pp. 1–6. doi: 10.1109/ICPES.2016.7584089.
[99] Y. Zhang, Y. Wang, H. Li, J.-B. Chang, and J. Yu, “A Firefly Algorithm and Elite Ant System-Trained Elman Neural Network for MPPT Algorithm of PV Array,” *International Journal of Photoenergy*, vol. 2022, pp. 1–16, Nov. 2022, doi: 10.1155/2022/5700570.
[100] Y.-P. Huang, M.-Y. Huang, and C.-E. Ye, “A Fusion Firefly Algorithm With Simplified Propagation for Photovoltaic MPPT Under Partial Shading Conditions,” *IEEE Trans. Sustain. Energy*, vol. 11, no. 4, pp. 2641–2652, Oct. 2020, doi: 10.1109/TSTE.2020.2968752.
[101] D. F. Teshome, C. H. Lee, Y. W. Lin, and K. L. Lian, “A Modified Firefly Algorithm for Photovoltaic Maximum Power Point Tracking Control Under Partial

Shading," *IEEE J. Emerg. Sel. Topics Power Electron.*, vol. 5, no. 2, pp. 661–671, Jun. 2017, doi: 10.1109/JESTPE.2016.2581858.
[102] N. A. Windarko, A. Tjahjono, D. O. Anggriawan, and M. H. Purnomo, "Maximum power point tracking of photovoltaic system using adaptive modified firefly algorithm," in *2015 International Electronics Symposium (IES)*, Surabaya, Indonesia: IEEE, Sep. 2015, pp. 31–35. doi: 10.1109/ELECSYM.2015.7380809.
[103] R. B. A. Koad, A. F. Zobaa, and A. El-Shahat, "A Novel MPPT Algorithm Based on Particle Swarm Optimization for Photovoltaic Systems," *IEEE Trans. Sustain. Energy*, vol. 8, no. 2, pp. 468–476, Apr. 2017, doi: 10.1109/TSTE.2016.2606421.
[104] T. L. Nguyen and K.-S. Low, "A Global Maximum Power Point Tracking Scheme Employing DIRECT Search Algorithm for Photovoltaic Systems," *IEEE Trans. Ind. Electron.*, vol. 57, no. 10, pp. 3456–3467, Oct. 2010, doi: 10.1109/TIE.2009.2039450.
[105] L. N. Palupi, T. Winarno, A. Pracoyo, and L. Ardhenta, "Adaptive voltage control for MPPT-firefly algorithm output in PV system," *IOP Conf. Ser.: Mater. Sci. Eng.*, vol. 732, p. 012048, Jan. 2020, doi: 10.1088/1757-899X/732/1/012048.
[106] S. Sheik Mohammed, D. Devaraj, and T. P. Imthias Ahamed, "Maximum power point tracking system for stand alone solar PV power system using Adaptive Neuro-Fuzzy Inference System," in *2016 Biennial International Conference on Power and Energy Systems: Towards Sustainable Energy (PESTSE)*, Bangalore: IEEE, Jan. 2016, pp. 1–4. doi: 10.1109/PESTSE.2016.7516536.
[107] A. G. Abo-Khalil, W. Alharbi, A.-R. Al-Qawasmi, M. Alobaid, and I. M. Alarifi, "Maximum Power Point Tracking of PV Systems under Partial Shading Conditions Based on Opposition-Based Learning Firefly Algorithm," *Sustainability*, vol. 13, no. 5, p. 2656, Mar. 2021, doi: 10.3390/su13052656.
[108] S. M. Sulthan, D. D., S. R. B., M. M. O., and V. Raj, "Development and analysis of a Two stage Hybrid MPPT algorithm for solar PV systems," *Energy Reports*, vol. 9, pp. 1502–1512, Oct. 2023, doi: 10.1016/j.egyr.2023.07.006.
[109] M. Seyedmahmoudian *et al.*, "Simulation and Hardware Implementation of New Maximum Power Point Tracking Technique for Partially Shaded PV System Using Hybrid DEPSO Method," *IEEE Trans. Sustain. Energy*, vol. 6, no. 3, pp. 850–862, Jul. 2015, doi: 10.1109/TSTE.2015.2413359.
[110] W. Hayder, E. Ogliari, A. Dolara, A. Abid, M. Ben Hamed, and L. Sbita, "Improved PSO: A Comparative Study in MPPT Algorithm for PV System Control under Partial Shading Conditions," *Energies*, vol. 13, no. 8, p. 2035, Apr. 2020, doi: 10.3390/en13082035.
[111] S. Hesari, "Design And Implementation Of Maximum Solar Power Tracking System Using Photovoltaic Panels," *IJRER*, no. v6i4, 2016, doi: 10.20508/ijrer.v6i4.4352.g6909.
[112] P. Dhivya and K. R. Kumar, "MPPT based control of sepic converter using firefly algorithm for solar PV system under partial shaded conditions," in *2017 International Conference on Innovations in Green Energy and Healthcare Technologies (IGEHT)*, Coimbatore, India: IEEE, Mar. 2017, pp. 1–8. doi: 10.1109/IGEHT.2017.8094081.

[113] A. Nusaif and A. Mahmood, “MPPT Algorithms (PSO, FA, and MFA) for PV System Under Partial Shading Condition, Case Study: BTS in Algazalia, Baghdad,” *ijSmartGrid*, Sep. 2020, doi: 10.20508/ijsmartgrid.v4i3.113.g99.
[114] J. Farzaneh, R. Keypour, and M. A. Khanesar, “A New Maximum Power Point Tracking Based on Modified Firefly Algorithm for PV System Under Partial Shading Conditions,” *Technology and Economics of Smart Grids and Sustainable Energy*, vol. 3, no. 1, p. 9, Jun. 2018, doi: 10.1007/s40866-018-0048-7.
[115] M. Agdam, A. Asbayou, M. Elyaqouti, A. Ihlal, and K. Assalaou, “MPPT of PV System Under Partial Shading Conditions Based on Bio-inspired Swarm Intelligence Technique,” *E3S Web Conf.*, vol. 297, p. 01051, 2021, doi: 10.1051/e3sconf/202129701051.
[116] A. Gil-Velasco and C. Aguilar-Castillo, “A Modification of the Perturb and Observe Method to Improve the Energy Harvesting of PV Systems under Partial Shading Conditions,” *Energies*, vol. 14, no. 9, p. 2521, Apr. 2021, doi: 10.3390/en14092521.
[117] M. S. Nkambule, A. N. Hasan, and A. Ali, “MPPT under partial shading conditions based on perturb & observe and incremental conductance,” in *2019 11th international conference on electrical and electronics engineering (ELECO)*, 2019, pp. 85–90. doi: 10.23919/ELECO47770.2019.8990426.
[118] A. Pandey and S. Srivastava, “Perturb & Observe MPPT Technique used for PV System Under different Environmental Conditions,” vol. 06, no. 04, 2019.
[119] J. Garcia-Morales, G. Femenias, and F. Riera-Palou, “Analysis and Optimization of FFR-Aided OFDMA-Based Heterogeneous Cellular Networks,” *IEEE Access*, vol. 4, pp. 5111–5127, 2016, doi: 10.1109/ACCESS.2016.2599026.
[120] M. Rehan and M. M. A. Awan, “Optimization of MPPT perturb and observe algorithm for a standalone solar PV system,” *Mehran Univ. res. j. eng. technol.*, vol. 43, no. 3, p. 136, Jul. 2024, doi: 10.22581/muet1982.3147.
[121] E. W. Mukti, A. Risdiyanto, Ant. A. Kristi, and R. Darussalam, “Particle Swarm Optimization (PSO) based Photovoltaic MPPT Algorithm under the Partial Shading Condition,” *J. Elektron. dan Telekomun.*, vol. 23, no. 2, p. 99, Dec. 2023, doi: 10.55981/jet.552.
[122] A. Lakhdara, T. Bahi, and A. Moussaoui, “PSO Control under Partial Shading Conditions,” *AJRESD*, vol. 2, no. 02, pp. 126–136, Dec. 2020, doi: 10.46657/ajresd.2020.2.2.5.